

UNIVERSIDAD AUTÓNOMA DE MADRID

ESCUELA POLITÉCNICA SUPERIOR



PROYECTO FIN DE CARRERA

MIMO ANTENNAS BASED ON THE EXCITATION OF CAR BODYWORK ELEMENTS

Ingeniería de Telecomunicación

Eva Masaguer Velasco
Mayo 2014

MIMO ANTENNAS BASED ON THE EXCITATION OF CAR BODYWORK ELEMENTS

AUTOR: Eva Masaguer Velasco
TUTOR: Jerzy Kowalewski

Grupo de RadioFrecuencia: Circuitos, Antenas y Sistemas
Escuela Politécnica Superior
Universidad Autónoma de Madrid
Mayo 2014

Resumen

De acuerdo con la teoría de los modos característicos, una distribución de corriente superficial arbitraria puede ser representada como una serie infinita de modos ortogonales de corrientes superficiales. Los patrones de directividad de los modos se determinan a través de formulación matemática y son ortogonales entre sí. Por lo tanto, los modos son apropiados para la síntesis de un patrón de directividad dado, así como para la integración de un sistema MIMO en un espacio limitado. Esto es debido al acoplamiento entre cada una de las antenas y su plataforma de referencia común. La distribución de corriente superficial en la plataforma de referencia es por lo tanto de gran importancia y por ello debe ser entendida y optimizada. Por lo tanto, la teoría de los modos característicos es un método para integrar y optimizar sistemas MIMO en un espacio dado.

El objetivo de este proyecto es desarrollar y verificar un sistema de antenas MIMO basado en la excitación de los elementos de la carrocería de un coche. Con el fin de excitar las corrientes superficiales en las piezas de carrocería, posibles estructuras de acoplamiento debe ser investigadas y desarrolladas. La banda de funcionamiento de este sistema se define desde 2.5 GHz hasta 2.7 GHz, frecuencias del standar LTE. Para alimentar las antenas que forman este sistema, se ha diseñado un circuito de línea microstrip compuesto por redes de adaptación, T-Juntion y Tapers.

Para verificar los resultados obtenidos en las simulaciones, se construirá un prototipo para cada uno de los modos característicos estudiados, para la posterior medición de su reflexión y de su patrón de radiación.

Por último, el sistema de antena MIMO se simulará y fabricará para la posterior medición de su reflexión y de su patrón de radiación. En este sistema MIMO se excitarán dos de los modos característicos estudiados.

Palabras clave

antenna, Multiple-Input Multiple-Output (MIMO), modos característicos, carrocería, diagrama de radiación, corriente superficial, microstrip, acoplamiento, parametros S, reflexión, adaptación, substrato, constante dieléctrica, pérdidas,

Abstract

According to the theory of characteristic modes an arbitrary surface current distribution can be represented as an infinite series of orthogonal surface current modes. The directivity patterns of the modes are determined by the mathematical formula and are orthogonal to each other. Thus, the modes are suitable for the synthesis of a given directivity pattern as well as for the integration of MIMO system in a limited space. This is due to a coupling between the individual antenna elements and the common reference platform. The surface current distribution on the reference platform is thereby of a great importance and therefore must be understood and optimized. Thus the theory of characteristic modes is a methodology to integrate and optimize a MIMO system in a given space.

The objective of this project is to develop and verify a MIMO antenna system based on the excitation of car bodywork elements. In order to excite the surface currents on the bodywork parts possible coupling structures should be investigated and developed. The operating band of this system is defined from 2.5 GHz to 2.7 GHz, frequencies in the LTE (Long Term Evolution) standard. To feed the antennas, a microstrip line circuit composed of matching networks, T-junction and Tapers has been designed.

To verify the results obtained in the simulations, a prototype for each of the studied characteristic modes is fabricated, for further investigation of its insertion loss, radiation pattern and efficiency.

Finally, the MIMO antenna system is simulated and manufactured for its further evaluation. In this MIMO system two of the studied characteristic modes are excited.

Key words

antenna, Multiple-Input Multiple-Output (MIMO), characteristic modes, bodywork, radiation pattern, surface current, microstrip, patches, coupling, S-parameters, reflection, matching, substrate, dielectric constant, losses

Agradecimientos

Una etapa antigua se acaba y empieza una nueva. Esta ha sido una etapa llena de sacrificios y esfuerzos, pero también a sido una etapa llena de experiencias y momentos inolvidables. En la Escuela Politécnica Superior de la Universidad Autónoma de Madrid saben como formar ingenieros para que cuando acabemos sepamos comernos el mundo. Por ello quiero agradecer de todo corazón a todos esos profesores que me han guiado en mi carrera espero algún día llegar a ser tan buena en mi trabajo como ellos.

En especial quiero agradecer a José Luis Masa Campos esta gran oportunidad que me ha dado de continuar mi carrera en el extranjero. El día que acudí a el con la descripción del proyecto, se lo leyó y me dio su visto bueno, porque el sabe muy bien que me estaba dando una oportunidad de oro.

También quiero agradecer este proyecto al profesor Bazil Taha Ahmed, acudí a el en primer lugar pensando que el era el especialista en antenas y el me dijo que tenía que ir a hablar con José Luis, no sin antes decirme: Me he leído la descripción del proyecto y es un proyecto complicado, ¿tu estás segura? Y yo sin pensármelo dos veces le conteste que estaba segura y pensé para mí misma: si fuese fácil no me gustaría.

Además quiero hacer una agradecimiento muy especial al profesor Juan Córcoles Ortega, por todas esas tutorías de COOP. Todas esas horas de formación me abrieron los ojos para darme cuenta de que el mundo de la radio frecuencia es donde quiero trabajar.

Por supuesto también quiero dar la gracias a mi tutor Jerzy Kowalewski, danke für die vielen Stunden deiner Zeit und alle deine Unterstützung.

Y sobretodo agradecer a mi familia todo su apoyo incondicional durante todos estos años, vosotros sois los que siempre estas ahí para guiar mis pasos y aunque sé que estos dos últimos años he estado lejos sabéis que siempre volveré. Además si luego os gusta ir de visita y que os enseñe los rincones más bonitos, asique no os podéis quejar. Lo veis, os dije que lo conseguiría.

Gracias a todos mis amigos de teleco con los que he compartido tantas horas de practicas y biblioteca, el final tantos veranos pasando calor en Madrid y tantas navidades haciendo practicas han dado sus frutos. No quiero hacer ninguna mención especial por que la lista me ocuparía otras 100 páginas peor ellos saben a quien me refiero ¿a que sí? Sin vosotros no habría llegado a donde esto ahora. Gracias Maya y Marta por estar siempre ahí aunque estuviésemos lejos.

No me olvido de mis amigos de toda la vida. Con vosotros tengo recuerdos imborrables y sé que siempre voy a poder contar con vosotros por muy lejos que me vaya sé que cuando vuelva estaréis aquí. Menos mal que ya se acabaron los domingos de llegar los primeros a la 24 horas para coger sitio y los veranos de buscar una sombra en cualquier sitio para no asarnos al sol. Aunque también echaré de menos esos momentos.

Por ultimo quiero acordarme también de todos mis amigos de Erasmus, el Erasmus fue un año maravilloso lleno de nuevas experiencias. Ir a la universidad a $-35^{\circ}C$, ir a la compra en trineo, quedar para hacer guerras de nieve y tirarnos todo el día en trineo (para luego tener moratones por todo el cuerpo), esos viajes de locura a laponia, tantas horas de aprender finlandés aunque sabíamos que luego nos iba a servir para poco, las horas en la sauna para luego tirarnos

al mar congelado. Todo esto no habría sido lo mismo sin todos vosotros, gracias.

Una etapa se cierra y otra se abre, pánico me da la que se abre, pero sé que siempre puedo contar con vosotros. Muchas gracias.

Eva

Contents

List of figures	xiii
List of Tables	xvii
1 Introduction	1
1.1 Motivation	1
1.2 Goals	1
1.3 Document Structure	2
2 State of the art	3
2.1 Introduction	3
2.2 Principles of Antennas	3
2.2.1 Concept of Antenna	3
2.2.2 Types of Antennas	4
2.2.3 Standard Frequency Bands	4
2.3 Input Impedance	5
2.4 Scattering Parameters (S Parameters)	5
2.5 Matching	7
2.6 Voltage Standing Wave Ratio (VSWR)	8
2.7 Field regions	8
2.8 Radiation Pattern	9
2.8.1 Radiation Pattern Lobes	9
2.8.2 Parameters of the radiation pattern	10
2.8.3 Radiation pattern types	11
2.9 Radiation Intensity, Directivity and Gain	11
2.9.1 Radiation Intensity	11
2.9.2 Directivity	11
2.9.3 Gain	12
2.10 Polarization	12
2.11 Bandwidth	13
2.12 Microstrip Line Theory	13

2.13	Multiple Input Multiple Output (MIMO) antennas	14
2.13.1	Diversity in MIMO Systems	14
2.13.2	Performance of MIMO	15
2.14	The Theory of Characteristic Modes	18
2.14.1	Mathematical Formulation of Characteristic Modes	18
2.15	Overview on possible automotive antenna technologies	20
2.15.1	Monopoles	20
2.15.2	Blade or Shark-fin antennas	21
2.15.3	On-glass antenna	22
2.15.4	Body integrated spiral antenna	22
2.15.5	Patch antenna	23
2.16	Antenna technology used in this project	23
3	Feeding Network for Inductive Coupling Elements	25
3.1	Introduction	25
3.2	Characteristic Modes of a rectangular metallic plate	26
3.3	Selective excitation of Characteristic Modes by different set of Inductive Coupling Elements (ICEs)	27
3.3.1	Single Inductive Coupling Element (ICE)	28
3.4	Feeding network using microstrip line technology	29
3.4.1	Inductive Coupling Element (ICE) ports	30
3.4.2	Matching circuits	31
3.4.3	T-Junction	34
3.4.4	Taper	34
3.4.5	Directivity Pattern	36
3.4.6	Final circuits	36
3.4.7	Fabricated circuits and measurements	37
3.4.8	Manual tuning of the matching network	39
3.4.9	Matching network at 2.8 GHz	40
3.5	Improved circuits	41
3.6	Study of the fabrication tolerance of the system	42
3.7	Conclusions	43
4	MIMO antennas system based on the excitation of car bodywork elements	45
4.1	Introduction	45
4.2	Requirements for vehicular antennas	45
4.3	Possible location of antennas in a car	45

4.3.1	Roof	46
4.3.2	Spoiler	46
4.3.3	Fender and bumper	46
4.3.4	Trunk cover	46
4.3.5	Side-Mirror	46
4.4	Location of the MIMO system	47
4.5	Design of the MIMO system	47
4.6	Inductive Coupling Elements in the MIMO system	49
4.7	Feeding network of the MIMO system	50
4.7.1	Inductive Coupling Element (ICE) ports of the MIMO system	50
4.7.2	Matching network of the MIMO system	50
4.7.3	T-Junction structure of the MIMO system	52
4.7.4	Taper structure of the MIMO system	53
4.7.5	Final circuit	54
4.7.6	Shorted stubs metallization	56
4.8	Definition of the Envelope Correlation Coefficient (ECC)	57
4.9	MIMO system with mode $J1$ and $J3$	58
4.10	Conclusions	59
5	Fabrication of the MIMO system	61
5.1	First fabricated MIMO system	62
5.1.1	Reflection coefficient measurements	62
5.1.2	Far field measurements	63
5.2	Second fabricated MIMO system	66
5.2.1	Reflection coefficient measurements	66
5.3	Fabricated MIMO system on the side-mirror	66
5.4	Conclusions	66
6	MIMO antenna system in the side-mirror	69
6.1	Introduction	69
6.2	Attachment of the MIMO system with the side-mirror	69
6.3	MIMO system in the side-mirror	70
6.4	Influence of painting the car bodywork elements	70
6.5	Feeding the MIMO system with a mini-coaxial cable	72
6.6	Other considerations in the design of the MIMO system for the side-mirror	73
6.7	Conclusions	74
7	Conclusions	75

8 Future work	77
Bibliography	78
Appendices	83
A Introducción	85
A.1 Motivación	85
A.2 Objetivos	86
A.3 Estructura del documento	86
B Conclusiones	89
B.1 Publicaciones	90
C Presupuesto	91
D Pliego de condiciones	93

List of Figures

2.1	Antennas' examples	3
2.2	Classification of antennas according to their frequency of operation	4
2.3	Antenna connected to a generator through a transmission line	7
2.4	Field regions of an antenna	8
2.5	Spherical coordinate system	9
2.6	Radiation pattern of an antenna	10
2.7	Linear plot of power pattern and its associated lobes and beamwidths	10
2.8	Radiation patterns [39]	11
2.9	Linear, Circular and Elliptical polarization [42]	12
2.10	Geometry of a microstrip line	13
2.11	WLANs generations	14
2.12	Comparison between SISO, SIMO, MISO and MIMO	15
2.13	Basic structure of a MIMO system	16
2.14	MIMO channel model	17
2.15	Current vectors for six eigenvector in a rectangular plate	19
2.16	Variation of the eigenvalues with frequency [1]	20
2.17	Mast antenna [43]	21
2.18	Blade or Shark-fin antenna[43]	21
2.19	BMW 3-Series E46 Sharkfin Antenna [43]	21
2.20	TV antennas on glass[24]	22
2.21	Body integrated spiral antenna [44]	22
2.22	Principal structure of a squared patch antenna[23]	23
3.1	Feeding network schema	25
3.2	Microstrip line of the feeding network	26
3.3	Eigenvalues as a function of frequency for the characteristic modes of the investigated metallic plate in free space [14]	26
3.4	Current distribution schematics for the first three characteristic modes	27
3.5	Sinusoidal behavior of the current distribution on the metallic plate [12],[14]	27
3.6	Concept for the selective excitation of the first three characteristic modes on a metallic plate by different sets of ICEs [12],[14]	28

3.7	Inductive Coupling Element at the edge of the metallic plate [12],[14]	28
3.8	Current distribution of the Inductive Coupling Element at the edge of the metallic plate	29
3.9	Feeding network: circuits structure	30
3.10	Feeding network: current distribution	30
3.11	Inductive Coupling Element port	31
3.12	Matching circuit using double-stub tuning	31
3.13	Matching circuit using the Smith Chart	32
3.14	Matching impedance circuit	32
3.15	Double-stub tuning example	33
3.16	Reflection coefficient of the matched ICE_{J1} , ICE_{J2} and ICE_{J3}	33
3.17	T-junction	34
3.18	Tapered element	35
3.19	Variation of the impedance for an Exponential taper [11]	35
3.20	Reflection coefficient of an Exponential taper [11]	35
3.21	Antenna's radiation pattern for three modes in 3D representation	36
3.22	Antenna's radiation pattern for three modes in 2D representation	36
3.23	Feeding network: final circuits	37
3.24	Feeding network: fabricated circuits	37
3.25	Reflection Coefficients (S_{11}) MODE J1	38
3.26	Reflection Coefficients (S_{11}) MODE J2	38
3.27	Reflection Coefficients (S_{11}) MODE J1	39
3.28	Results of the manual tuning of the fabricated circuits	40
3.29	Reflection Coefficients (S_{11}) MODE J2 matched in simulation at 2.8 GHz	41
3.30	Fabricated circuit MODE J2 matched in simulation at 2.8 GHz	41
3.31	Metallized via	42
3.32	Dimensions of the improved matching circuits	42
3.33	Reflection coefficient final metallized circuits	43
3.34	Positive tolerance	43
3.35	Negative tolerance	44
4.1	Suitable antenna placement on a regular passenger car	46
4.2	Microstrip line of the MIMO system	47
4.3	Generic car mirror	48
4.4	MIMO system in the side-mirror	48
4.5	Inductive Coupling Elements for the characteristic modes in the MIMO system	49
4.6	Structure of the Inductive Coupling Elements in the MIMO system	49

4.7	Location of the Inductive Coupling Element ports in the MIMO system	50
4.8	Location of the matching network in the MIMO system	51
4.9	Matching network using ADS	51
4.10	T-junctions structures in the MIMO system	53
4.11	Taper structure in the MIMO system on details	53
4.12	Taper structure in the MIMO system	54
4.13	Final circuit of the MIMO system	54
4.14	Reflection coefficient MIMO system	55
4.15	Reflection coefficient MIMO system	55
4.16	Antenna's radiation pattern for the MIMO system in 3D representation	56
4.17	Shorted stubs metallization for the MIMO system	56
4.18	Reflection coefficient MIMO system, shorted stubs metallization	57
4.19	Envelope Correlation Coefficient (ECC)	58
4.20	MIMO system, mode $J1$ and $J3$	58
4.21	Reflection coefficiente MIMO system with modes $J1$ and $J3$	59
5.1	Microstrip line of the MIMO system	61
5.2	First fabricated MIMO antenna	62
5.3	Measurement mode $J3$	62
5.4	Reflection coefficient first fabricated MIMO antenna system	63
5.5	Anechoic chamber in the Institut für Hochfrequenztechnik und Elektronik (IHE)	63
5.6	Measured directivity pattern at 2.2 GHz for $\theta = 90^\circ$ for mode $J2$	64
5.7	Simulated directivity pattern at 2.2 GHz for $\theta = 90^\circ$ for mode $J2$	64
5.8	Measured directivity pattern at 2.2 GHz for $\theta = 90^\circ$ for mode $J3$	65
5.9	Simulated directivity pattern at 2.2 GHz for $\theta = 90^\circ$ for mode $J3$	65
5.10	Second fabricated MIMO antenna	66
5.11	Reflection coefficient second fabricated MIMO antenna system	67
5.12	Fabricated MIMO system in the side-mirror	67
6.1	MIMO system in the side-mirror	69
6.2	Glued MIMO system	70
6.3	Attached MIMO system to the side-mirror	71
6.4	Isolated MIMO system to the side-mirror	71
6.5	Tuning for the MIMO system	71
6.6	Painted MIMO system	72
6.7	Painted MIMO system	72
6.8	Feeding the MIMO system with a coaxial cable	73

6.9	Offset of the mode J2	73
8.1	Multi-layer MIMO system	77
8.2	SMA connected at the end of the microstrip line port	77

List of Tables

2.1	Frequency Bands	4
2.2	Two-port circuit S parameters description	6
3.1	Final matching network Mode J1	42
3.2	Final matching network Mode J2	42
3.3	Final matching network Mode J3	42
4.1	Width values (W) of the microstrip line	47
4.2	Values of the load impedance (ZL) for each of the matching networks	51
4.3	Matching network 1 MODE J3	52
4.4	Matching network 2 MODE J2	52
4.5	Matching network 3 MODE J2	52
4.6	Matching network 4 MODE J3	52
5.1	Width values (W) of the microstrip line	61

1

Introduction

1.1 Motivation

In recent years, people spent more and more time in their cars this means that the cars are essential in our society. Consequently everyday consumers demand more services from their cars. This demand leads into an increasing development of new vehicles technologies. This new vehicles technologies promote the improvement of different factors such as the size of the product, the reduction of the product price and better adaptation of the product to the environment. Ergo there is a constant research and development of new solutions that provide a high Quality of Service. The increasing amount of services like radio, GPS navigation, TV or telephone request a continuous increased of the number of antennas installed on a car. However the number of suitable locations for the antennas at the car is decreasing.

The demand for more services requires higher data rates which can be realized by Multiple-Input Multiple-Output (MIMO) antenna systems [22, 23, 24]. MIMO is an essential part of all future mobile wireless standards [18]. Therefore, the design of a MIMO antenna system for vehicles is of great attention in the the automobile industry.

Also as an adequate location of the antenna system is reduced, either by design specifications or potential interference with other electronic equipment, the use of reduced-size antennas must be considered. Thus the design of a MIMO system based on the generation of characteristic modes in car body elements [1, 2, 3, 4, 5, 6, 7] appears to be a promising solution to cover the increasing demand of mobile services in cars. If to the advantage of the higher data rate and the reduced size, the ease of manufacturing and the low cost of microstrip circuits is added, an optimal antenna for communication system can be designed.

Due to the named reasons a MIMO antenna system [13, 15, 18] based on excitation of car bodywork elements using Inductive Coupling Elements with a microstrip feeding network is developed and verified in this project.

1.2 Goals

The overall aim of this project is the design, construction and measurement of an MIMO antenna system applying Inductive Coupling Elements. The operating band of this antenna is

from 2.5 GHz to 2.7 GHz, which is the frequency band use by LTE (Long Term Evolution).

The objectives of this project are the following:

1. Study of possibilities for multimode excitation of car bodywork elements
2. Design and optimization of Inductive Coupling Elements in a metallic plate
3. Design of a feeding network for the Inductive Coupling Elements using microstrip elements and matching networks
4. Fabrication of a prototype antennas for different characteristic modes
5. Design of a MIMO system using Inductive Coupling Elements with the feeding network
6. Fabrication of the MIMO system

1.3 Document Structure

This document is structured as follows:

- **Chapter 1: Introduction**

Introducing the motivation for the project, its objectives and the structure of memory.

- **Chapter 2: State of the art**

Description of state of the art, deepening into MIMO systems, the characteristic modes and microstrip technology.

- **Chapter 3: Feeding Network for Inductive Coupling Elements**

The complete design of the feeding network is organized into three parts:

- Design and characterization of the Inductive Coupling Elements
- Design of the feeding network for each of the Characteristic Modes
- Manufacture of prototypes and experimental verification

- **Chapter 4: MIMO antennas system based on the excitation of car bodywork elements**

Design of the MIMO system applying the acquired knowledge of Inductive Coupling Elements on generation of characteristic modes.

- **Chapter 5: Fabrication of the MIMO system**

The fabrication process of the MIMO system and the experimental results are detailed in this chapter.

- **Chapter 6: MIMO antennas system on the side-mirror**

Final implementation of the MIMO system in the side-mirror is described in this chapter.

- **Chapter 7: Future Work**

Finally, this chapter suggests possible improvements and future lines of work.

2

State of the art

2.1 Introduction

This chapter explains basic concepts of antennas and gives a brief introduction to the theory of waveguides and microstrip lines used in this project.

2.2 Principles of Antennas

2.2.1 Concept of Antenna

Antennas are the parts of the wireless systems designed specifically to radiate and receive electromagnetic waves. An antenna can also be defined as a device that changes guided waves, which are conducted by transmission lines, into waves propagating in free space.

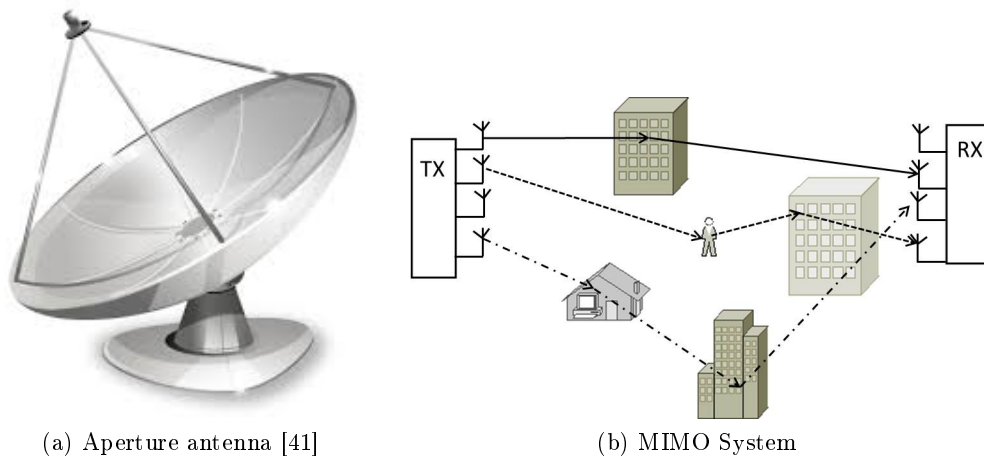


Figure 2.1: Antennas' examples

2.2.2 Types of Antennas

The antennas are classified into directional and omnidirectional antennas.

- A directional antenna is capable of concentrating most of the radiated energy in a localized manner, thus increase the power transmitted to the receiver or from the source and send unwanted interference introduced by unwanted sources.
- An omnidirectional antenna radiates electromagnetic waves uniformly in all directions.

According to the radiation mode four groups of antennas can be defined: elements, progressive wave, arrays and aperture antennas. The figure 2.2 shows this antennas classification according to their operating frequency of the antenna.

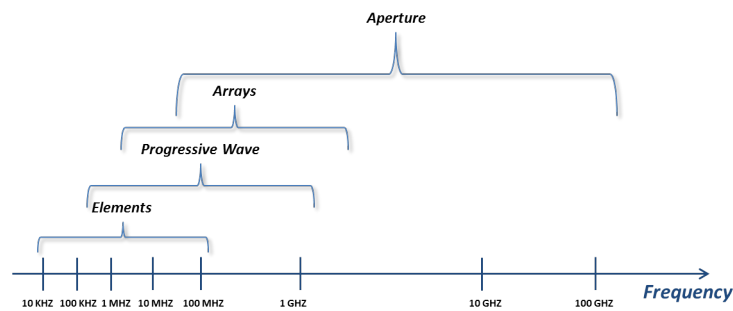


Figure 2.2: Classification of antennas according to their frequency of operation

2.2.3 Standard Frequency Bands

Acronym	Name	Wavelength	Frequency Range	Applications
VLF	Very low frequency	30.000 m to 10.000 m	10 KHz to 30 KHz	Navigation and sonar
LF	Low frequency	10.000 m to 1.000 m	30 KHz to 300 KHz	Radio beacons and Navigational aids
MF	Medium Frequency	1.000 m to 100 m	300 KHz to 3 MHz	AM broadcasting, maritime radio, direction finding
HF	High Frequency	100 m to 10 m	3 MHz to 30 MHz	Telephone, telegraph, amateur radio, ship-to-coast and ship-to-aircraft comm
VHF	Very High Frequency	10 m to 1 m	30 MHz to 300 MHz	Television, FM broadcasting, air traffic control, police and taxi mobile radio
UHF	Ultra High Frequency	1 m to 10 cm	300 MHz to 3 GHz	Television, satellite communication, radiosonde and surveillance radar
SHF	Super High Frequency	10 cm to 1 cm	3 GHz to 30 GHz	Airborne radar, microwave links and satellite communication
EHF	Extremely High Frequency	1 cm to 1 mm	30 GHz to 300 GHz	Radar

Table 2.1: Frequency Bands

2.3 Input Impedance

The input impedance is defined as the impedance presented by an antenna at its port or the ratio of the voltage to current at the port or the ratio of the appropriate components of the electric or magnetic fields at a point [10].

The input impedance Z_A , given in the formula 2.1, consists in two parts:

- The real part R_A known as the resistive part of the antenna's impedance
- The imaginary part X_A known as the reactance part of the antenna's impedance

$$Z_A = R_A(\omega) + jX_A(\omega) \quad (2.1)$$

Generally the resistive part R_A consists of two components:

- The radiation resistance of the antenna (R_r):

$$R_r = \frac{2P_{rad}}{|I_A|^2} \quad (2.2)$$

- The loss resistance of the antenna (R_L):

$$R_L = \frac{2(P_{in} - P_{rad})}{|I_A|^2} \quad (2.3)$$

Both components are related by the following equation:

$$R_a = R_r + R_L \quad (2.4)$$

This division allows one to distinguish between the power radiated by the antenna P_r (2.5) and the power dissipated as heat P_L (2.6), where I_0 is the current value at the antennas port:

$$P_r = \frac{1}{2}|I_0|^2 R_r \quad (2.5)$$

$$P_L = \frac{1}{2}|I_0|^2 R_L \quad (2.6)$$

In addition, if the imaginary part of the input impedance $X_A(\omega)$ is zero at a certain frequency, it is said that the antenna is resonant at this frequency.

2.4 Scattering Parameters (S Parameters)

At RF (Radio Frequency) and microwave frequencies direct measurements of impedance Z or admittance Y is difficult due to the unavailability of equipment to measure total current or voltage. Furthermore it is difficult to obtain perfect open/short conditions and the active devices may be unstable under open/short conditions.

A more consistent representation with the concepts of incident waves, reflected and transmitted is the scattering matrix or S-parameters. S-parameters are the reflection and transmission

coefficients between the incident and reflected wave. These parameters describe completely a device's behavior under linear conditions at a given frequency range. Each parameter is characterized by magnitude and phase. Although they are applicable to any frequency, the S-parameters are primarily used for networks operating at radio frequency (RF) and microwave frequencies. In general, for practical networks the S-parameters change with the frequency, that is why the frequency should be specified for any measurement of S-parameters, as well as the characteristic impedance.

In the context of the S-parameters, dispersion refers to the way in which the currents and voltages that are displaced in a transmission line are affected when they meet a discontinuity due to the introduction of a network in a transmission line.

Some microwave circuits can be characterized as a two-port network, where the first port is the physical input port of the circuit and the second is the output terminal.

Following explains the method to calculate the S-parameters of a 2-port circuit. The relation between the reflected waves, the incident and scattering parameter matrix is given by:

$$\begin{bmatrix} b_1 \\ b_2 \end{bmatrix} = \begin{bmatrix} s_{11} & s_{12} \\ s_{21} & s_{22} \end{bmatrix} \begin{bmatrix} a_1 \\ a_2 \end{bmatrix} \quad (2.7)$$

To calculate the parameter S_{ji} is necessary that each port of the network ends in its respective characteristic impedance except for the i -th, which will connect to a generator that produces the incident wave a_i . Therefore, the rest of incident waves are zero. Substituting and solving from S-parameters matrix, the parameter S_{ji} is:

$$S_{ji} = \left(\frac{b_j}{a_i} \right)_{a_i \neq 0, \forall K \neq i} \quad (2.8)$$

The description of the S-parameters of a 2-port circuit is shown in the table 2.2.

Parameter	Coefficient	Description	Formula
S_{11}	Input reflection	Power reflected in port 1 when fed with an incident wave in port 1	$S_{11} = \frac{b_1}{a_1}$ when $a_2 = 0$
S_{12}	Transmission or inverse gain	Power that reaches port 2 when the circuit is fed from port 2	$S_{12} = \frac{b_1}{a_2}$ when $a_1 = 0$
S_{21}	Transmission or direct gain	Power that reaches port 2 when the circuit is fed from port 1	$S_{21} = \frac{b_2}{a_1}$ when $a_2 = 0$
S_{22}	Output reflection	Power reflected in port 2 when fed with an incident wave in port 2	$S_{22} = \frac{b_2}{a_2}$ when $a_1 = 0$

Table 2.2: Two-port circuit S parameters description

From the S-parameters described in the table 2.2 the parameters in the equations 2.9, 2.10, 2.11 and 2.12 can define.

$$|S_{ii}|^2 = \frac{\text{Power reflected at port } i}{\text{Power fed at port } i} \quad (2.9)$$

$$\text{Input return loss}(dB) = -20 \log |S_{ii}| \quad (2.10)$$

$$|S_{ji}|^2 = \frac{\text{Power transmitted at port } j}{\text{Power fed at port } i} \quad (2.11)$$

$$\text{Insertion loss(dB)} = -20 \log |S_{ji}| \quad (2.12)$$

2.5 Matching

For proper operation, an antenna must be connected to the transmitter or to the receiver through a transmission line.

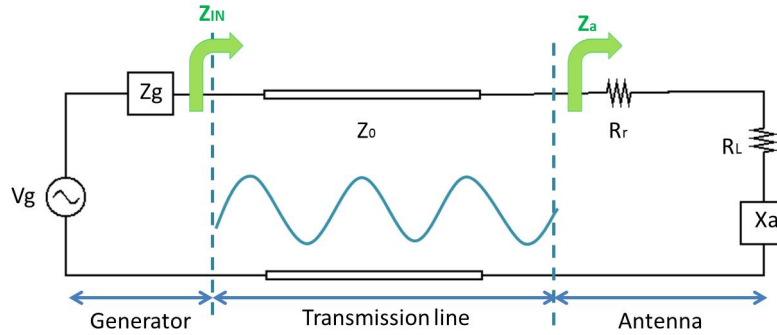


Figure 2.3: Antenna connected to a generator through a transmission line

In the Figure 2.3 the following parameters are schematized :

- Z_0 : characteristic impedance of the transmission line
- Z_A : input impedance of the antenna
- A generator V_g with the impedance $Z_g = R_g + jX_g$
- An antenna with load impedance $Z_a = R_a + jX_a = (R_r + R_L) + jX_a$
- The impedance seen by the generator is $Z_{IN} = R_{IN} + jX_{IN}$

The S_{11} parameter measures the power reflected at the input port of the antenna, giving an idea of the power transfer from the antenna. The S_{11} parameter can be defined in terms of impedance:

$$S_{11} = |\Gamma| = \frac{Z_a - Z_0}{Z_a + Z_0} \quad (2.13)$$

The input power to the network is defined as:

$$P_{IN} = \frac{1}{2} |I|^2 R_{IN} = \frac{1}{2} \left| \frac{V_g}{Z_g + Z_{IN}} \right|^2 R_{IN} \quad (2.14)$$

Maximum impedance matching occurs if $Z_g = Z_{IN}^*$. Transferred power is maximized at the point of maximum impedance matching. In this way the generator delivers the maximum power to the transmission line, the expression of the maximum power is:

$$P_{IN} = \frac{1}{2} \left| \frac{V_g}{Z_{IN}^* + Z_{IN}} \right|^2 R_{IN} = \frac{1}{2} \left| \frac{V_g}{R_g} \right|^2 R_{IN} \quad (2.15)$$

2.6 Voltage Standing Wave Ratio (VSWR)

In a radio frequency circuit for supplying power to an antenna, the impedance of the transmission line should be well matched to the characteristic impedance of the antenna. The VSWR parameter is a numerical measure that describes how well the antenna impedance is matched to the transmission line:

$$VSWR = \frac{V_{max}}{V_{min}} = \frac{1 + |\Gamma|}{1 - |\Gamma|} \quad (2.16)$$

Where $\Gamma = S_{11}$, in most of the cases.

The SWR is always a real positive number. The SWR can take on any value from 1 to infinity. For the perfect impedance match situation, $|\Gamma| = S_{11} = 0$, and $VSWR = 1$.

2.7 Field regions

The radiation field from an antenna is characterized by the complex Poynting vector $E \times H^*$ in which E is the electric field and H is the magnetic field. Close to the antenna the Poynting vector is imaginary (reactive) and (E, H) decay more rapidly than $1/r$, while further away it is real (radiating) and (E, H) decay as $1/r$. These two types of fields dominate in different regions in space around the antenna. Based on this characterization of the Poynting vector, the space around the antenna is divided into three regions depending on the distance:

- **Reactive near field:** this region is the area closest to the antenna. The extent of this region is $0 < R < 0.62\sqrt{\frac{D^3}{\lambda}}$, where λ is the wavelength and D is the largest dimension of the antenna. In this space the Poynting vector is predominantly reactive (non-radiating) and it has all three components in spherical coordinates (r, θ, ϕ) . In this region, the electric and magnetic fields are out of phase by 90 degrees to each other (recall that for propagating or radiating fields, the fields are orthogonal (perpendicular) but are in phase).
- **Radiating near-field (Fresnel):** beyond the immediate neighbourhood of the reactive field the radiating field begins to dominate. The extent of this region is $0.62\sqrt{\frac{D^3}{\lambda}} < R < \frac{2D^2}{\lambda}$.
- **Far-field (Fraunhofer) region:** Beyond the radiating near-field region $\frac{2D^2}{\lambda} < R < \infty$. In this region the Poynting vector is real (only radiating fields) and it only has two components in the spherical coordinates (θ, ϕ) .

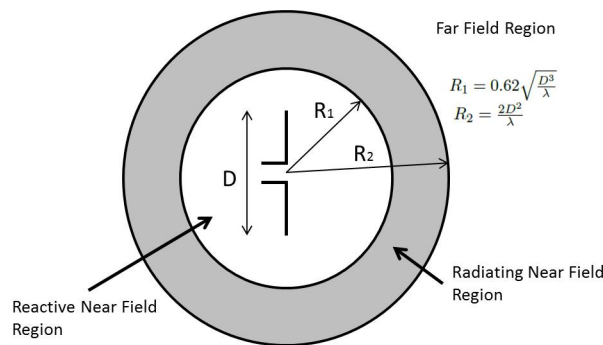


Figure 2.4: Field regions of an antenna

2.8 Radiation Pattern

An antenna radiation pattern is a graphical representation of the radiation properties of the antenna according to its spatial coordinates.

The most common manner representation of the radiation pattern uses a spherical coordinates system. This system is formed by the following coordinates, see Figure 2.5:

- Radius from the origin (r)
- θ the azimuth angle, angle relative to the axis x
- ϕ the elevation angle, angle relative to the axis z

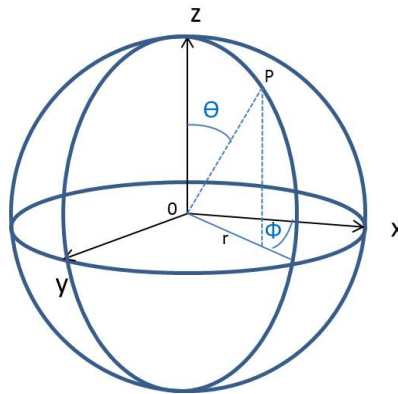


Figure 2.5: Spherical coordinate system

2.8.1 Radiation Pattern Lobes

The radiation pattern is the three-dimensional representation of the average value of the Poynting vector associated with an antenna. It is divided into lobes, closed regions where the radiation is continuous. The lobes are separated by areas in which there is no radiation, null areas of the radiation pattern.

In the Figure 2.6 can be seen the following parts of the radiation pattern:

- **Direction of propagation:** direction of maximum radiation of the antenna
- **Main lobe:** Region of the radiation pattern that contains the direction of maximum radiation
- **Grating lobe:** A lobe, other than the main lobe, produced by an array antenna when the inter element spacing is sufficiently large to permit the in-phase addition of radiated fields in more than one direction [10].
- **Side lobes:** lobes that are adjacent to the main lobe
- **Back lobe:** lobe which is in the opposite direction to the principal

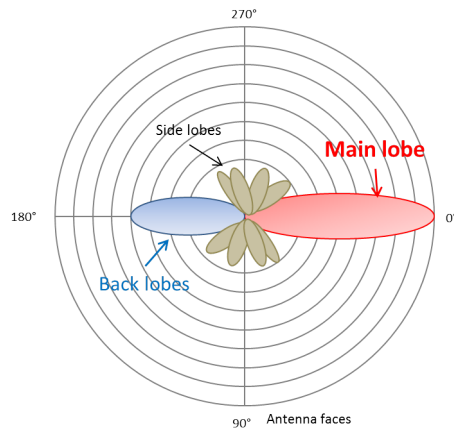


Figure 2.6: Radiation pattern of an antenna

2.8.2 Parameters of the radiation pattern

The Figure 2.7 illustrates the following parameters of the radiation pattern:

- **Side lobe level (SLL):** Relation in dB between the maximum value of the main lobe and the maximum amplitude value of the side lobes
- **Half Power Beamwidth (HPBW):** is the angular separation in which the magnitude of the radiation pattern decreases by 50% (or -3 dB) from the peak of the main beam
- **First-Null Beamwidth (FNBW):** is the angular separation between the first nulls of the pattern

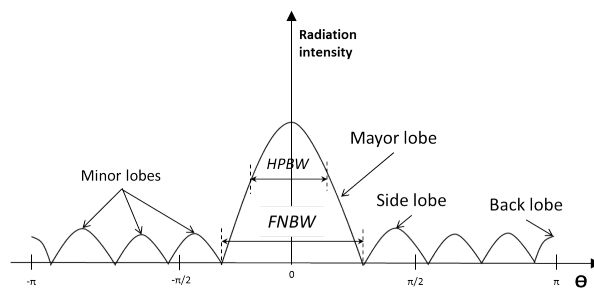


Figure 2.7: Linear plot of power pattern and its associated lobes and beamwidths

2.8.3 Radiation pattern types

The radiation pattern can be classified as:

1. **Isotropic:** it represents the theoretical form of lossless antenna , in this radiation pattern the density of the radiated power is the same in all directions (see Fig.2.8a)
2. **Omnidirectional:** the radiation pattern present a rotational symmetry respect to an axis (see Fig.2.8b)
3. **Directional:** in this case the directivity of the antenna is concentrate in one given direction (see Fig.2.8c)

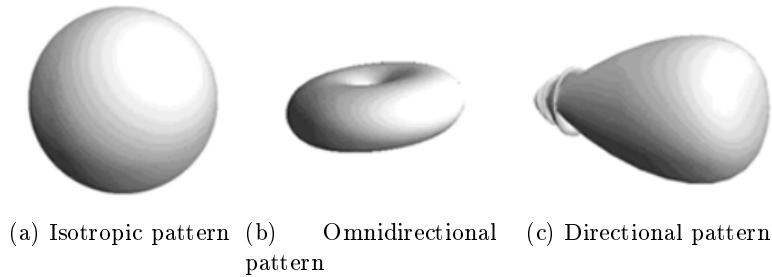


Figure 2.8: Radiation patterns [39]

2.9 Radiation Intensity, Directivity and Gain

2.9.1 Radiation Intensity

The intensity of radiation is the power radiated per unit of solid angle in certain direction. The units are watts per steradian. This parameter is independent of the distance at which the transmitting antenna is located. The relationship between radiation intensity $K(\theta, \varphi)$ and radiated power density $P(\theta, \varphi)$ is:

$$K(\theta, \varphi) = P(\theta, \varphi)r^2 \quad (2.17)$$

The total radiated power can be calculated by integrating the radiation intensity in all directions of the space

$$W_r = \int \int K(\theta, \varphi)d\Omega W_r = \int \int K(\theta, \varphi)\sin\theta d\theta d\varphi \quad (2.18)$$

2.9.2 Directivity

The directivity is defined as the ratio of the radiation intensity of the antenna in a given direction and the radiation intensity from a source isotropic by the same amount of power:

$$D(\theta, \varphi) = \frac{U(\theta, \varphi)}{U_0} = \frac{4\pi U_0}{P_{rad}} \quad (2.19)$$

If not specified, the direction of maximum radiation intensity is implied:

$$D(\theta, \varphi) = \frac{U_{max}}{U_0} = \frac{4\pi U_{max}}{P_{rad}} \quad (2.20)$$

2.9.3 Gain

The gain of an antenna is defined as the ratio of power density radiated in one direction to the power density radiated by an isotropic antenna in the same direction. Both antennas are placed at the same distance and the with the same input power (P_{in}).

$$G(\theta, \varphi) = \frac{4\pi U_{max}}{P_{in}} \quad (2.21)$$

If the angular direction is not specified, it is understood that the gain refers to the direction of maximum radiation:

$$G = \frac{4\pi U_{max}}{P_{in}} \quad (2.22)$$

The gain is related to directivity by the efficiency η . The relation is given in 2.23.

$$G(\theta, \varphi) = D(\theta, \varphi)\eta \quad (2.23)$$

Efficiency can be defined as the ratio of the power radiated by an antenna and the power delivered to it. The efficiency is a number between 0 and 1. If an antenna has no ohmic losses and no dielectric losses, directivity and gain are equal.

2.10 Polarization

The polarization of an antenna is the polarization of the wave radiated by the antenna in a given direction. The polarization of a wave is determined by the geometrical shape of the end vector representing the changes of the electric field depending on the time, in a given position. For waves with sinusoidal variation that figure is generally an ellipse.

Linear polarization occurs when the phase of two orthogonal components of the electric field equals an integer multiple of π radians. Circular polarization occurs when the amplitudes are equal and the phase difference between the components is $\frac{\pi}{2}$ or $\frac{3\pi}{2}$, in this case the figure traced by the electric field is a circle. The polarization is elliptical in other cases. This three polarizations can be seen in the Figure 2.9.

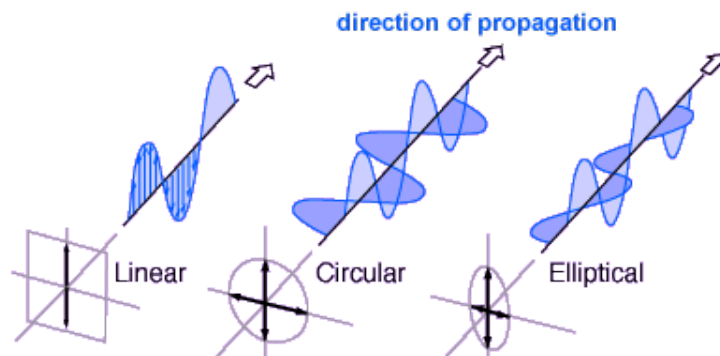


Figure 2.9: Linear, Circular and Elliptical polarization [42]

2.11 Bandwidth

All antennas are limited to operate properly within one or more frequency bands. The bandwidth (BW) is the frequency range in which the antenna parameters satisfy certain characteristics. The analytical expression of the bandwidth is:

$$BW = \frac{f_{max} - f_{min}}{f_0} \quad (2.24)$$

where f_{max} and f_{min} are the maximum and minimum frequencies respectively that limit the bandwidth and f_0 is the center frequency.

2.12 Microstrip Line Theory

Microstrip line is one of the most popular types of planar transmission lines. The main reasons why this transmission line is so popular is that it can be fabricated by photolithographic processes and it can easily be miniaturized and integrated with both passive and active microwave components. The design of a microstrip line (Fig.2.19a) consisting of a conductor of width W printed on a thin, grounded dielectric substrate of thickness h and relative permittivity ϵ_r .

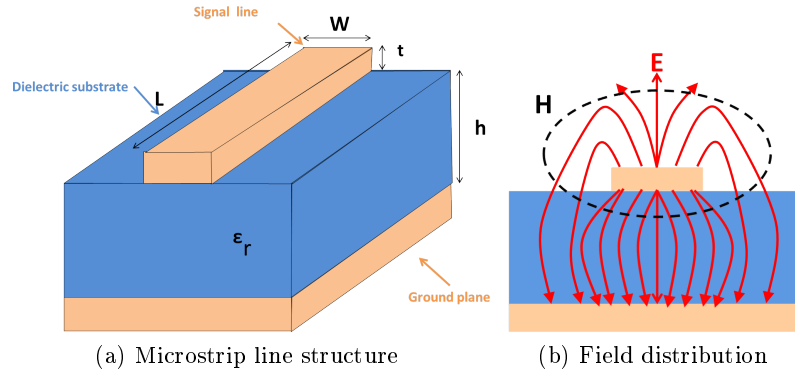


Figure 2.10: Geometry of a microstrip line

This type of transmission line is formed by two conductors, the signal line and the ground plane, separated from each other by a dielectric substrate. Besides the signal line is where all the fields are contained. Some fraction of these field lines are radiated in the air region above the microstrip line. This is the reason why microstrip lines do not conduct pure TEM modes. In most practical applications the dielectric substrate is electrically very thin ($h \ll \lambda$) thereby the fields that propagate are quasi-TEM.

The presence of two dielectrics (the substrate and the air) requires defining a new dielectric constant called effective dielectric constant. This constant is defined by the following formula:

$$\epsilon_{refec} = \begin{cases} \frac{\epsilon_r + 1}{2} + \frac{\epsilon_r - 1}{2} \cdot \left[\left(1 + 12 \frac{h}{W}\right)^{-0.5} + 0.004 \left(1 - \frac{W}{h}\right)^2 \right] & \text{when } \frac{W}{h} \leq 1 \\ \frac{\epsilon_r + 1}{2} + \frac{\epsilon_r - 1}{2} \cdot \left(1 + 12 \frac{h}{W}\right)^{-0.5} & \text{when } \frac{W}{h} > 1 \end{cases} \quad (2.25)$$

Using the above Formula 2.25 the wavelength is calculated as follows:

$$\lambda_{\mu strip} = \frac{\lambda_0}{\sqrt{\epsilon_{refec}}} \quad (2.26)$$

Further from ϵ_{refec} [Formula 2.25] you can get the characteristic impedance of the microstrip line. This characteristic impedance is defined by the Formula 2.27.

$$Z_{\mu strip} = \begin{cases} \frac{60}{\sqrt{\epsilon_{refec}}} \cdot \ln\left(\frac{8h}{W} + \frac{W}{4h}\right) & \text{when } \frac{W}{h} \leq 1 \\ \frac{120\pi}{\sqrt{\epsilon_{refec}} \left[\frac{W}{h} + 1.393 + 0.667 \cdot \ln\left(\frac{W}{h} + 1.444\right) \right]} & \text{when } \frac{W}{h} > 1 \end{cases} \quad (2.27)$$

2.13 Multiple Input Multiple Output (MIMO) antennas

The wireless communication has been very successful over the years in all environments, either in offices or domestic environments wireless local area networks provide high functionality with low cost.

However, the data rates achieved in the actual's wireless networks (WLANs) is still limited compared to wired LAN. After the 802.11a, the 802.11b standar and the widespread 802.11g standard appeared, whose rate is five times higher than the first standard, but its 54Mbps are still far from the 1000Mbps Gigabit Ethernet using wired networks. Furthermore the scope and performance offered by the WLANs standards are quite improvable.

The Multiple-Input Multiple-Output (MIMO) technology is developed to solve many of these problems in the near future, offering faster throughput, greater coverage distances, greater channel capacity and reliability, all without increasing the bandwidth and power transmitted. However MIMO technology is not only available for WLANs. It is the current trend of international research in wireless and many types of WPAN and WMAN networks. Moreover mobile communication systems are or will be equipped with this technology.

Figure 2.11 shows the evolution of the different standards according to their data transfer rate and the covert distance range. In this figure we can see the increase in data transfer rate of the different standards and how the different generations of communications are distinguished according to their standards.

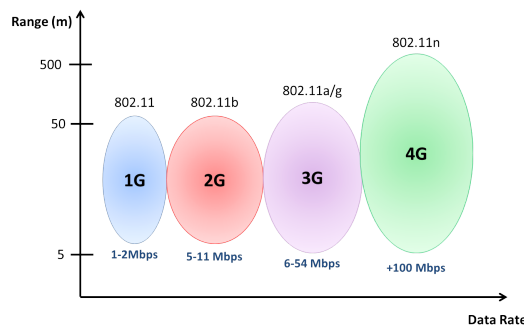


Figure 2.11: WLANs generations

2.13.1 Diversity in MIMO Systems

Diversity occurs when there are multiple copies of the transmitted signal, and depending on where this diversity occurs one can distinguish the following classes: time diversity, frequency diversity, space diversity, polarization diversity and users diversity.

The MIMO systems are focus on spatial diversity. The space diversity can be defined as the use of different propagation paths for transmitting or receiving the signal. In wireless communications the space diversity is achieved through the used of several antennas, this means that multiple antennas are used for transmission and/or reception indistinctly.

Depending on the number of antennas that are at both ends of the communication channel one can distinguish the following systems, which can be considered as starting points of the MIMO technology:

- **SISO (Single Input, Single Output):** communication system that utilizes a single transmitting antenna and a single receiving antenna.
- **MISO (Multiple Input, Single Output):** communication system that uses two or more transmitting antennas but only one receiving antenna. Also known as transmit diversity.
- **SIMO (Single Input, Multiple Output):** communication system that utilizes a single transmitting antenna and two or more receiving antennas. It is known as diversity reception.

According to this classification, MIMO is a communication system that uses two or more antennas at the transmitting end and two or more antennas at the receiver end. This means that it uses space diversity through the use of multiple antennas at transmit and receive sides.

The described systems can be diagrammatically represented as shown in figure 2.12.

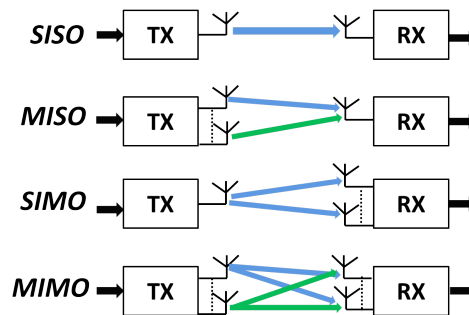


Figure 2.12: Comparison between SISO, SIMO, MISO and MIMO

2.13.2 Performance of MIMO

Multipath. Radio channel distortions

One can say that between a transmitter located at a point A and a receiver at point B there is a primary path, which we define as the most direct between the two points. Inevitably not all that transmit signals between these points follow this path. Signals suffer many reflections and/or refractions with various obstacles in their path, such as mountains, buildings or even the same layers of the atmosphere. Therefore, the transmitted signals take multiple different paths to reach the receiver. This is called multipath and is a feature presents in radio channels for all wireless communication systems.

The signals that go through these secondary paths reach the receiver delayed in time, then we say that we have an offset with respect to the primary signal. Depending on offset, constructive or destructive interference will occur causing sums or degradation of the original signal. The signal seen by the receiver, which is a linear combination of the multipath signals with the primary signal, will suffer interference that will cause the degradation of the final signal.

Besides multipath distortion, wireless channels may suffer the following distortions:

- ISI or Inter-Symbolic Interference: caused by multipath

- Fading: also caused by multipath propagation and scattering effects suffered by the signal
- CCI or Co-Channel Interference: caused when two stations broadcast at the same frequency in the same channel
- Time-varying channel (Doppler): when transmitting stations and/or receiver are moving
- Thermal noise: inherent in electronic devices themselves

All these distortions cause a significant reduction in data transmission rate and an increase in errors.

How MIMO systems work

The multipath propagation was considered a problem for the radio communications. However, during the 90s, several researchers from Stanford University and Bell Laboratories showed that could be exploited to multiply the capacity of wireless systems. This is the main idea of the performance of MIMO systems.

The basic structure of a MIMO system is shown in the Figure 2.13:

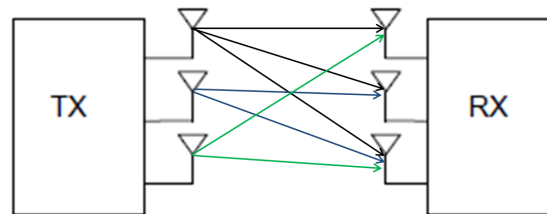


Figure 2.13: Basic structure of a MIMO system

In this system M_t transmit antennas and M_r receive antennas are used. Processing is performed in transmission and reception. This system takes advantage of $M_t \times M_r$ physical channels. These channels depend on the conditions of propagation and separation between the antennas. The greater the uncorrelation between those channels, the greater the system capacity is.

MIMO systems take advantage of multipath in the following way: each multipath route is treated as a different channel, creating a kind of virtual connections on which the signal is transmitted. By using multiple spatially separated antennas, these virtual connections can be leveraged to transmit more data, thereby the throughput will be multiplied. The maximum rate per channel will grow linearly with the number of different data substreams that are transmitted on the same channel. Furthermore, due to the diversity of antennas, it will also increase the distance covered.

Benefits of MIMO systems

MIMO technology improves the performance of any wireless communication system, multiplying its spectral efficiency. This results in the following benefits for our MIMO network or device:

- **Bit rate.** MIMO systems multiply the transmission rate without consuming more spectrum, allowing simultaneous transmission of multiple data frames. The throughput is increased as the number of parallel signals transmitted through the same radio channel at the same time

- **Spectral efficiency.** MIMO systems are the only systems that improve spectral efficiency by multiplying at least twice transmitted bits per Hz
- **Number of users.** the increase in capacity increases the number of users that may simultaneously connect to our network on the same frequency channel.
- **Coverage.** because of the diversity techniques, larger distances are achieved without increasing the transmission power. With a single access point one can provide coverage for a larger space region.
- **Reliability.** reliability increases as MIMO error probability is lower.
- **Cost.** A smaller number of devices are needed because a single access point can support more users, since improved with the same power scope, reducing the cost of our network.

Mathematical description of MIMO systems

To conclude this section, a MIMO system is characterized mathematically. One can represent the mathematical model of a MIMO system such as shown in 2.14. It is assumed that the channel is random and without memory.

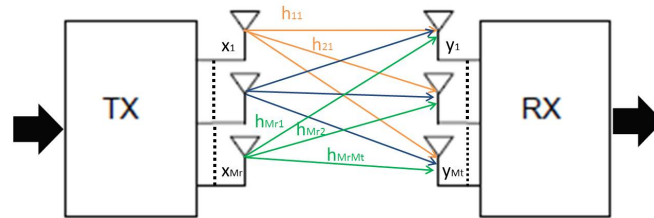


Figure 2.14: MIMO channel model

The input and output relation in an instant of time will be:

$$y(t) = Hx(t) + n(t) \quad (2.28)$$

Where:

- $x(t)$ is the transmitted data vector, with dimension $M_t \times 1$
- $y(t)$ is the received data vector and has dimension $M_r \times 1$
- $n(t)$ is the noise vector AWGN (Additive White Gaussian Noise), whose dimensions are $M_r \times 1$
- H is the MIMO channel matrix with dimension $M_r \times M_t$

Being M_t the number of transmit antennas and M_r the number of receiving antennas.

In this way we have a simple model with matrices of complex numbers (see equation 2.29):

$$[H] = \begin{bmatrix} h_{11} & h_{12} & \cdots & h_{1M_t} \\ h_{21} & h_{22} & \cdots & h_{2M_t} \\ \vdots & \ddots & \ddots & \vdots \\ h_{M_r 1} & h_{M_r 2} & \cdots & h_{M_r M_t} \end{bmatrix} \quad (2.29)$$

Each term of the matrix represents a different signal path, affected by the transmit antennas and receive antennas and the propagation.

MIMO channel capacity

The MIMO systems have an associated capacity which marks the theoretical limit of the system. This capacity is the maximum bit rate that can be transmitted over the channel with an error probability lower than the given threshold. The use of multiple antennas increase the total channel capacity compared to a single antenna case. Higher bit rates with arbitrarily small error probabilities can be achieved using the same bandwidth.

The MIMO channel capacity is defined by the formula 2.30

$$C_{MIMO}[bps] = E \left[\log_2 \left(\det \left| I + \frac{1}{\sigma^2} H Q H^* \right| \right) \right] \quad (2.30)$$

Where:

- H is the MIMO channel matrix with dimension $M_t \times M_r$
- Q is the is the covariance matrix of the transmission vector $x(t)$
- σ is the noise power at the receiver input

2.14 The Theory of Characteristic Modes

The characteristic modes are real current modes that can be computed numerically for conducting bodies of an arbitrary shape. The characteristic modes make a modal analysis of conducting objects possible. In addition, base on the theory of the characteristic modes the current distribution can be studied. Therefore the use of characteristic modes is helpful antenna design, because the radiation pattern of the antenna can be interpreted.

This is because they provide a physical interpretation of the radiation phenomena taking place on the antenna.

The Theory of Characteristic Modes was first developed by Garbacz [2] and was later refined by Harrington and Mautz in the seventies [3, 4]. It was originally applied to antenna-shape synthesis [5, 6] and to control of obstacle scattering by reactive loading [7]. It was also applied to the analysis of slots in conducting cylinders [8] or in perfectly conducting planes [9].

The characteristic modes do not depend on any kind of excitation, they only depend on the shape and size of the conducting object. Therefore the antenna design using characteristic modes can be performed in two steps. The first step is to optimize the size and shape of the radiating element. Changing the size of the element the resonance frequency of the mode will be modified. If apart of changing the size of element also the element shape is changed, not only the resonance frequency of the mode will be modified, also the radiating properties of the mode will change.

2.14.1 Mathematical Formulation of Characteristic Modes

From the mathematical formulation in [1, 2] the characteristic modes can be obtain as the eigenfunctions of the following particular weighted eigenvalue equation:

$$X \left(\vec{J}_n \right) = \lambda_n R \left(\vec{J}_n \right) \quad (2.31)$$

where the λ_n are the eigenvalues, the \vec{J}_n are the eigenvectors, and R and X are the real and imaginary part of the impedance operator respectively. Where the impedance operator is defined as:

$$Z = R + jX \quad (2.32)$$

Moreover, all eigenvalues λ_n and all eigenvectors \vec{J}_n can be chosen real. The magnitude of the eigenvalues λ_n gives information about how well the associated mode radiates.

In this project the used conducting object has a rectangular shape, so from now the explanation of the characteristic modes will focus on a rectangular plate. The surface current density distribution on a rectangular plate can be expressed as a linear superposition of the characteristic modes:

$$J = \sum_n a_n J_n = \sum_n \frac{V_n^i J_n}{1 + j\lambda_n} \quad (2.33)$$

The term V_n^i in the equation 2.33 is called the modal-excitation coefficient and it is defined as:

$$V_n^i = \langle J_n, E^i \rangle = \oint_n J_n \bullet E^i ds \quad (2.34)$$

The modal-excitation coefficient accounts for the way the position, magnitude and phase of the applied excitation influence the contribution of each mode to the total current, J . Thereby the product $V_n^i J_n$ in the equation 2.33 models the coupling between the excitation and the n^{th} mode. This product also determines if a particular mode is excited by the antenna feed or by the incident field.

The Figure 2.15 illustrate an schematic of the current distribution for six eigenvectors of a rectangular plate. As can be seen in this, the eigenvector J_0 has a special inductive behavior, as its currents flow in concentric loops on the plate. The eigenvector J_1 and J_2 are characterized by horizontal and vertical currents, respectively. Finally the eigenvector J_3 , J_4 and J_5 are high-order modes that might be taken into consideration only at the highest frequencies.

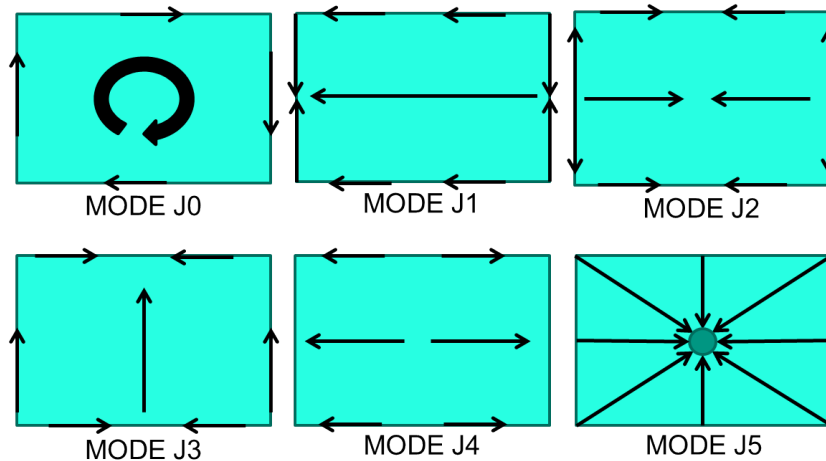


Figure 2.15: Current vectors for six eigenvector in a rectangular plate

Taking into account that the resonance frequency of the characteristic mode occurs when its associated eigenvalue is zero ($|\lambda_n = 0|$), it can ensure that the lower is the magnitude of the

eigenvalue, the more efficiently the characteristic mode will be excited. In addition, the sign of the eigenvalue determines which of the fields, electric or magnetic, contributes more to the characteristic mode. If the sign of the eigenvalue is positive ($\lambda_n > 0$), the mode contributes to store magnetic energy. In contrast if the sign of the eigenvalue is negative ($\lambda_n < 0$), the mode contributes to store electric energy.

The Figure 2.16 shows the variation of the eigenvalues for the six current modes of the rectangular plate presented in the Figure 2.15. In the Figure 2.16 it can be observed that all the eigenvalues start being negative, they resonate ($\lambda_n = 0$) and finally they keep a small constant positive value.

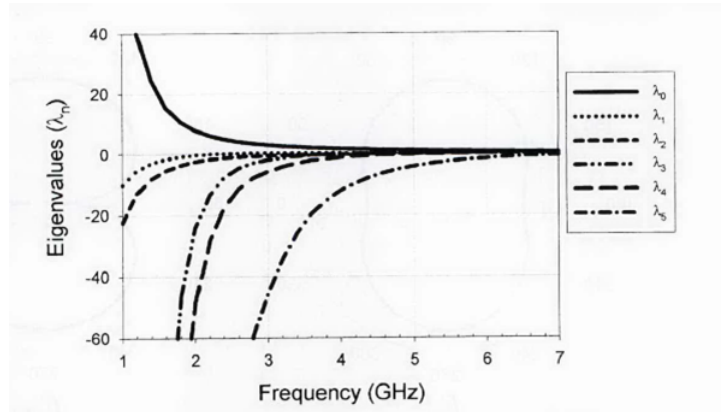


Figure 2.16: Variation of the eigenvalues with frequency [1]

2.15 Overview on possible automotive antenna technologies

In this section, a short overview about the most popular antenna technologies used in cars is given. To find the ideal location for an antenna on a car, the service, the frequency band and selected antenna technology must be considered.

2.15.1 Monopoles

Monopole antennas are the most popular antenna type, as they are very easy to manufacture, easy to implement and very cheap. A monopole antenna consists of a rod of around $\lambda/4$ length supported in a plastic platform. To install the antenna on the roof of the car it is only necessary to make a hole in the metallic structure of the car in order to connect the feeding cable of the antenna.

Monopoles provide a broad range of applications in every frequency band, from VHF sound broadcasting up to Car-2-Car communication at 5.9 GHz. The monopole can be placed on the roof center, on an edge of the roof or on the frame, or even on a bumper or fender. The monopole antenna requires a direct connection to ground, meaning the metallic structure of the vehicle. The monopole will not work efficiently when the metallic ground is small in comparison to the wavelength λ . However, aesthetically speaking, the current trend of designers is to avoid the use of monopoles antennas, especially in premium cars. An example of this monopoles antennas are mast antennas, this type of antenna is described in detail in the next subsections.

Mast antennas

The low frequency and relatively high signal strengths encountered in AM and FM car radio systems have allowed the use of uncomplicated antenna systems in the past. The most common antenna traditionally used for these bands is the mast antenna. The mast antenna consists of a conductive rod used to form a monopole antenna. This conductive rod has a length of approximately one quarter wavelength ($\lambda/4$), which equates to approximately 75 cm in the middle of the FM band [43]. Moreover an amplifier is used to boost the signal level to compensate for the poor performance obtained by the antenna length. Locating such an antenna in the backside of the roof (Fig.2.17) gives the best radiation performance, with the antenna elevated above obstructions and surrounded by a conducting ground plane of approximately equal extent in all directions. Despite this, the front or rear fender is usually preferred for aesthetic reasons.



Figure 2.17: Mast antenna [43]

2.15.2 Blade or Shark-fin antennas

Nowadays shark-fin antennas have become very popular in premium cars, thus there are many varieties of this type of antenna. Shark-fin antennas are commonly a collection of several antennas. Most designs consist of multiple narrowband antennas all located together under a single housing. This housing is shaped like a blade or dorsal fin, and is usually located on the roof towards the rear of the vehicle. An examples of shark-fin designs is shown in the Figure 2.18.

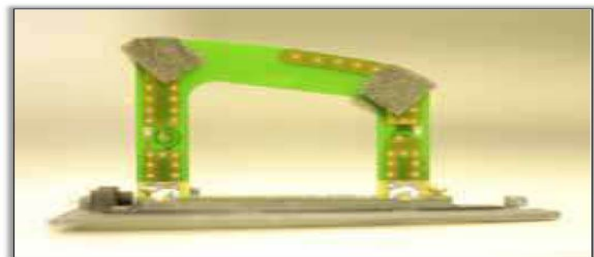


Figure 2.18: Blade or Shark-fin antenna[43]

The Figure 2.19 shows an early shark-fin antenna design for the BMW 3-Series (E46) for cellular phone frequencies. The antenna consists of a cast steel base and a fin-shaped cover made from an ABS and Polycarbonate polymer. Radiating elements are on both sides of an FR-4 circuit board which stands erect in the middle of the device. Rubber gaskets are used to seal the inner components from the environment [43].



(a) Shark-fin on vehicle roof



(b) Shark-fin with radome removed showing filters

Figure 2.19: BMW 3-Series E46 Sharkfin Antenna [43]

2.15.3 On-glass antenna

This antenna type became popular in premium cars industry in the 1980, when design issues became increasingly important. With this technique the antenna structure can be hidden from the user's eyes.

The on-glass antenna technique follows a loop antenna principle. In this way the metallic car structure becomes part of the antenna and the glass is used as the slot in the metal structure. The coupling of the slot with a thin conductor, the slot resonates and can be used as an antenna. The design of this system can take a lot of time as it depends on the characteristics of the glass, its shape and its position with respect to the metal of the car. So changing the shape of the car will change the on-glass antenna characteristics. An example of the use of this technology are the on-glass antennas, described in the next subsection.

TV antennas on glass

In the Figure 2.20 an analogue TV antenna system in rear quarter glass is shown. In this TV antennas on glass system the antennas are printed on the rear quarter glass and have four branches. The antennas are arranged symmetrically on the left and right sides of the vehicle. The design includes some meandering elements which give a long electrical length in a small space. Other branches of the design include slanted and short horizontal elements. this system provides improved performance over a rod antenna, and is capable of operating in the range from 90 MHz to 770 MHz.

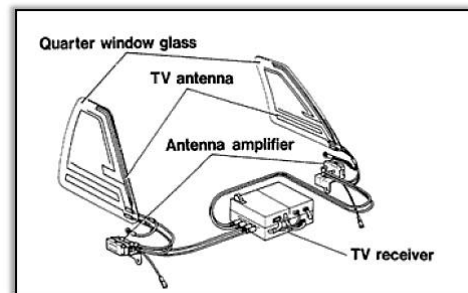


Figure 2.20: TV antennas on glass[24]

2.15.4 Body integrated spiral antenna

Fortbildungszentrum für Technik und Umwelt (FTU) researchers investigated the possibility of mounting a cavity-backed spiral antenna in the trunk lid of a car [25]. The four arm spiral antenna produced is approximately 40 cm in diameter and is backed by a metallic cavity (Figure 2.21).

The spiral supports two modes of radiation depending on how the signal is fed into the structure. The first mode is a coplanar waveguide (CPW) mode which creates a null at zenith (ie. directly above the antenna) with omni-directional radiation around the sides of the device. This mode generates a radiation pattern that is suitable for terrestrial services. The second mode, known as the coupled slot line (CSL) mode feeds only two of the four arms, creating a circularly polarised radiator with a maximum at zenith (directly overhead).

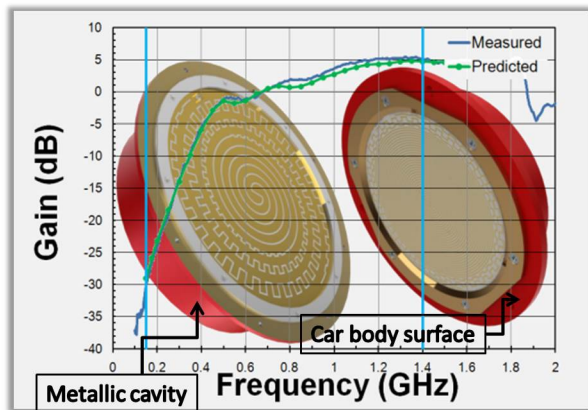


Figure 2.21: Body integrated spiral antenna [44]

2.15.5 Patch antenna

A patch antenna is a flattened monopole. The Figure 2.22 shows the principal structure of a patch antenna. A metallic plate of about half wavelength is placed over a metallic ground plane, which are separated either by air or a low loss dielectric material. The RF is ideally fed directly to the radiating patch.

This antenna technology is getting more and more popular in the automotive industry. At first this type of antenna can be used for a large number of applications, from high frequency applications such as GPS reception at 1.5 GHz or SDARS satellite broadcasting radio reception at 2.3 GHz up to WLAN and Car-2-Car Communication at 5/6 GHz. However nowadays this technology can be seen in telephone antennas for GSM and CDMA at 800/900 MHz.

As a patch antenna is completely flat it can be installed anywhere in the vehicle such as, e.g. behind a fender or bumper or in a plastic trunk cover. Patch antennas require a large metallic ground structure, preferably flat of minimum λ around the antenna. If the car cannot fulfill this requirement at the position with its surrounding metallic structure, then the patch antenna shall provide its own ground plane in the antenna structure.

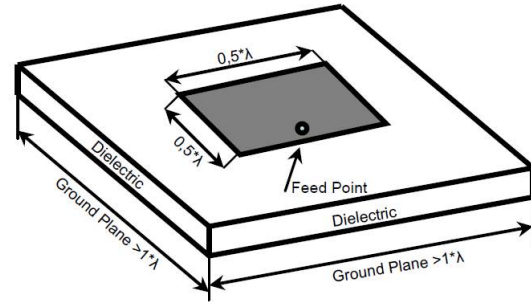


Figure 2.22: Principal structure of a squared patch antenna[23]

2.16 Antenna technology used in this project

The antenna technology used in this project is based on the excitation of bodywork elements. Using coupling structures, surface currents are generated in the bodywork elements. To feed these coupling structures, a feeding network using microstrip lines will be designed. This antenna technology covers a bandwidth impossible to be covered for some of the antennas technology described in the previous section. The main advantage of this technology is to be able to cover the Long Term Evolution (LTE) standard bandwidth, in this way the antennas system implemented in this project will achieve high speed data rates.

Moreover this antenna technology can be used in several applications such as mobile satellite communications systems, direct broadcast television (DBS), wireless LAN'S and GPS systems.

Furthermore the small size of this antenna, makes this system a perfect system aesthetically speaking, as it is almost invisible to the user. The easy design of this system makes it easy to be integrated in the car. Besides this antenna technology can be implemented in any shape. Hence this antenna technology can be manufactured in large quantities.

In the following chapters, the used of the characteristic modes to design a MIMO antenna system placed in a vehicle is studied. First the characteristic modes will be study performing some prototypes circuits. Then the characteristic modes will be apply to design a MIMO antenna system. And finally the behavior of the MIMO system in the vehicle will be study.

3

Feeding Network for Inductive Coupling Elements

3.1 Introduction

This chapter will explain the design of three circuits used for feeding the MIMO system. The basic concepts of each element of the multi-port systems are schematized in the Figure 3.1. These circuits are composed of matching networks, phase shifters and Inductive and Coupling Elements (ICE).

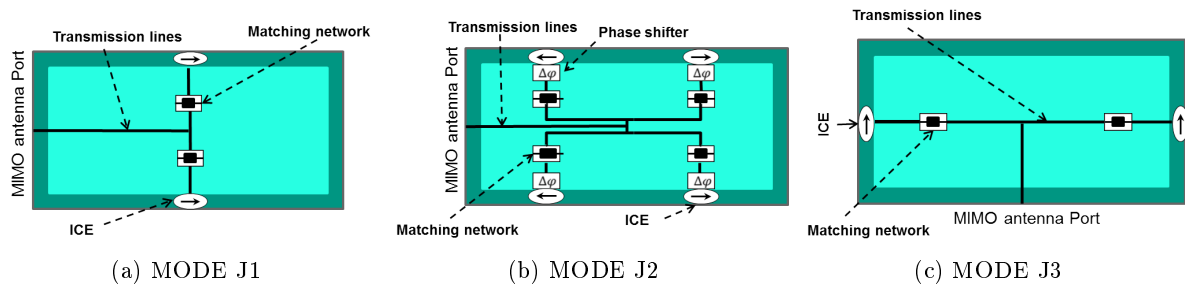


Figure 3.1: Feeding network schema

The presented circuits are designed and fabricated in microstrip line technology, for this reason they are suitable for mass production. The specifications of the microstrip line used are shown in Figure 3.2. The material used for the design of this microstrip line is ROGERS RO4003. ROGERS RO4003 is a glass reinforced hydrocarbon/ceramic laminate. This material fulfills the following features:

- Not-PTFE
- Excellent high frequency performance due to low dielectric tolerance and loss
- Stable electrical properties versus frequency
- Low thermal coefficient of dielectric constant
- Low Z-Axis expansion

- Low in-plane expansion coefficient
- Excellent dimensional stability

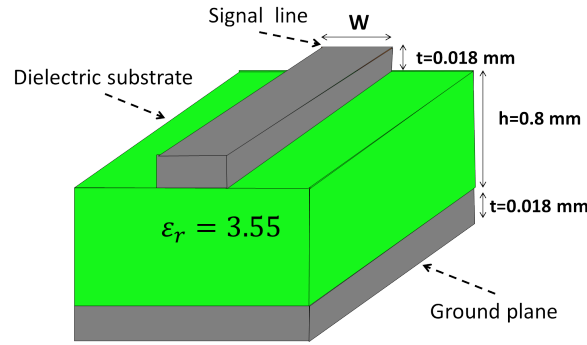


Figure 3.2: Microstrip line of the feeding network

3.2 Characteristic Modes of a rectangular metallic plate

This project is based on the study of different characteristic modes of a rectangular metallic plate. The dimensions of the studied metallic plate are: length= $\lambda = 120$ mm and width= $\lambda/2 = 60$ mm.

The theory of the characteristic modes in a rectangular metallic plate is explained in the section 2.14. This section describes how each of the characteristic modes can be excited most efficiently near its resonant frequency ($f_{res,n}$). The resonant frequency occurs when $|\lambda_n = 0|$. The Figure 3.3 shows the values of the first five characteristic modes J_n with horizontal and vertical currents and the first two characteristic modes J_{0n} which represent current loops on the metallic plate.

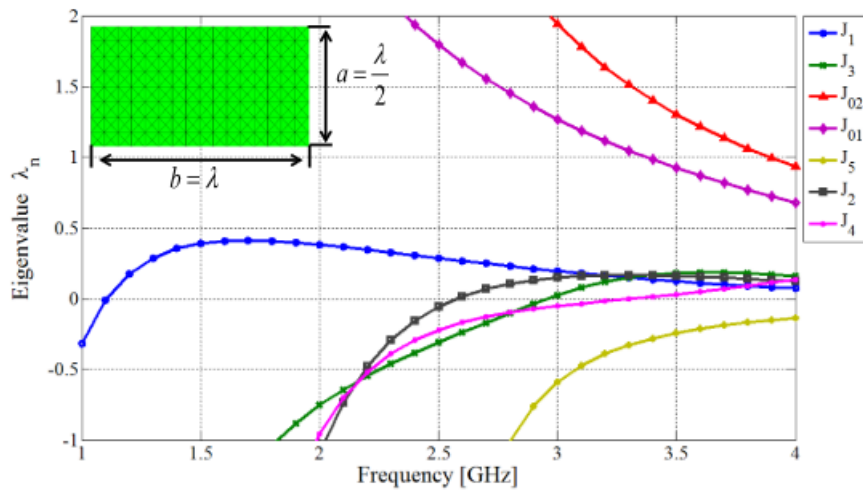


Figure 3.3: Eigenvalues as a function of frequency for the characteristic modes of the investigated metallic plate in free space [14]

The aim of this project is to design an antenna system operating from 2.5 GHz to 2.7 GHz (LTE frequency band), in order to achieve high data rates. As it can be seen in Figure 3.3, the characteristic modes J_1 , J_2 and J_3 are resonant in the desired frequency range ($2.5 \leq f[GHz] \leq 2.7$).

Figure 3.4 illustrates the current distribution at the first resonance for the three eigenmodes of the studied rectangular metallic plate. As can be seen in this figure, the eigenvectors J_1 and J_3 which are characterized by horizontal and vertical currents, respectively, present current distribution of a half wavelength along the major and the minor axes of the metallic plate. Moreover the eigenvector J_2 presents a current distribution of one wavelength along the major axes.

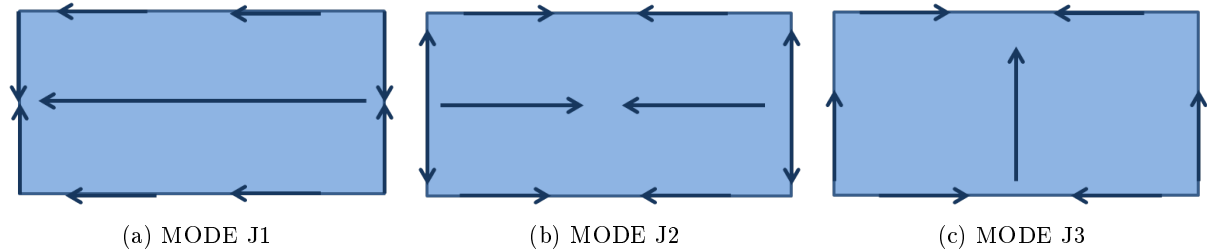


Figure 3.4: Current distribution schematics for the first three characteristic modes

3.3 Selective excitation of Characteristic Modes by different set of Inductive Coupling Elements (ICEs)

The current distributions of the characteristic modes are mainly characterized by a sinusoidal behavior at the edges of the metallic plate. The Figure 3.5 illustrates this sinusoidal behavior for the first three characteristic modes. The points at which the amplitude of current is maximum and minimum for each of the three selected characteristic modes can be seen in this figure.

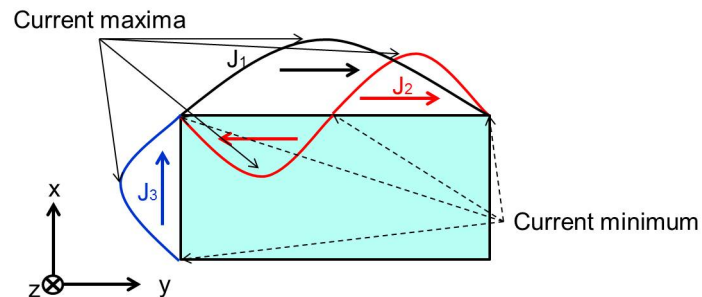


Figure 3.5: Sinusoidal behavior of the current distribution on the metallic plate [12],[14]

For the first mode (J_1), the current magnitude is minimal at the ends of the major axis of the metallic plate and maximal in the center of the major axis of the metallic plate.

Whereas, for second mode (J_2), the current magnitude is minimal at the ends and in the center of the major axis of the metallic plate and maximal at the quarter length and two quarter length of the major axis of the metallic plate.

Finally, for the third mode (J_3), the current magnitude is minimal at the ends of the minor axis of the metallic plate and maximal in the center of the minor axis of the metallic plate.

Besides of the current distribution, the electric field and the current distribution will have a phase difference of 90° . I.e, the electric field will be minimum when the current maximal and vice versa.

Based on these observation, the optimal Inductive Coupling Elements (ICEs) position inside of the metallic plate at maximum current is chosen. Taking advantage of these changes in the current distribution, the Inductive Coupling Elements (ICEs) will be placed. The location of the ICEs, for a metallic plate with dimensions $\lambda \times \lambda/2$, can be seen in the Figure 3.6.

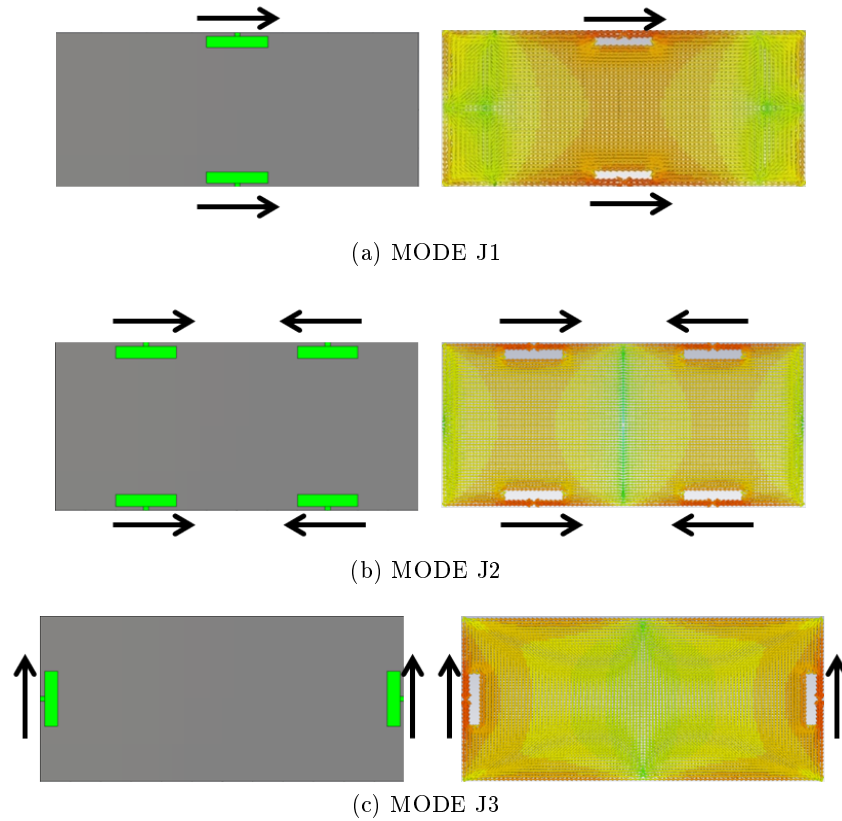


Figure 3.6: Concept for the selective excitation of the first three characteristic modes on a metallic plate by different sets of ICEs [12],[14]

3.3.1 Single Inductive Coupling Element (ICE)

The Inductive Coupling Element (ICE) structure used in this project is based on the previous designs proposed in [12] and [14]. The Figure 3.7 presents in detail the Inductive Coupling Element (ICE) embedded at the edge of the rectangular metallic plate. In this figure, the width of the coplanar coupling element is $r=1.43$ mm, the length of the arm is $l_c=20$ mm and the width of the arm is $s=4.3$ mm. The direction of the current excited by the embedded Inductive Coupling Element (ICE) is schematized in the Figure 3.7.

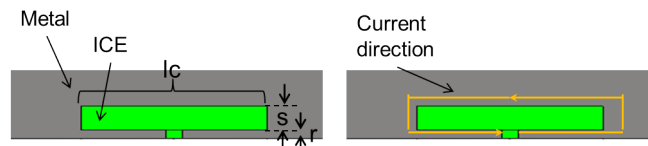


Figure 3.7: Inductive Coupling Element at the edge of the metallic plate [12],[14]

The closeness of the arm to the boundary of the metallic plate ($r=1.43$ mm) will almost cancel the fields at far distances. However the current distribution of the specific characteristic mode will spread wider on the metallic plate. In this way the excited current will generate the

modal distribution on the metallic plate. This small excited current will contribute to fields at far distance. Furthermore, the current distribution on both sides of the arm has to be identical. Thus the loop has to be electrically small, i.e. $l_c \ll \lambda$ [12, 14].

The Figure 3.8 shows the same current distribution as in the Figure 3.7. This current distribution had been simulated with the CST program. In the Figure 3.8 the direction of the current distribution around the ICE at the edge of the metallic plate can be seen.

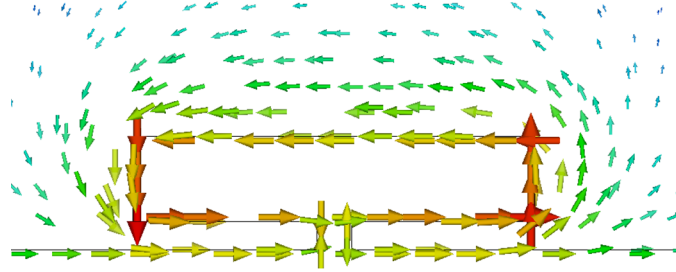


Figure 3.8: Current distribution of the Inductive Coupling Element at the edge of the metallic plate

3.4 Feeding network using microstrip line technology

After designing the Inductive Coupling Elements (ICEs) it is necessary to create the feeding network for each characteristic mode. This feeding network is located in the back side (reverse side) of the metallic plate, separated from the metallic plate by the dielectric material. The final structures of these feeding networks are shown in the Figure 3.9. In this figure the three circuits for each of the three characteristic modes can be seen. In addition in this figure the location of the ICE elements is sketched for a better visualization and a better comprehension of the circuit. In the Figure 3.10 the current distribution of each circuit from the Figure 3.9 can be seen. In the Figure 3.10 the current direction is represented by a yellow arrow.

These three circuits are composed of T-junctions, matching circuits and transmission lines. Apart from the mentioned structures a taper has been included in the design of the second circuit. As the second circuit includes all the different elements of the feeding network, the explanation of the different feeding network elements will be based on the second circuit. In the following subsections the design and implementation of the different feeding network elements are described.

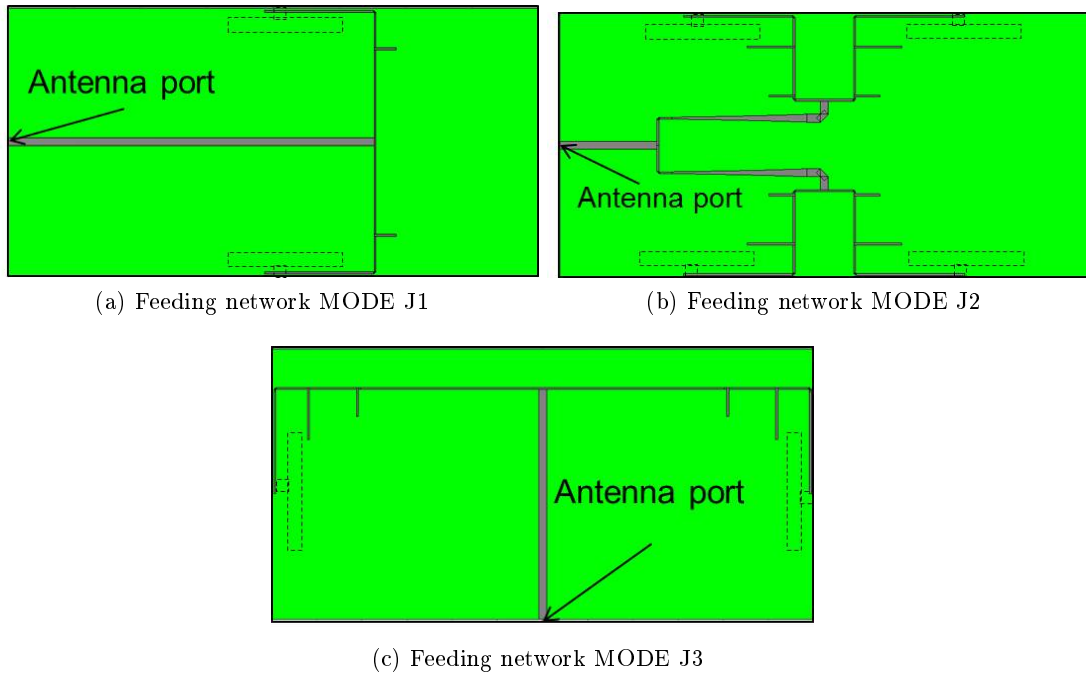


Figure 3.9: Feeding network: circuits structure

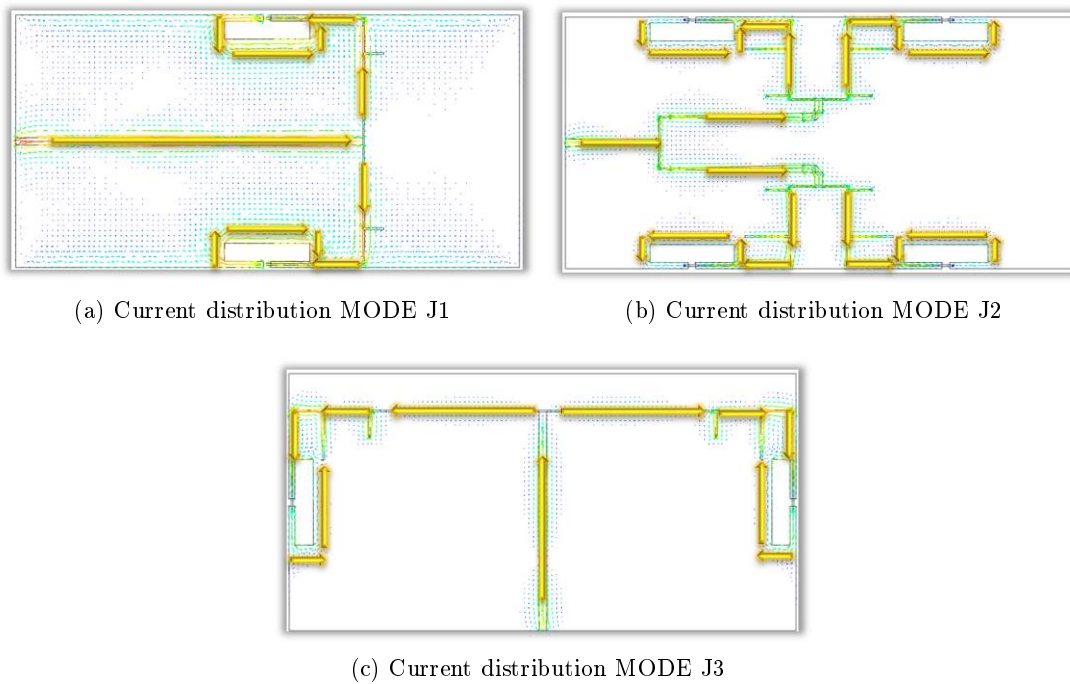


Figure 3.10: Feeding network: current distribution

3.4.1 Inductive Coupling Element (ICE) ports

The first step in the design of the feeding network is to design an ICE port. This port is located in the back side of the metallic plate, as shown in Figure 3.11. This port is connected to the top metal layer through a VIA as it is shown in the Figure 3.15b. As can be seen in Figure 3.15a, to connect the port with the VIA a slot line had been used. Between the slot line and the port there is a bend, these bend induces an opposite phase in the circuit. This opposite phase

induced in the Inductive Coupling Elements is obtained by feeding them from the opposite side (one from the left side and the other from the right). Thanks to this opposite phase it is not necessary to implement a phase shifter component for the second mode circuit. The length of the slot line is $l_s=24.8$ mm and the input impedance of this port is set to $100\ \Omega$.

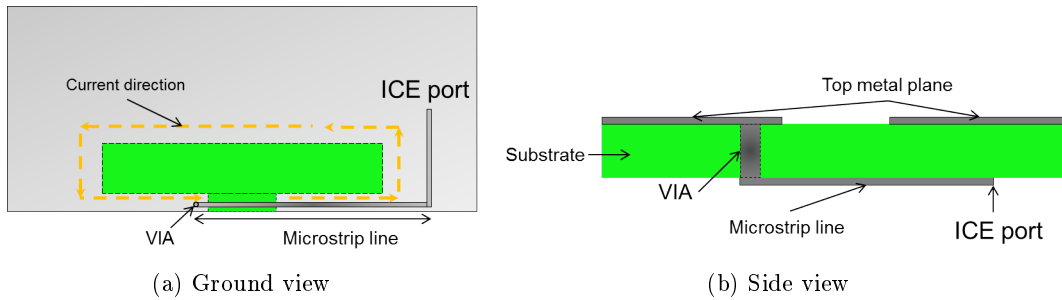


Figure 3.11: Inductive Coupling Element port

3.4.2 Matching circuits

The next step in the realization of the feeding network is to design the impedance matching circuits. The selected center frequency for this design is 2.6 GHz. These impedance matching circuits are composed of double-stubs in parallel as is shown in the Figure 3.12. For the design of these impedance matching circuits the methods of Richard's transformation and Kuroda identities were studied. However, these methods were discarded because its realization as a real circuit was impossible. For this reason, to calculate the length of the stubs the double-stub tuning method was used [11]. Varying the length of this stubs the impedance matching of the ICE-antenna can be achieved.

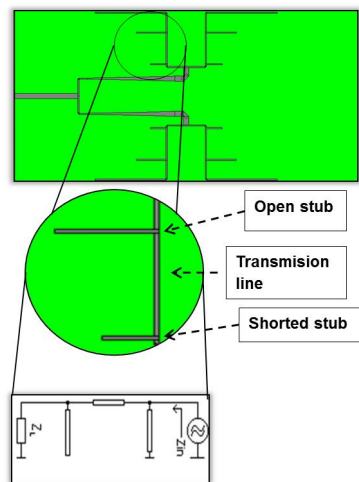


Figure 3.12: Matching circuit using double-stub tuning

The Figure 3.13 shows the smith chart used for the design of the impedance matching circuit. The starting point of the impedance matching circuit design is the impedance Z_L , which is the value of the impedance measured at the end of the ICE port. As the stubs are in parallel it is necessary to work with admittances in the smith chart. The load admittance is $Y_L = \frac{1}{Z_L}$. An open stub is added to the matching circuit in order to compensate the imaginary part of the admittance Y_L , thus getting to the admittance Y_A . The admittance Y_A has only real part, but the value of Y_A is smaller than $100\ \Omega$, so the matching point is not reached yet. To continue with the matching circuit design a transmission line is added, getting to the admittance

Y_B . The value of the Y_B is $100 - j(\text{ImaginaryValue})\Omega$. Therefore the last step would be to eliminate this *ImaginaryValue*. For this purpose it is required to add a shorted stub in parallel. After adding this last stub we have reached the matching impedance point where $Z_{IN} = 100\Omega$.

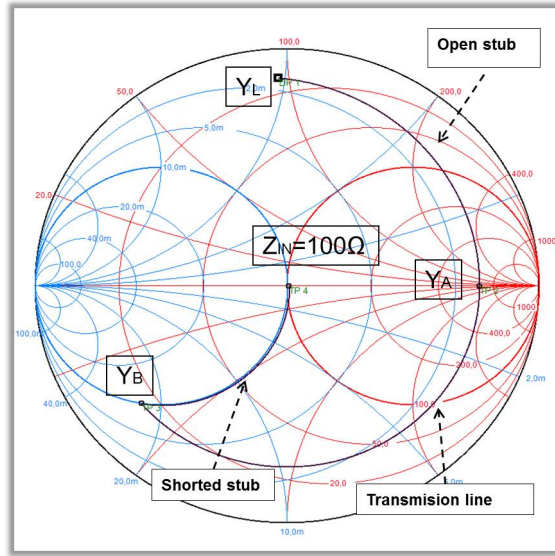


Figure 3.13: Matching circuit using the Smith Chart

The Figure 3.14 shows a schema of the matching impedance circuit, clarifying the location of the impedances Z_A and Z_B in the circuit. Also following an example of the design of the matching network is introduced.

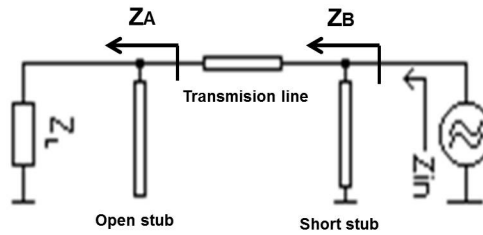


Figure 3.14: Matching impedance circuit

Example: double-stub tuning

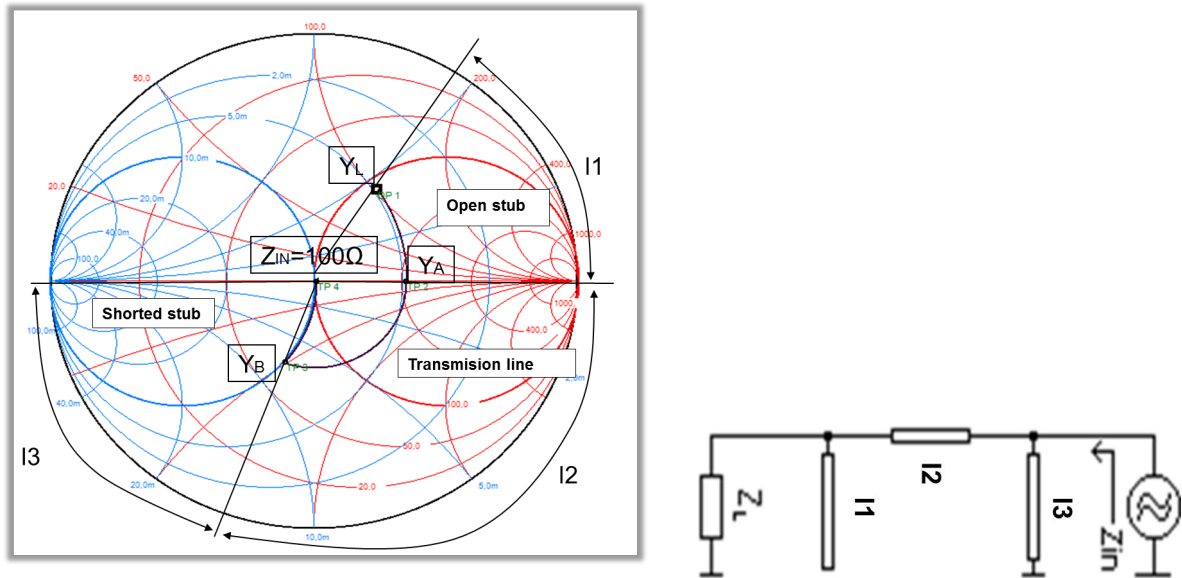
The goal of this example is to clarify how a matching circuit is designed. In this example the load impedance $Z_L = 111.68 + j103.23\Omega$ wants to be matched to $Z_0 = 100\Omega$. The normalized load impedance is $Z_L = 1.1168 + j1.0323\Omega$. From now on all the values will be normalized. As the stubs are in parallel it is necessary to work with admittances in the smith chart. The load normalized admittance is $Y_L = \frac{1}{Z_L} = 0.48 - j0.448\Omega$.

An open stub is added to compensate the imaginary part of the admittance Y_L , thus getting the normalized admittance $Y_A = 0.48\Omega$. The admittance Y_A has only real part, but this value is smaller than normalized characteristic admittance $Y_0 = 1\Omega$ so the matching point is not reached yet.

To continue the circuit design a transmission line is added, getting to the normalized admittance $Y_B = 1 - j0.756\Omega$. Therefore the last step would be to eliminate this the imaginary

part of Y_B . For this purpose it is necessary to add a shorted stub. After adding this last stub we have reached the matching impedance point, where the denormalized impedance is $Z_{IN} = 100 \Omega$.

The Figure 3.14 shows the smith chart used for these example and a schema of the matching impedance circuit. In this figure the length of the stub is represented as $l1 = 0.0668\lambda = 4.09 \text{ mm}$, $l2 = 0.1515\lambda = 9.27 \text{ mm}$ and $l3 = 0.1489\lambda = 9.11 \text{ mm}$, for $\lambda = 61.23 \text{ mm}$.



(a) Smith chart diagram for the operation of double-stub tuner (b) Double-stub tuning circuit

Figure 3.15: Double-stub tuning example

Reflection coefficient

The reflection coefficient obtained after adding the matching circuits to the feeding network is shown in the Figure 3.16. It can be seen that using matching circuits the matching of the circuit is achieved. The only drawback of using matching circuits is that the operational bandwidth of the antenna is narrow in the case of the characteristic modes J_2 and J_3 .

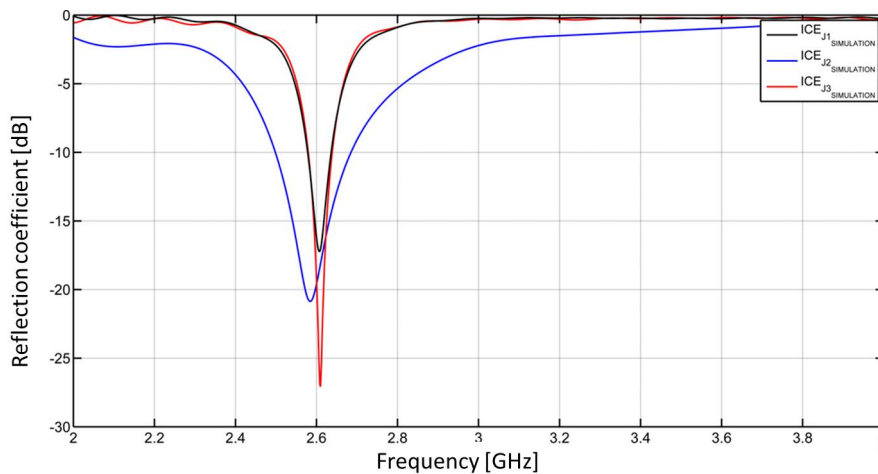


Figure 3.16: Reflection coefficient of the matched ICE_{J1} , ICE_{J2} and ICE_{J3}

3.4.3 T-Junction

The next step in the design of feeding network is to connect the branches of the matching circuits. For this purpose T-Junction structures have been used. Figure 3.17 visualizes the appearance of the T-junction element.

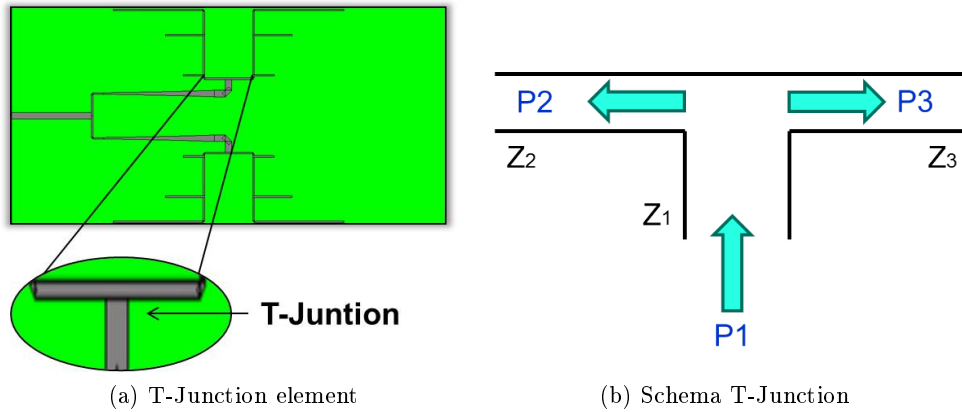


Figure 3.17: T-junction

The use of this circuit allows us to obtain the desired impedance value (50Ω) at the ICE port. The value of this impedance may be calculated using the formula 3.1.

$$Z_1 = \frac{Z_2 * Z_3}{Z_2 + Z_3} = \frac{100\Omega * 100\Omega}{100\Omega + 100\Omega} = 50\Omega \quad (3.1)$$

In 3.17b, P_1 is the value of the power fed to the T-junction and P_2 and P_3 are the values of power distributed to each of the circuit branches. By proper design of the T-junction, the same amount of power fed can be obtained for both circuit branches as shown by formulas 3.2, 3.3 and 3.4.

$$P_2 = P_1 \left(\frac{Z_1}{Z_2} \right) \quad (3.2)$$

$$P_3 = P_1 \left(\frac{Z_1}{Z_3} \right) \quad (3.3)$$

$$P_3 = P_2 \quad (3.4)$$

3.4.4 Taper

To continue with the circuit design it is essential to use a taper structure for the second circuit. Another possibility is to use $\lambda/4$ transmission line. The width of the $\lambda/4$ transmission line is greater than the current width of the microstrip line, this discontinuity causes a small reflection. To avoid this small reflection it has been decided to use a tapered structure.

Triangular taper, Klopfenstein taper and exponential taper were studied. Due to its length, the exponential taper was selected for the design of this circuit. In the Figure 3.18 the structure of the exponential taper can be seen.

The initial impedance of one of the ports is 50Ω and using the exponential taper this impedance is transformed to 100Ω of the other port. The formula 3.6 and the Figure 3.19 show the variation of impedance for the exponential taper.

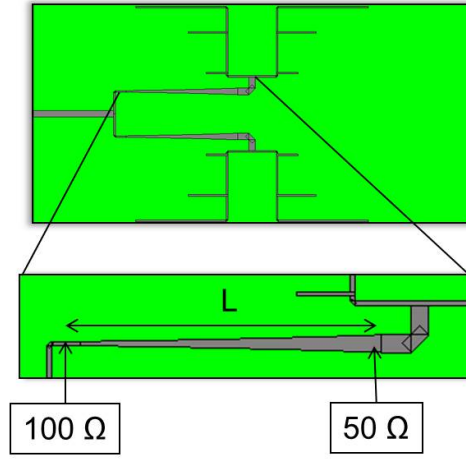


Figure 3.18: Tapered element

$$Z(z) = \exp(az) \quad \text{for } 0 < z < L \quad (3.5)$$

$$\text{where } a = \frac{1}{L} \ln\left(\frac{Z_L}{Z_0}\right) \quad (3.6)$$

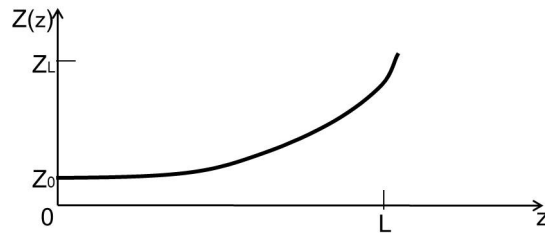


Figure 3.19: Variation of the impedance for an Exponential taper [11]

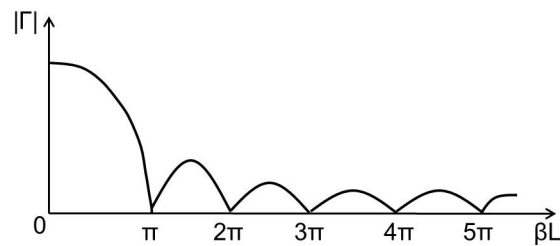


Figure 3.20: Reflection coefficient of an Exponential taper [11]

For the equation 3.6, the variable L represents the value of the length of the exponential taper. The value of this variable has been calculated using the Figure 3.20. From this, it can be seen that the first null value of the reflection coefficient occurs when $\beta L = \pi$, therefore the calculated value of the taper length is:

$$L = \frac{\pi}{\beta} = \frac{\pi}{\frac{2\pi}{\lambda}} = \frac{\lambda}{2} = 30.6195 \text{ mm} \quad (3.7)$$

3.4.5 Directivity Pattern

In this section the radiation pattern for each characteristic mode are described. The radiation pattern of the characteristic modes changes depending on the elevation (θ) and azimuth (ψ) axis.

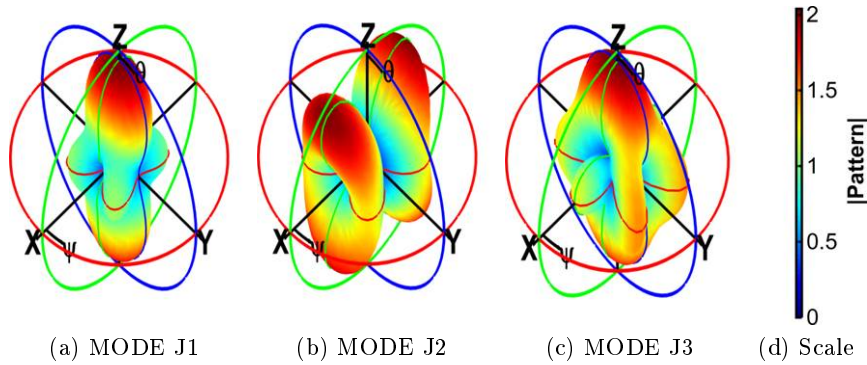


Figure 3.21: Antenna’s radiation pattern for three modes in 3D representation

For the first mode, the directivity is minimum at $\theta = 0^\circ$ when $\psi = 0^\circ$ and $\psi = 180^\circ$ (see Figure 3.22a). The radiation of the first mode becomes maximum broadside to the antenna, that is when $\psi = 0^\circ$ and $\theta = 90^\circ$ and $\theta = 180^\circ$ (see Figure 3.22a). Furthermore, for the second mode the directivity is minimum at $\theta = 0^\circ$ when $\psi = 0^\circ$. The radiation of the second mode becomes maximum broadside to the antenna, when $\theta = 45^\circ$ and $\psi = 45^\circ$ (see Figure 3.22b). Finally, for the third mode, the directivity is minimum at $\theta = 90^\circ$ when $\psi = 90^\circ$. The radiation pattern of the third mode becomes maximum broadside to the antenna, that is when $\theta = 0^\circ$ and $\psi = 0^\circ$ (see Figure 3.22c).

The Figure 3.22 represents the same radiation patterns as shown in the Figure 3.21. The Figure 3.22 is a flat representation of the radiation patterns, allowing a better visualization of the above explanations.

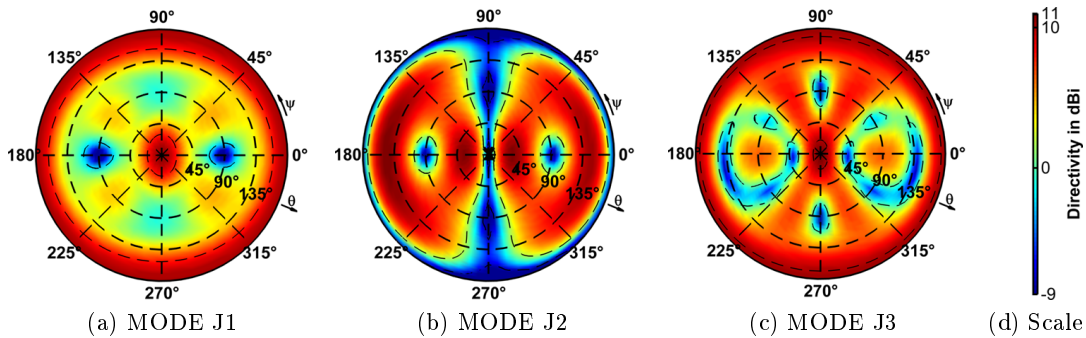


Figure 3.22: Antenna’s radiation pattern for three modes in 2D representation

3.4.6 Final circuits

The last step to complete the design of this feeding network is to extend the microstrip lines to the limit of the metallic plate. In this way the SMA connectors can be placed, it will enable the connection of the antenna to RF-front-end and measurement devices. In the Figure 3.23 the final result of this feeding network for each of the three characteristic modes can be seen.

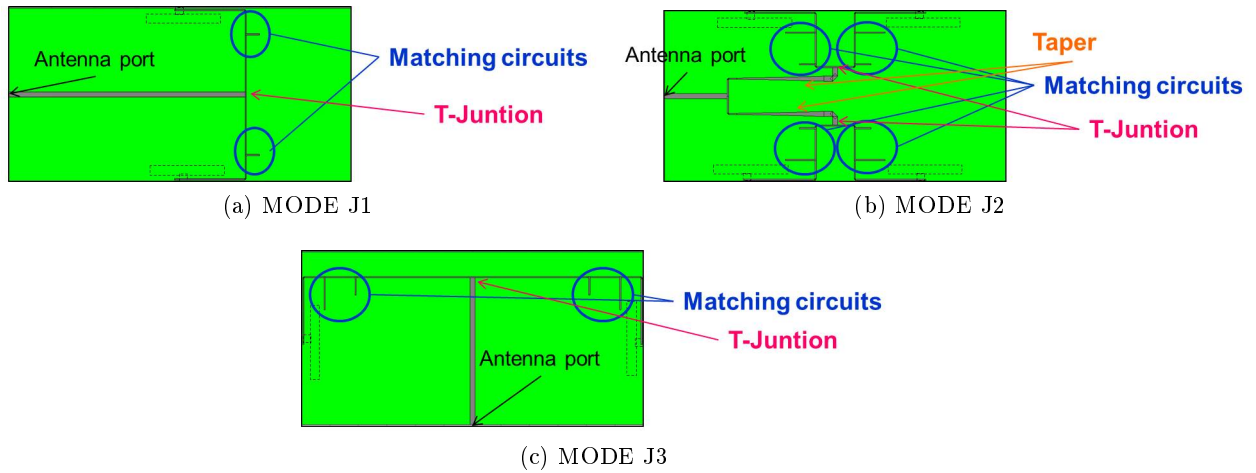


Figure 3.23: Feeding network: final circuits

3.4.7 Fabricated circuits and measurements

Once completed the design and simulation of circuits, the final step is to manufacture and measure these circuits. In order to verify the performance of the fabricated circuits (Fig.3.24), the reflection coefficient of each circuit has been measure by PNA (Series Network Analyzer, E8363B, Agilent Technologies). The Figure 3.24 shows the front and back of the fabricated circuits for each of the three characteristic modes.

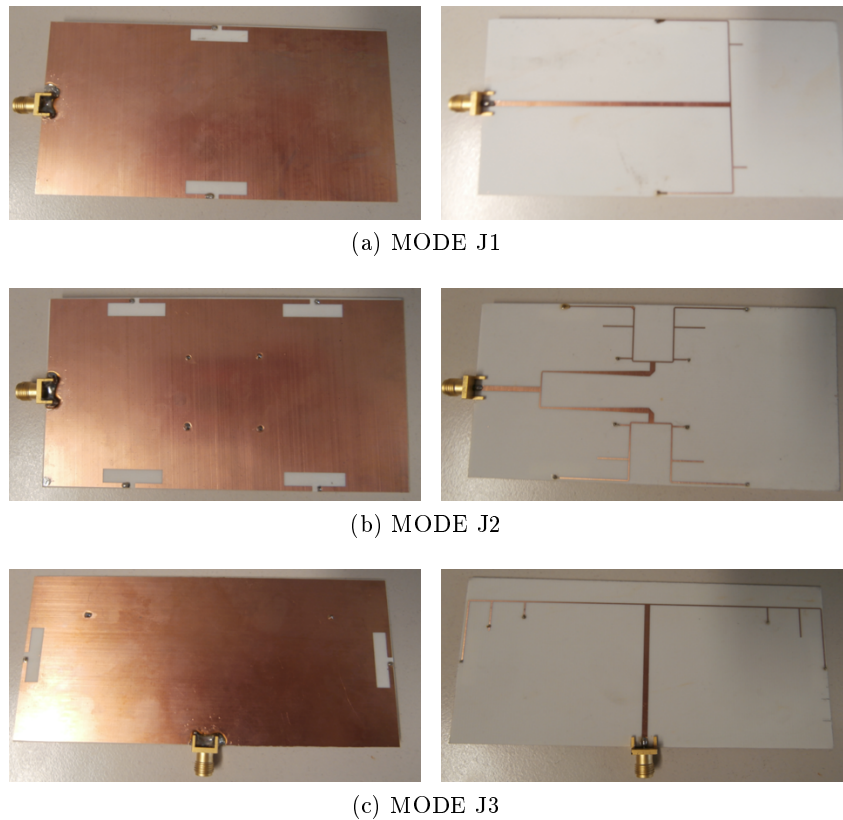


Figure 3.24: Feeding network: fabricated circuits

After the fabrication, the next step is to measure the circuits. The results of the measurements of each of the circuits are shown in the Figures 3.25, 3.26 and 3.27. For this circuits

the total operational bandwidth is from 2.5 GHz to 2.7 GHz. In the figures 3.25, 3.26 and 3.27, BW_{-6dB} represents the useful bandwidth from which the reflection coefficient is below -6 dB. The BW_{-6dB} bandwidth describes the range of frequencies over which the antenna can properly radiate or receive energy.

In the case of the *MODEJ1* (Figure 3.25), simulation results show that $BW_{-6dB} = 2.44$ GHz-2.776 GHz. This means that the simulated circuit covers the 100% of the total operational bandwidth. The measurements results shows that the fabricated circuit does not function as expected, probably because of the manual fabrication of the vias.

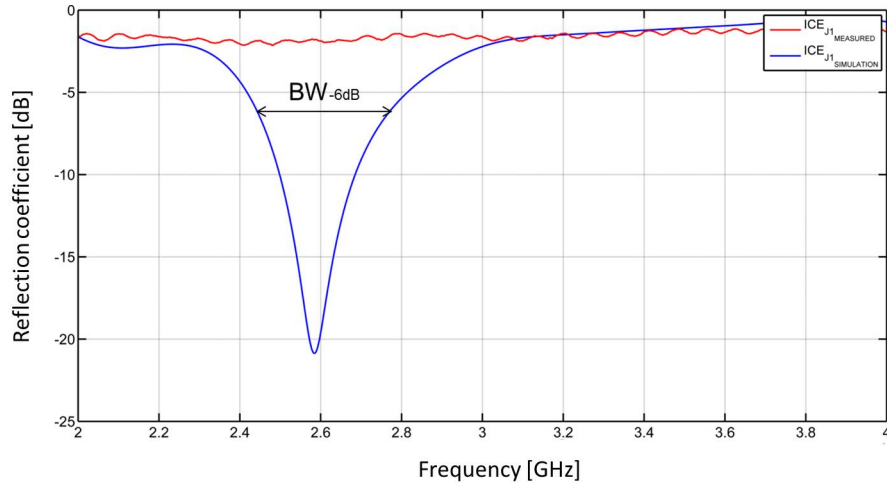


Figure 3.25: Reflection Coefficients (S_{11}) MODE J1

For the *MODEJ2* (Figure 3.26), simulation results show that $BW_{-6dB} = 2.56$ GHz-2.658 GHz. This means that the simulated circuit has a narrower bandwidth probably because of the used of double stub tuning matching networks. The simulated circuit covers the 49% of the total operational bandwidth. Moreover, the simulated circuit shows a very good matching of -27 dB at 2.6 GHz. And last but not least the frequency of operation for the fabricated circuit is shifted to 2.4 GHz in comparison to 2.6 GHz in the simulation.

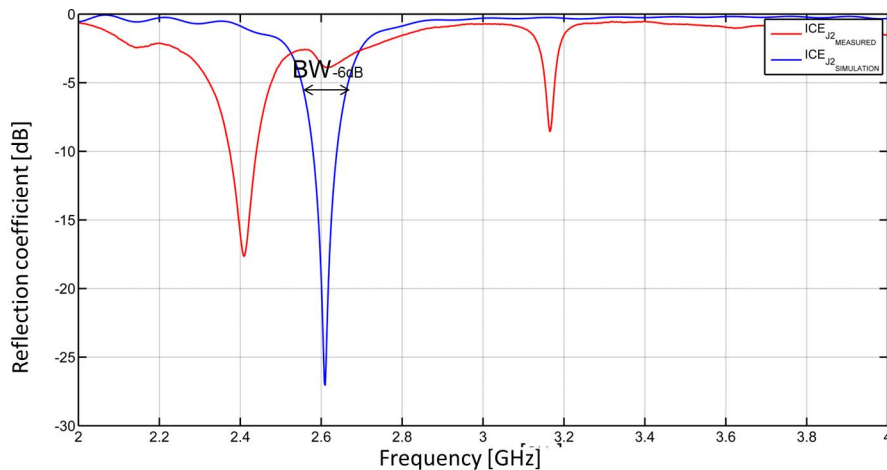


Figure 3.26: Reflection Coefficients (S_{11}) MODE J2

Finally for the *MODEJ3* (Figure 3.27), simulation results show that $BW_{-6dB} = 2.556 \text{ GHz} - 2.66 \text{ GHz}$. This means that, as in the previous case, the simulated circuit has a narrower bandwidth probably because of the used of double stub tuning matching networks. The simulated circuit covers the 52% of the total operational bandwidth. Moreover, the simulated circuit shows a very good matching of -22 dB at 2.6 GHz . And last but not least the fabricated circuit behaves similar to the simulated circuit, although it has a small frequency shift to 2.645 GHz in comparison to 2.6 GHz in the simulation.

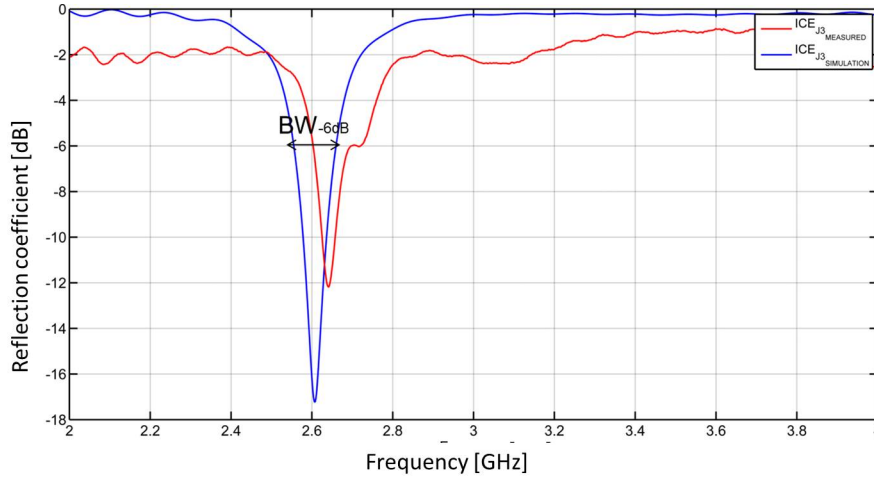
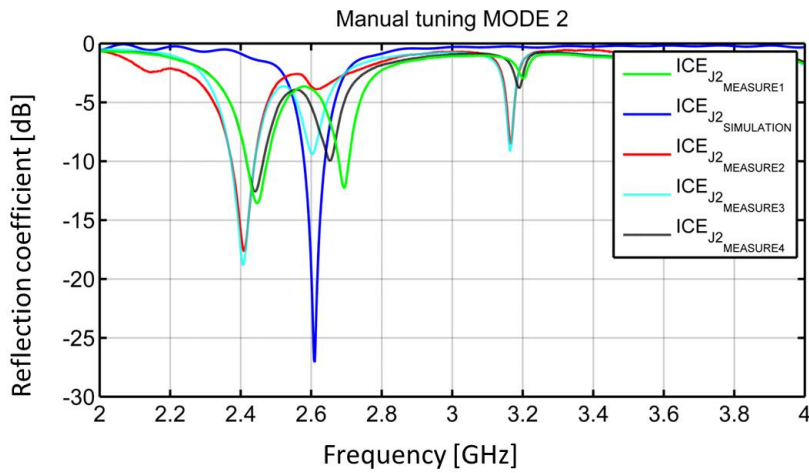


Figure 3.27: Reflection Coefficients (S_{11}) MODE J1

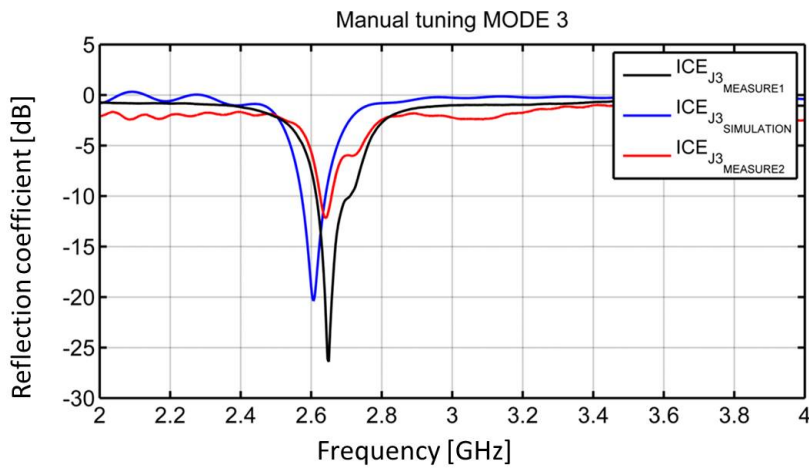
3.4.8 Manual tuning of the matching network

As the results of the measurements do not correspond with the simulation, the next step is to find how to improve these results. Therefore manual deembedding in order to determine the position of mismatch in the circuit should be conducted. One of the critical points in the circuit design is the matching circuit. To verify that the problem is in the matching circuit, it is necessary to remove part of the metal from the open circuit stub. Decreasing the length of the open stub, the matching frequency of the circuit changes as it can be seen in the Figure 3.28. By decreasing the length of the open stub the matching frequency starts to get closer to the desired frequency (2.6 GHz), thus the circuit presents a smaller frequency shift.

To conclude, it can be said that if the matching network changes the system performance will improve. Therefore the following sections show various improvements of the previous circuits, as well as a study of the tolerance of the system.



(a) MODE J2



(b) MODE J3

Figure 3.28: Results of the manual tuning of the fabricated circuits

3.4.9 Matching network at 2.8 GHz

Another way to improve the circuit behavior is to study how the fabricated circuit behaves. For example in the case of the MODE J2, for the fabricated circuit the operation frequency is shifted 200 MHz. To avoid this frequency shift, a circuit matched to 2.8 GHz has been designed and fabricated. The goal of this section is to verify that if the simulated circuit is designed for 2.8 GHz, the fabricated circuit will be matched at 2.6 GHz, due to the frequency shift that the fabricated circuit has shown in the previous circuits (section 3.4.7).

The three previous circuits were etched. For the fabrication of the circuit in this section the CNC machine from the "Escuela Politécnica Superior de la Universidad Autónoma de Madrid" had been used. The CNC machine was used in order to avoid manufacturing errors .

The Figure 3.29 shows the three different reflection coefficients taken into account in this section. In this figure $ICE_{J2}^{DESIRED}$ represents the desired behavior of the simulated reflection coefficient which is matched at 2.6 GHz. $ICE_{J2.8GHz}$ represents simulated reflection coefficient which is matched at 2.8 GHz. And $ICE_{J2}^{MEASURED}$ represents measured reflection coefficient which is matched at 2.8 GHz.

As can be seen in the Figure 3.29, the fabricated circuit is matched at 2.8 GHz, without presenting any frequency shift. Confirming that the frequency shift in the previous circuits

(section 3.4.7) is due to a manufacturing problem. Probably if the circuits of the section 3.4.7 were fabricated with the CNC machine this manufacturing problem would be avoid.

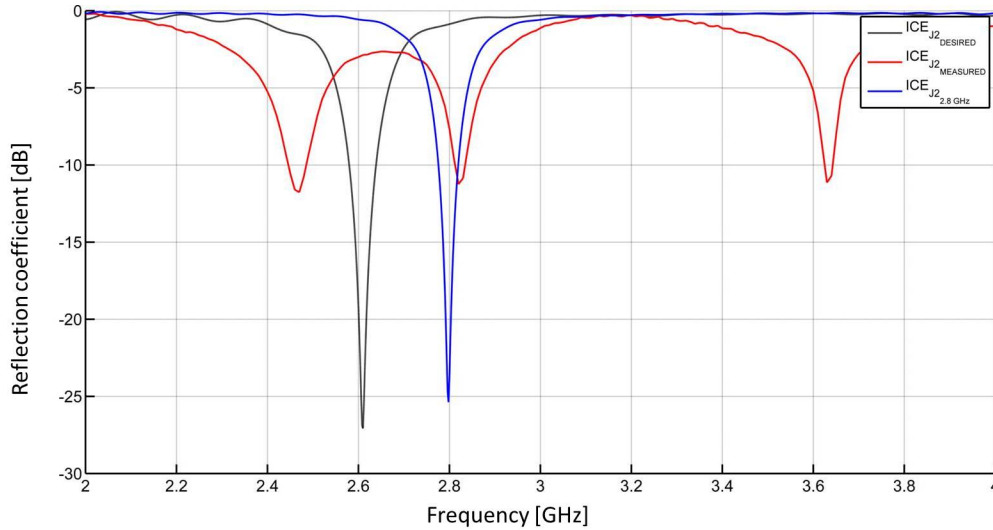


Figure 3.29: Reflection Coefficients (S_{11}) MODE J2 matched in simulation at 2.8 GHz

Finally, the Figure 3.30 shows the fabricated circuit for this section.

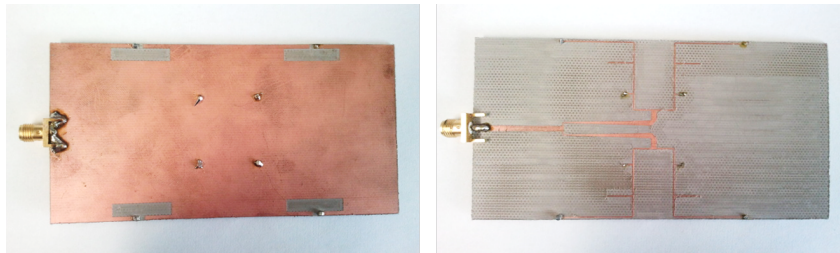


Figure 3.30: Fabricated circuit MODE J2 matched in simulation at 2.8 GHz

3.5 Improved circuits

With the aim of improving the system performance, new circuits with different matching networks have been designed. In the case of first mode circuit, the matching network with double stub is now used since the use of a matching network with a single stub could be the reason why the fabricated circuit did not behave properly. Another improvement of the system aims to improve the soldering of the vias and the shorted stubs. In order to improve adherence of the solder and the metal layer, a metallic circle is placed around the bore. Adding this improvement is only necessary to change the length of the shorted stubs to achieve the desired matching frequency. The Figure 3.31 shows an example of one the vias with this circular metallization around.

The Figure 3.32 presents three matching networks used for each of the circuits. Furthermore in Tables 3.1, 3.2 and 3.3 each of the lengths of the components of these matching network are specified .

Finally, Figure 3.33 shows the reflection coefficients for each of the three circuits. It can be seen the use of a circular path around the vias and the shorted stubs does not reduce the bandwidth of the circuit and it does not affect behavior of the circuits in the simulation.

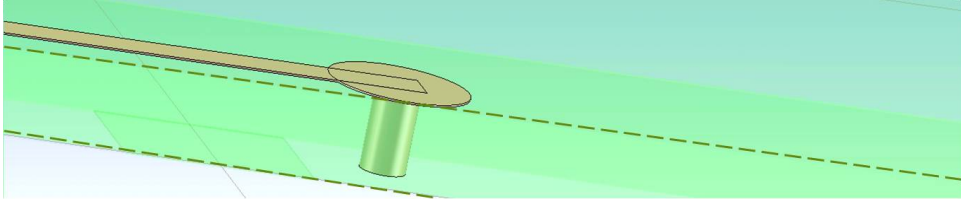


Figure 3.31: Metallized via

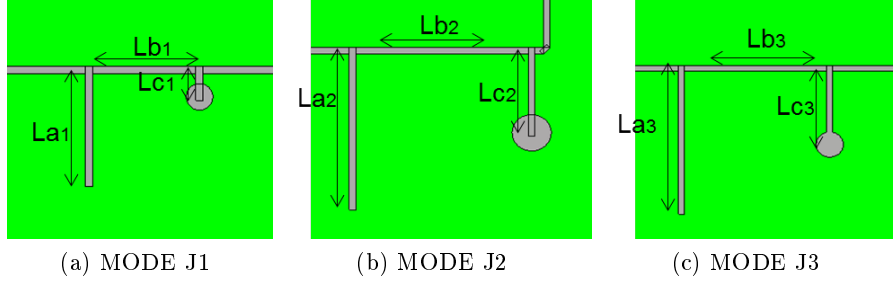


Figure 3.32: Dimensions of the improved matching circuits

Final lengths of the elements of the matching network MODE 1	
La_1	7 mm
Lb_1	6 mm
Lc_1	2 mm

Table 3.1: Final matching network Mode J1

Final lengths of the elements of the matching network MODE 2	
La_2	11.072 mm
Lb_2	10.692 mm
Lc_2	5.909 mm

Table 3.2: Final matching network Mode J2

Final lengths of the elements of the matching network MODE 3	
La_3	11.753 mm
Lb_3	10.435 mm
Lc_3	6.455 mm

Table 3.3: Final matching network Mode J3

3.6 Study of the fabrication tolerance of the system

Due to the manufacturing process, the fabrication errors occur in the circuit. Thus the fabrication tolerance of the circuit should be investigated. The two most common errors occur at the edges of the metal plate. The CNC machine can remove too much metal or otherwise the CNC machine can remove too much substrate at the edges of the metal plate. To test the effect of these two errors, the tolerance of the circuit has been studied in this section.

The Figure 3.34 shows a graphical representation of the circuit with excessive substrate around the metallic plate, where x represents the width of the excessive substrate around the metallic plate. In addition, the Figure 3.34b represents the variation of the reflection coefficient

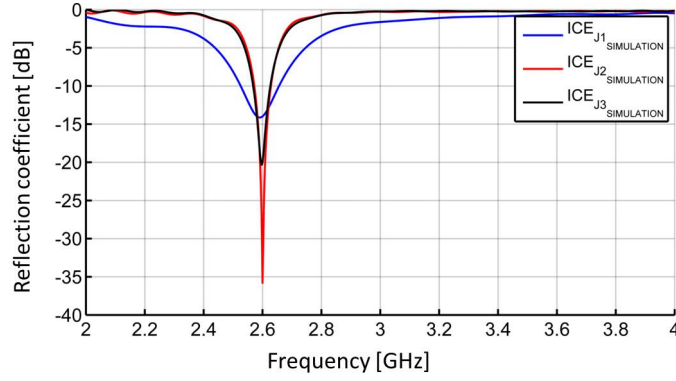
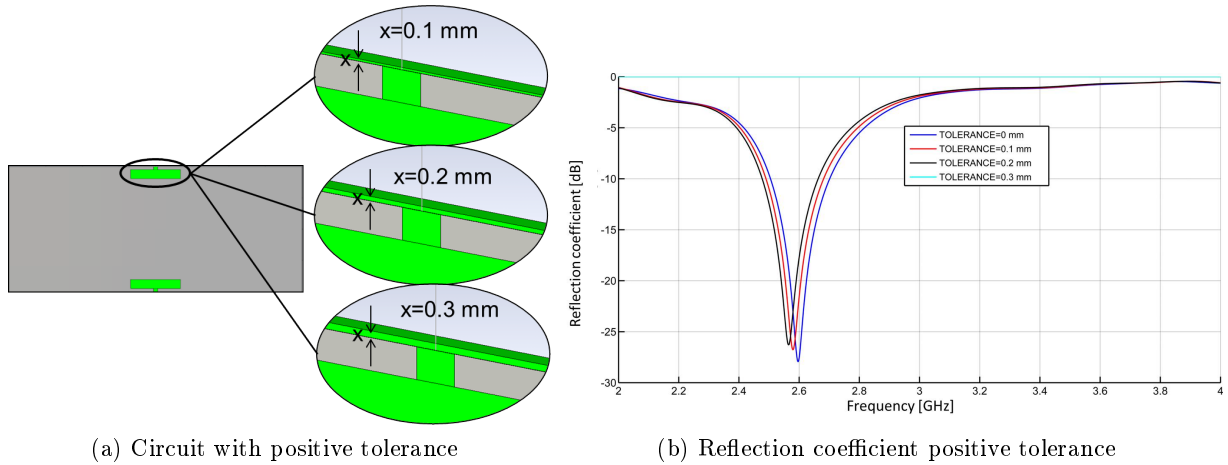


Figure 3.33: Reflection coefficient final metallized circuits

depending on x . It can be seen that increasing x causes a frequency shift of the operation frequency. The frequency shift is smaller than 20 MHz for x smaller than 0.3 mm. Therefore an excess of substrate around the metallic plate would not be a serious problem if the excess is lower than 0.3 mm.



(a) Circuit with positive tolerance

(b) Reflection coefficient positive tolerance

Figure 3.34: Positive tolerance

The Figure 4.4 shows a graphical representation of the circuit when the CNC machine removes too much substrate around the circuit. In this figure x represents the width of the lack of substrate around the circuit. The Figure 3.35b represents the variation of the reflection coefficient depending on x . It can be seen that decreasing x causes a frequency shift. This frequency shift is smaller than 200 MHz for x bigger than -0.5 mm. Therefore a lack of substrate around the circuit would not be a serious problem if the lack is lower than -0.5 mm.

To sum up, as it is shown in the study of the fabrication tolerance of the system, the circuit is tolerant of small errors. If the errors are small the phase shift in the circuit will be always less than 200 MHz.

3.7 Conclusions

In this sections it has been demonstrated that the excitation of the characteristic modes on a metallic plate can be used to design a MIMO antenna. From the simulations results, from the design of the system and from the behavior of the system at different frequencies some conclusions can be drawn.

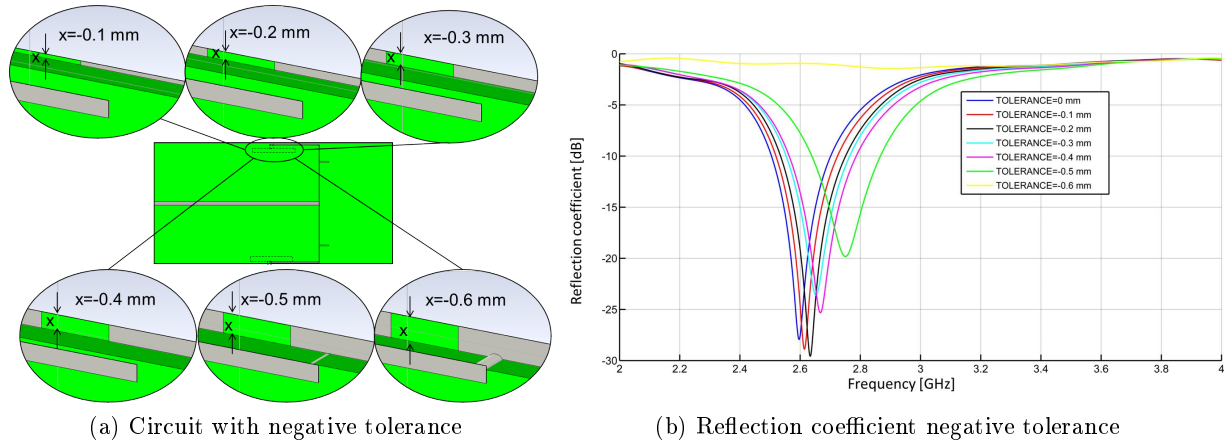


Figure 3.35: Negative tolerance

Firstly, the results of the reflection coefficient for the different modes show that an inductive coupling elements can be successfully matched using double tuning stubs circuits. Moreover, the simulations shown that the antennas system can be build for 2.6 GHz.

Secondly, it can be concluded from the simulation that the circuit for the first characteristic mode has the best performance. The useful bandwidth of the circuit for the first characteristic mode is larger than the bandwidth for the other two circuits for the other two characteristic modes. Additionally, the matching of the first circuit is simpler than for the other two circuits, because the value of the measured impedance at the end of the ICE port is closer to $100\ \Omega$, i.e. the value of the imaginary part of this measured impedance is almost zero.

Finally, the measurements of the fabricated circuits show that this fabricated circuits do not function as expected from the simulation. However the fabricated circuits can be redesigned in order to improve their performance, as demonstrated in the sections 3.4.8 and 3.5.

4

MIMO antennas system based on the excitation of car bodywork elements

4.1 Introduction

The early vehicles radio systems were limited to the use of AM and FM radio. Nowadays the customers demand more services in their vehicles, such as remote key-less entry, satellite navigation and others. Each of these wireless services requires the incorporation of antennas capable to receive and transmit signals in the appropriate frequency range. In order to cover these services, the use of a MIMO system as implemented in this project is required.

4.2 Requirements for vehicular antennas

In order to have a good reception in a vehicle, an antenna must satisfy several requirements. In this section some of these requirements are listed.

The first and most obvious is that the antenna must be able to receive from any direction around the car. In many cases the use of a single antenna is not enough to cover these first requirement. Therefore it is better to use a system of multiple antennas as the one implemented in this project. Another significant factor is the distance between ground and the antennas system. The higher the antenna system is placed over ground, the better it can receive and transmit.

Finally, another of the factors to consider in the design of an antenna system is the proximity of the engine. The engine generates noise and vibration that could disturb the reception of the antenna system. Thereby the antenna system should be placed as far as possible from the engine, but taking all other requirements mentioned before into account.

4.3 Possible location of antennas in a car

There are many possible locations to place antennas on a vehicle, but not all of them are good for each type of car. Following some of the most common locations of antenna systems on a car are mentioned. The Figure 4.1 shows a graphical representation of these locations.

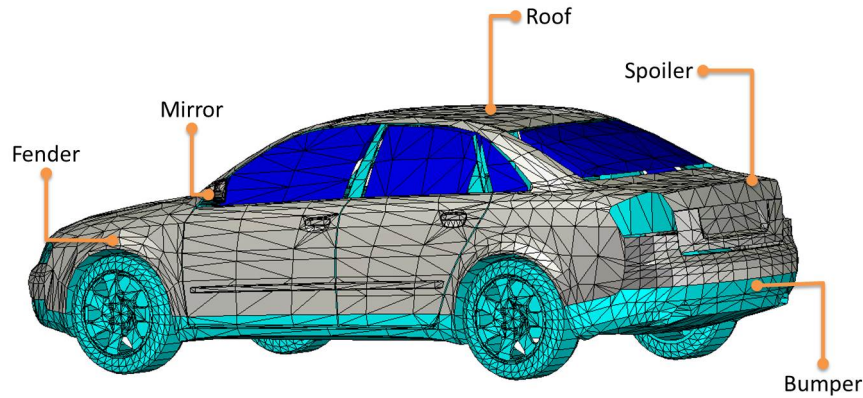


Figure 4.1: Suitable antenna placement on a regular passenger car

4.3.1 Roof

The roof is the most used location for positioning the antenna in a car. The roof is the highest point of the car above ground and it does not have any element around the antenna that interferences with the reception. Thus placing the antenna on the roof is one of the best options for most of the vehicles, except convertibles.

4.3.2 Spoiler

Some sport cars are equipped with a spoiler for better down force on higher speeds. Racing cars use the spoiler for telemetry communication systems. Moreover regular hatchback cars can have a little spoiler, in which an antenna's system can be implemented.

4.3.3 Fender and bumper

Fenders and bumpers may be another attractive location for an antenna. However, special care must be taken for easy repair, as bumper and fenders can crash. Also it should be taken into consideration that engine noise and low height above ground might degrade antenna performance.

4.3.4 Trunk cover

As an alternative to the roof, the trunk cover is another promising location for the antenna, especially in the case of convertible cars. However, the trunk cover must be made of plastic or a double-layer structure with metal frame and plastic cover on top.

4.3.5 Side-Mirror

The current trend of car designers is to put huge side-mirrors in the vehicles to facilitate driver's visibility. The side-mirrors can incorporate a large number of antennas working at high frequency. Some side-mirrors are large enough to contain antennas for wireless services above 1 GHz, such as the Car-2-Car communication in 5.9 GHz.

4.4 Location of the MIMO system

There are a number of factors to be considered to design an antenna system enabling good reception in wireless systems. As stated in the section 4.2, the antenna must be as high as possible above ground for long path transmission. Moreover, the antenna must be unobstructed to have a good communication in all directions.

To fulfill these requirements, the antenna system designed in this project is placed in the side-mirror of the car. In this way the system is far enough from the ground, it does not have metal elements near the system that could disturb the reception or the transmission of the signal and it can be used in convertible cars. In addition, to avoid possible loss of the signal in case of damage of the side-mirror, this system will be implemented in both side-mirrors.

4.5 Design of the MIMO system

The first step in the design of this MIMO system was to consider which material will be used. In this case the system will be located on the side-mirror of the car. As this location has a curved shape, it is essential to use a flexible material which could be manipulated without the use of machines. For this purpose the first option was to use Kapton, but the dimensions of this material are not suitable for this system. Therefore the best option was to use an existing material in the IHE department. The material that fulfills this flexibility feature is ROGERS *RT5880*. The specifications of the microstrip line created in this project using ROGERS *RT5880* are shown in Figure 4.2. In addition, in the table 4.1 the width values of the microstrip line are listed.

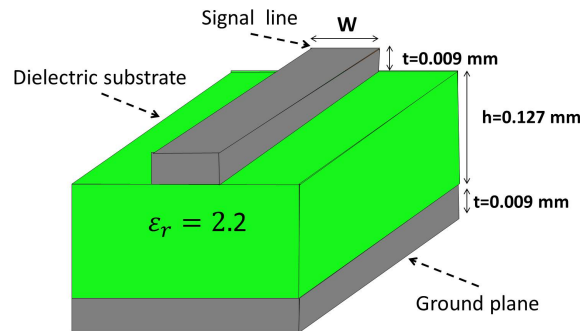


Figure 4.2: Microstrip line of the MIMO system

Width values (W) of the microstrip line	
W_{50}	0.3797 mm
W_{25}	0.9815 mm
$W_{12.5}$	2.219 mm

Table 4.1: Width values (W) of the microstrip line

The next step in the design of this MIMO system was to choose a generic mirror and measure its dimensions. The selected generic mirror is shown in the Figure 4.3. The MIMO system will be located in the metallic part of the side-mirror. The location of the MIMO system is indicated in the Figure 4.4a with a blue curve. The dimensions of this part of the side mirror are specified in the Figure 4.4b.

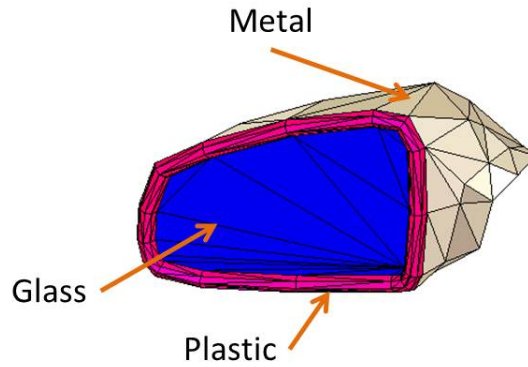
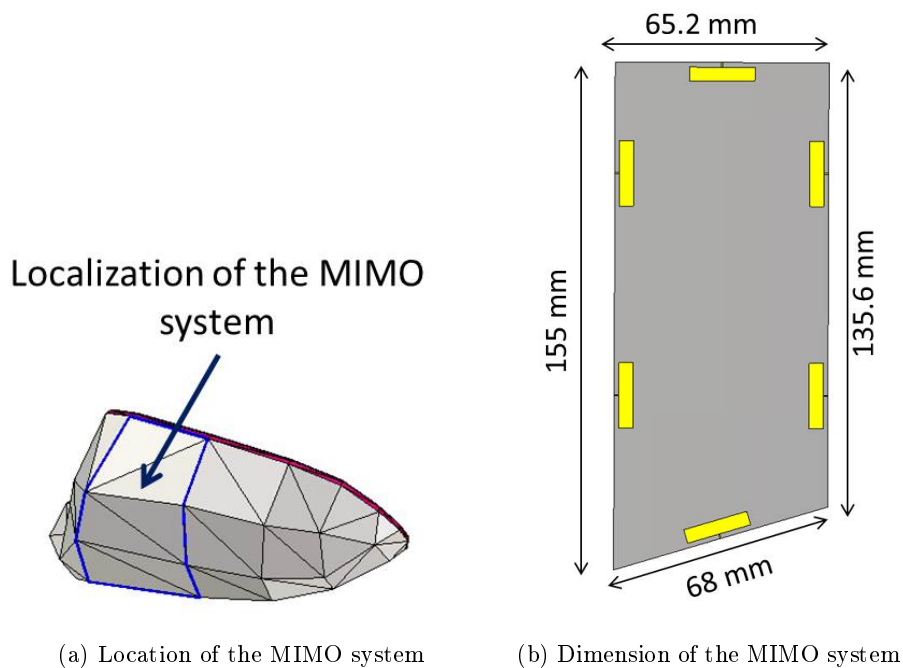


Figure 4.3: Generic car mirror



(a) Location of the MIMO system

(b) Dimension of the MIMO system

Figure 4.4: MIMO system in the side-mirror

The third step in the design of this MIMO system was to decide the type of structure that it is going to be implemented. The first idea was to design a multi-layer system with each of the characteristic mode elements in different layers. However, this idea was discarded because one of the goals of this project is to fabricate the system and the design of a multi-layer system makes the fabrication more complex. For this reason, a double-layer microstrip line MIMO system was build.

The last step to decide how this MIMO system should operate, was to decide which characteristics modes would be excited in the structure. Because of the shape of the structure, it was decided to implement the characteristic modes $J2$ and $J3$. The used of the combination of this two characteristic modes will generate a beneficial directivity pattern, allowing a reception from all the directions. The following sections explain in detail the architecture and the function of this MIMO system.

4.6 Inductive Coupling Elements in the MIMO system

Applying the acquired knowledge of Inductive Coupling Elements (section 3.3 and 3.3.1), in this section the location of the Inductive Coupling Elements in this MIMO system is chosen.

In the Figure 4.5 the position of the Inductive Coupling Elements for each of the characteristic modes inside of the structure can be seen. The dimensions of this Inductive Coupling Elements are the same as in the section 3.3.1, these dimensions have remained the same for the reasons explained in the section 3.3.1.

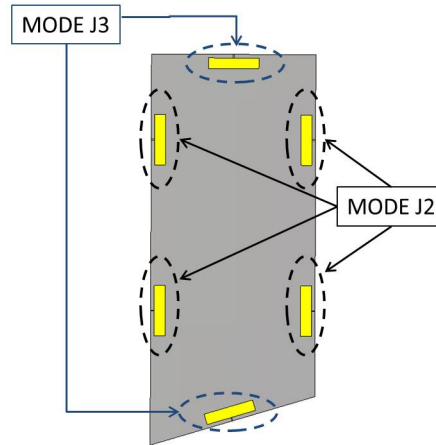


Figure 4.5: Inductive Coupling Elements for the characteristic modes in the MIMO system

The figure 4.6 explains the symmetry of the circuit. In this figure it can be seen that the Inductive Coupling Elements of the characteristic mode $J2$ are facing two to two, i.e. ICE₂ is in front of ICE₆ and ICE₃ is in front of ICE₅. Moreover the distance between ICE₂ and ICE₃ is that same than between ICE₅ and ICE₆.

In the case of the $J3$ mode, this Inductive Coupling Elements (ICE₁ and ICE₄) are located in the center of the mirror side of the structure as corresponds to the third characteristic mode.

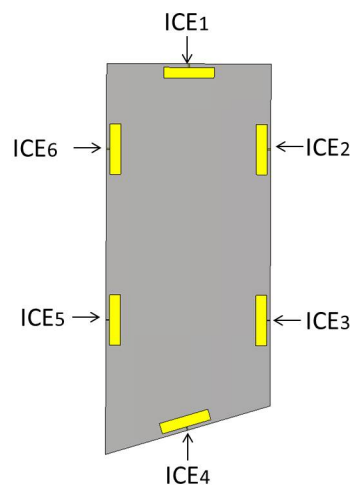


Figure 4.6: Structure of the Inductive Coupling Elements in the MIMO system

4.7 Feeding network of the MIMO system

After selecting the characteristic modes for the implementation of the MIMO system and observing the behavior of the current distribution in the system, the next step is to proceed with the design of the feeding network. For the feeding network of this MIMO system it is necessary to implement six matching networks, three T-junction elements and a taper element. The implementation of these elements is explained in detail in the following sections.

4.7.1 Inductive Coupling Element (ICE) ports of the MIMO system

The design of the Inductive Coupling Element ports was explained in the section 3.4.1. For this MIMO system is necessary to use six of this Inductive Coupling Element ports, one for each Inductive Coupling Element. The location of this Inductive Coupling Element ports can be seen in the Figure 4.7.

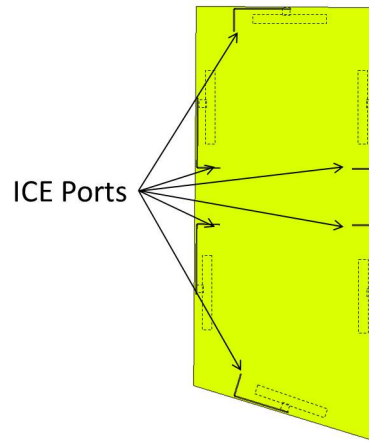


Figure 4.7: Location of the Inductive Coupling Element ports in the MIMO system

4.7.2 Matching network of the MIMO system

Given the mirror symmetry of the Inductive Coupling Elements of the mode J_2 , the matching network for the ICE_2 can have the same dimensions as the matching network for the ICE_3 . For the same reason the matching network for the ICE_5 can have the same dimensions as the matching network for the ICE_6 . Therefore it is necessary to implement four different matching networks for this MIMO system. The location of these four matching networks can be seen in the Figure 4.8.

The calculations of the dimensions of the matching networks are performed in the same manner as in the section 3.4.2. With the difference that in this case as the simulation was very time consuming, it was decided to use the Advanced Design System (ADS) program to study the behavior of the matching circuits.

As it was explained in the section 3.4.2, the length of the stubs for the double tuning stub can be calculated using the Smith V3.10 program. However with the help of the Advanced Design System (ADS) program the behavior of the reflection coefficient can be observed. An example of the matching circuits implemented with the Advanced Design System (ADS) program is shown in the Figure 4.9.

The value of the load impedance matched with each of these matching networks are given in the table 4.2.

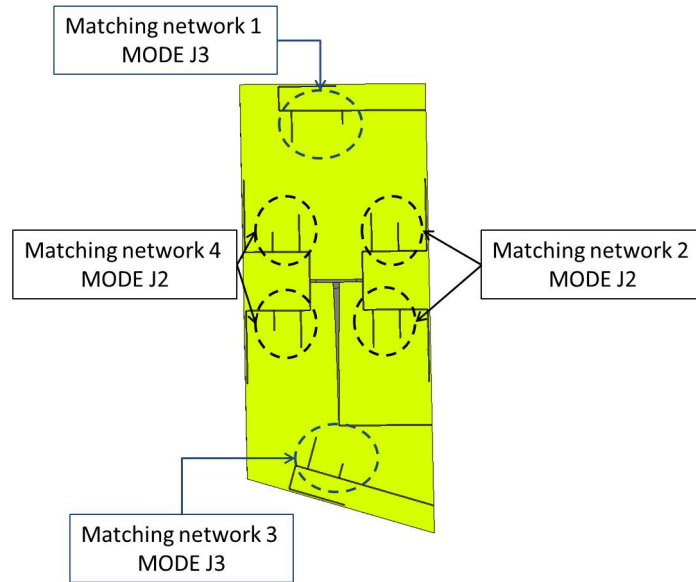


Figure 4.8: Location of the matching network in the MIMO system

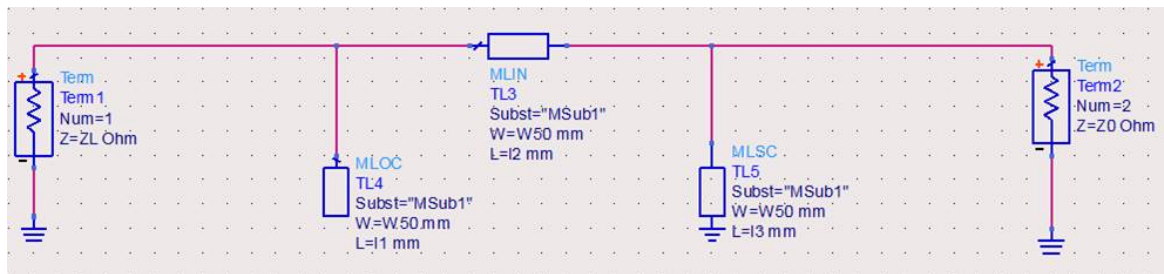


Figure 4.9: Matching network using ADS

Name of the load impedance(Z_L)	Values of the load impedance (Z_L)	Description
Z_{L1}	$1.263 + j20.403 \Omega$	Load impedance for the matching network 1 MODE J3
Z_{L2}	$1.56 + j44.48 \Omega$	Load impedance for the matching network 2 MODE J2
Z_{L3}	$1.635 + j26.419 \Omega$	Load impedance for the matching network 3 MODE J2
Z_{L4}	$1.684 + j44.566 \Omega$	Load impedance for the matching network 4 MODE J3

Table 4.2: Values of the load impedance (Z_L) for each of the matching networks

The tables 4.3, 4.4, 4.5 and 4.6 show in detail the length each of the stubs used in each of the matching networks.

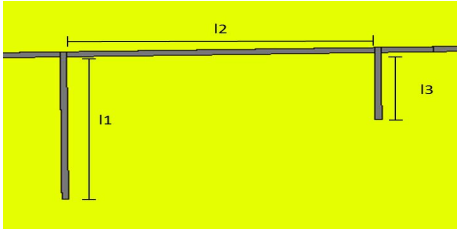
Matching network in CST	Values of the length
	$l_1=11 \text{ mm}$ $l_2=17.5 \text{ mm}$ $l_3=5.4 \text{ mm}$

Table 4.3: Matching network 1 MODE J3

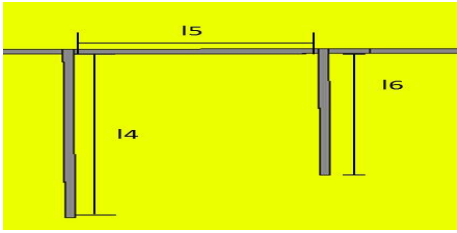
Matching network in CST	Values of the length
	$l_4=9 \text{ mm}$ $l_5=1 \text{ mm}$ $l_6=13.3 \text{ mm}$

Table 4.4: Matching network 2 MODE J2

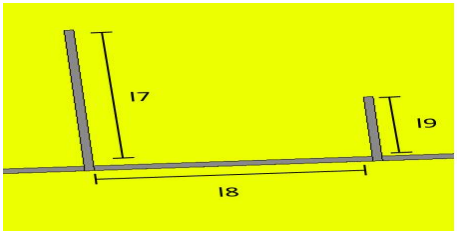
Matching network in CST	Values of the length
	$l_7=11.5 \text{ mm}$ $l_8=11 \text{ mm}$ $l_9=5.25 \text{ mm}$

Table 4.5: Matching network 3 MODE J2

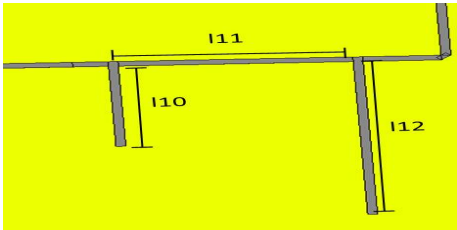
Matching network in CST	Values of the length
	$l_{10}=7 \text{ mm}$ $l_{11}=9 \text{ mm}$ $l_{12}=13 \text{ mm}$

Table 4.6: Matching network 4 MODE J3

4.7.3 T-Junction structure of the MIMO system

The next step in the design of this MIMO system is to connect the matching network number 2 with the matching network number 4. For this purpose T-Junction structures have

been used. The characteristics of such T-junction structure had been explained in the section 3.4.3. The Figure 4.10 shows the appearance of the T-junction elements. In this figure it can be seen that the structure called T-junction 1 is used to join the two matching networks of the matching network number 3, the structure called T-junction 2 is used to join the two matching networks of the matching network number 2 and the structure called T-junction 3 is used to join the structures T-junction 1 and T-junction 2.

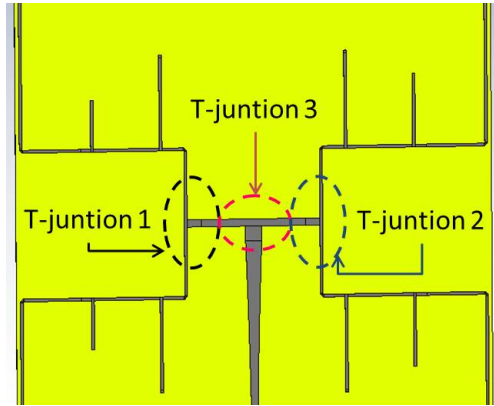


Figure 4.10: T-junctions structures in the MIMO system

The value of the impedance at the end of the T-junction 1 and T-junction 2 structures is $25\ \Omega$. Consequently the value of the impedance at the end of the T-junction 3 structure is $12.5\ \Omega$. The value of this impedance may be calculated using the formulas 4.1 and 4.2.

$$Z_1 = \frac{50\ \Omega * 50\ \Omega}{50\ \Omega + 50\ \Omega} = 25\ \Omega \quad (4.1)$$

$$Z_2 = \frac{25\ \Omega * 25\ \Omega}{25\ \Omega + 25\ \Omega} = 12.5\ \Omega \quad (4.2)$$

4.7.4 Taper structure of the MIMO system

The next and last element used in the design of this MIMO system is a exponential taper. The characteristics of this exponential taper had been detailed in the section 3.4.4. As can be seen in the Figure 4.12, the initial impedance at the end of the the T-junction number 3 is $12.5\ \Omega$ and using the exponential taper this impedance is transformed to $50\ \Omega$. Thereby the desired value of the impedance at the end of the port is obtain.

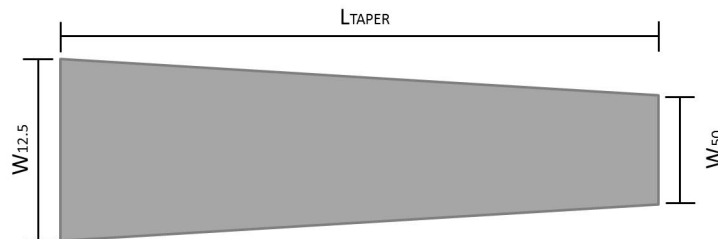


Figure 4.11: Taper structure in the MIMO system on details

In the Figure 4.11 the taper structure is described in detail. In this figure the width at the beginning of the taper is $W_{12.5} = 2.219\ \text{mm}$ and the end of the taper the width is $W_{50} = 0.3797\ \text{mm}$. Moreover the length of the taper is $L_{TAPER} = 42.2\ \text{mm}$.



Figure 4.12: Taper structure in the MIMO system

4.7.5 Final circuit

The last step to complete the design of this feeding network is to extend the microstrip lines to the limit of the metallic plate. In this way the SMA connectors that will enable the connection of the antenna to RF-front-end and measurement devices can be soldered. In the Figure 4.13 the final result of the feeding network can be seen. Given the structure of the circuit it is not possible to connect the two ports of the characteristic mode $J3$ using microstrip lines. Therefore it was decided to use a cable to combine these two ports. The connection between the two port of the characteristic mode $J3$ can be seen in the Figure 4.13b.

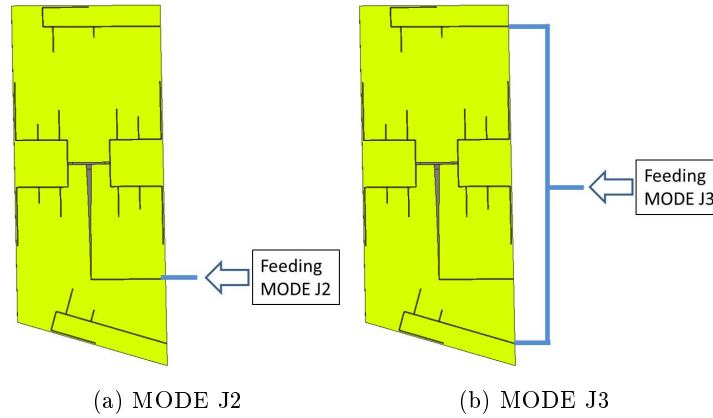


Figure 4.13: Final circuit of the MIMO system

Reflection coefficient of the MIMO system

In this circuit the total operation bandwidth is from 2.5 GHz to 2.7 GHz. Figures 4.14 and 4.15, BW_{-6dB} represents the useful bandwidth in which the reflection coefficient is below -6 dB. The BW_{-6dB} bandwidth describes the range of frequencies over which the antenna can properly radiate or receive energy.

In the case of the $MODEJ2$ (Figure 4.14), $BW_{-6dB} = 2.578$ GHz-2.618 GHz. This means that the characteristic $MODEJ2$ covers the 20% of the total operation bandwidth. Moreover, the this mode shows a very good matching of -37.8 dB at 2.6 GHz.

In the case of the $MODEJ3$ (Figure 4.15), $BW_{-6dB} = 2.584$ GHz-2.622 GHz. This means that the characteristic $MODEJ3$ covers the 19% of the total operation bandwidth. Moreover, the this mode shows a very good matching of -8.9 dB at 2.6 GHz.

Directivity Pattern of the MIMO system

In this section the radiation pattern of the MIMO system is described. The radiation pattern of the MIMO system changes depending on the elevation (THETA) and azimuth (PHI)

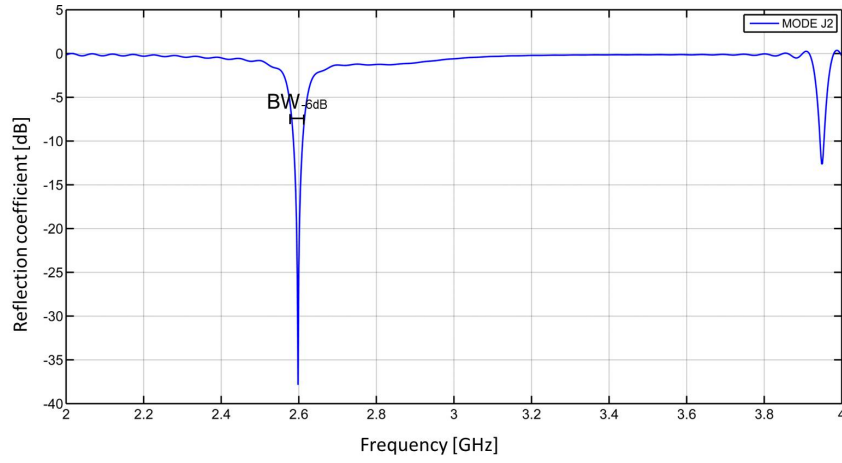


Figure 4.14: Reflection coefficient MIMO system

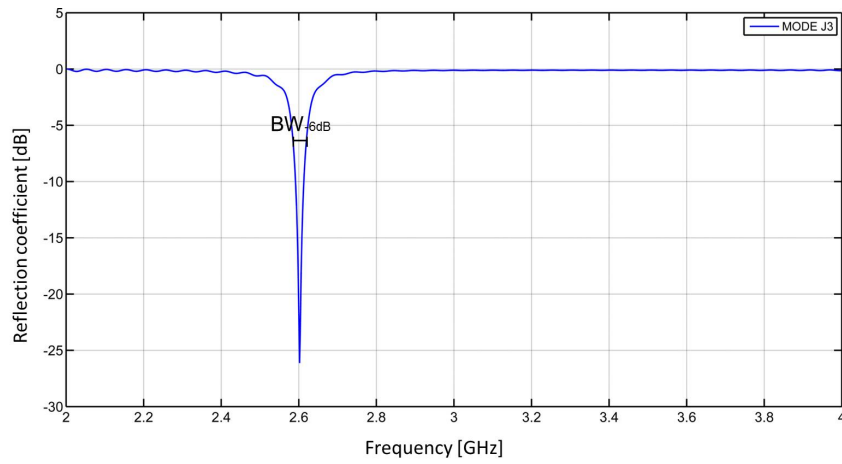


Figure 4.15: Reflection coefficient MIMO system

axis. The Figure 4.16a represents the radiation pattern produced by the characteristic mode $J2$. The Figure 4.16b represent the radiation pattern produced by the characteristic mode $J3$. Observing these figures it can be concluded that the system is able to get an omnidirectional radiation.

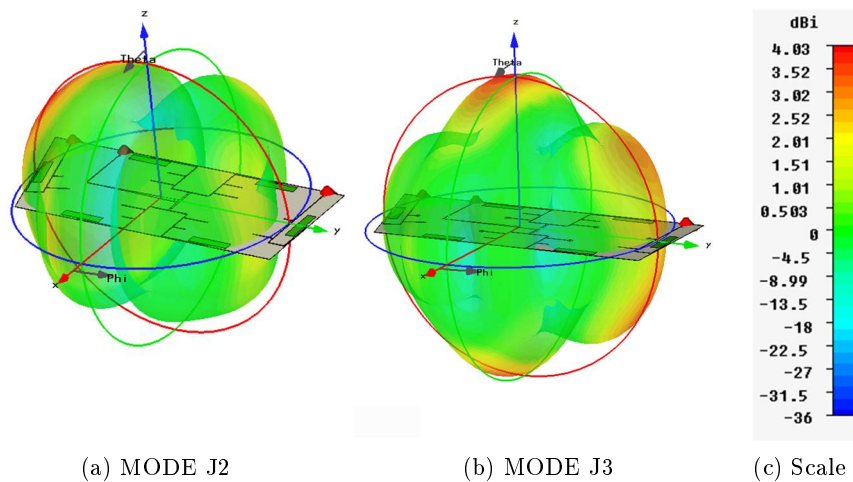


Figure 4.16: Antenna's radiation pattern for the MIMO system in 3D representation

4.7.6 Shorted stubs metallization

One of the improvements seen in the section 3.5 was the metallization around the vias in order to improve the soldering of this vias. In the case of this MIMO system the metallization of the vias was made at the end of the shorted stubs, in this way possible tolerance errors can be avoided. The final MIMO system was etched, i.e. the CNC was not used to fabricate the MIMO system. In the Figure 4.17 the final MIMO system with the metallized shorted stub can be seen in detail.

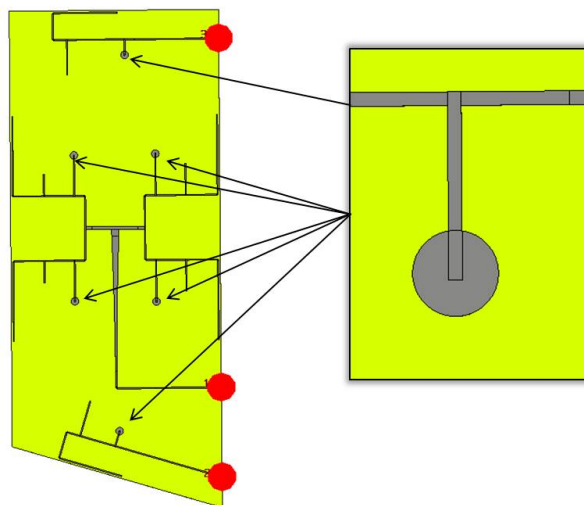
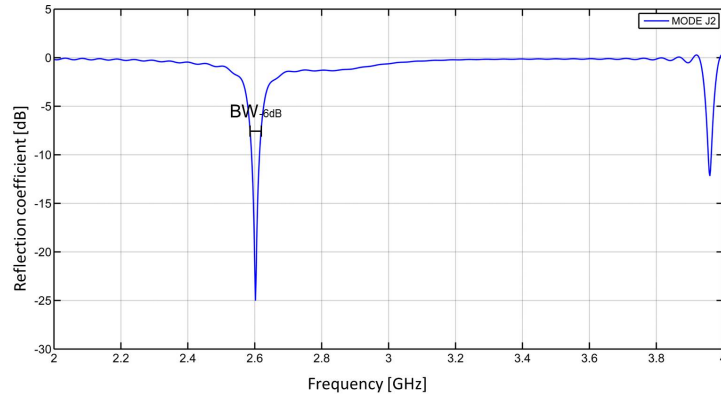
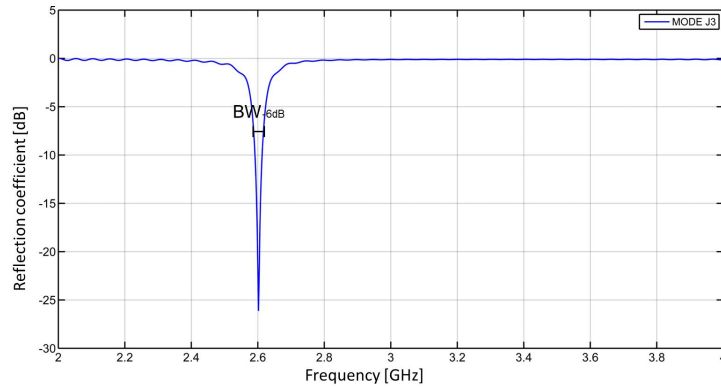


Figure 4.17: Shorted stubs metallization for the MIMO system

The Figure 4.18 shows the reflection coefficient for the final MIMO system with the metallized shorted stub. In the figure 4.18b it can be seen that the matching for the mode $J3$ improves if the shorted stub metallization is used.



(a) MODE J2



(b) MODE J3

Figure 4.18: Reflection coefficient MIMO system, shorted stubs metallization

4.8 Definition of the Envelope Correlation Coefficient (ECC)

The Envelope Correlation Coefficient (ECC) is an important parameter to be considered while developing a MIMO antenna system. The mutual coupling between the antennas degrades the performance of a diversity antenna system. Therefore antenna designers try to design antenna systems that minimize coupling between ports while meeting the input matching requirements [32]. Usually, the envelope correlation coefficients are presented to evaluate some of the diversity capabilities of a multiple-antenna system [33]. The lower will the value of the ECC be the better will be the performance of the antenna system be. The envelope correlation for a two-antenna system is defined in the equation 4.3.

$$\rho_e = \frac{|\int \int_{4\pi} \vec{F}_1(\theta, \phi) d\Omega \bullet \vec{F}_2(\theta, \phi) d\Omega|^2}{\int \int_{4\pi} |\vec{F}_1(\theta, \phi)|^2 d\Omega \int \int_{4\pi} |\vec{F}_2(\theta, \phi)|^2 d\Omega} \quad (4.3)$$

In the equation 4.3, $\vec{F}_1(\theta, \phi)$ is the field radiation pattern of the antenna system when only the port i is excited and all other ports are terminated to 50Ω load. In this equation, \bullet denotes the Hermitian product.

Recent research has shown that the envelope correlation can be well defined by a simple closed form equation that relates the scattering parameters of the multi-antenna system [35]. This approach has the advantage that it is not necessary to know the radiation pattern of the antenna system and that the explicit influence of mutual coupling and input match is revealed. The envelope correlation coefficient in terms of the S-parameter of the antenna system can be

seen in the equation 4.4.

$$\rho_e = \frac{|S_{11}^* S_{12} + S_{21}^* S_{22}|^2}{(1 - |S_{11}|^2 - |S_{21}|^2)(1 - |S_{22}|^2 - |S_{12}|^2)} \quad (4.4)$$

The Figure 4.19 represents the Envelope Correlation Coefficient (ECC) for the MIMO antenna system implemented in this chapter.

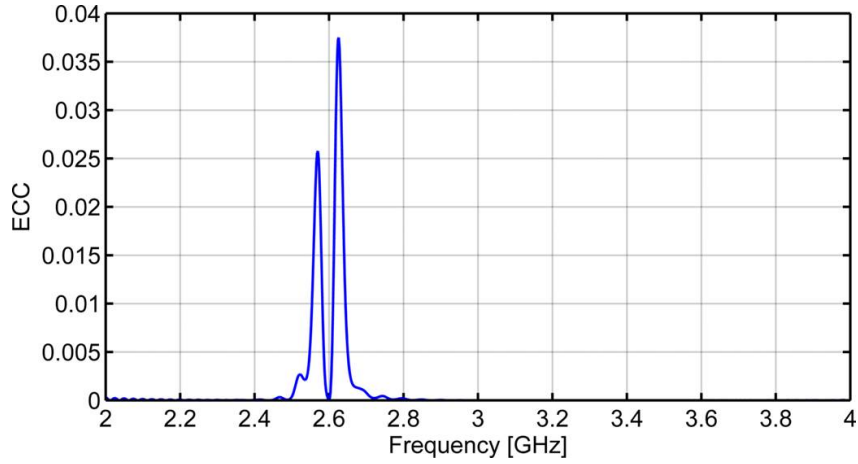
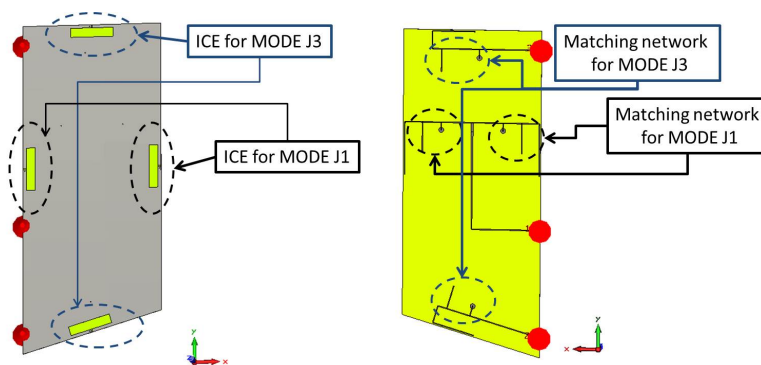


Figure 4.19: Envelope Correlation Coefficient (ECC)

Comparing the results of the ECC obtained in [33] with the results from the Figure 4.19, it can be concluded that the envelope correlation coefficient has a small value in the frequency range from 2 GHz to 4 GHz. Hence it can be concluded that this system has a high performance

4.9 MIMO system with mode $J1$ and $J3$

In the previous sections a MIMO system exciting the characteristic modes $J2$ and $J3$ have been designed. In this section, a MIMO system exciting the characteristic modes $J1$ and $J3$ is presented. At first the idea of generating the $J1$ mode for a MIMO system was discarded since the fabricated prototype for this mode did not function correctly. However, in the simulation for the mode $J1$, it was shown that the excitations of this mode allowed a larger operational bandwidth. The structure of this MIMO system can be seen in the Figure 4.20.



(a) MIMO system, mode $J1$ and $J3$ (b) MIMO system, mode $J1$ and $J3$

Figure 4.20: MIMO system, mode $J1$ and $J3$

The Figure 4.21 shows the reflection coefficient for the MIMO system designed in this section. As can be seen in this figure the BW_{-6dB} bandwidth describes the range of frequencies over which the antenna has sufficient matching.

In the case of the $MODEJ1$ (Figure 4.21), the bandwidth is $BW_{-6dB} = 2.58 \text{ GHz} - 2.62 \text{ GHz}$. This means that the characteristic $MODEJ1$ covers the 20% of the total operation bandwidth. Moreover, the this mode shows a very good matching of -9.5 dB at 2.6 GHz .

In the case of the $MODEJ3$ (Figure 4.21), the bandwidth is $BW_{-6dB} = 2.572 \text{ GHz} - 2.62 \text{ GHz}$. This means that the characteristic $MODEJ3$ covers the 24% of the total operation bandwidth. Moreover, the this mode shows a very good matching of -24.4 dB at 2.6 GHz .

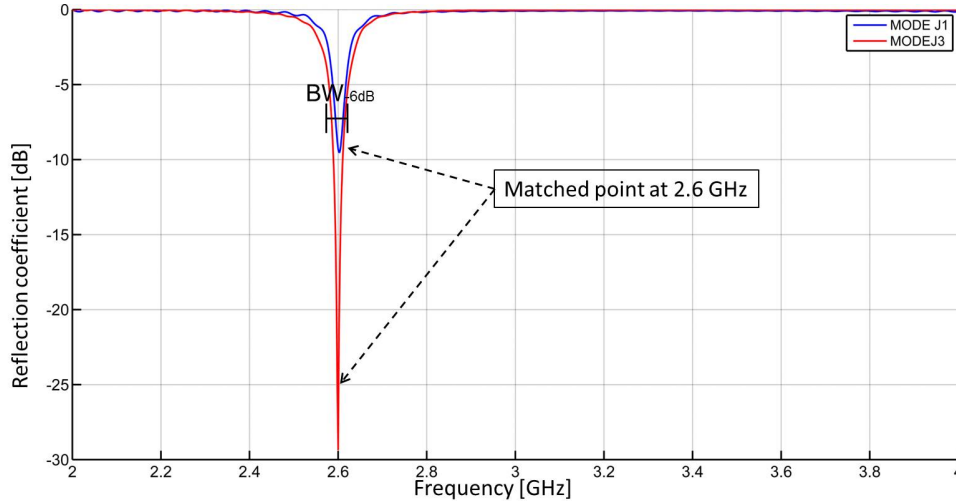


Figure 4.21: Reflection coefficient MIMO system with modes $J1$ and $J3$

The useful bandwidth of this MIMO system does not increase too much in comparison to the previous MIMO system. But the design of this system proves that a MIMO system exciting the mode $J1$ can be also designed.

4.10 Conclusions

From the simulation results conclusions can be drawn from the reflection coefficient representation and the different radiations patters.

In first place, the reflection coefficient of each of the characteristic modes used in the two MIMO systems described in this chapter show that a MIMO system matched at 2.6 GHz can be fabricated using Inductive Coupling Elements and a microstrip line as a feeding network.

Secondly, the simulated radiation patterns show that the combination of the radiation patter from the second mode and the radiation patter from the third mode can cover a great reception area. It happens the same in the combination of the first and third mode.

In the next chapter, the fabrication of the MIMO antenna system that combines the modes $J2$ and $J3$ is described.

5

Fabrication of the MIMO system

Once the design and simulation of the MIMO antenna system described in the previous chapter, the final step is to manufacture and measure this system is completed. At the point of the work when the prototype should be fabricated the ROGERS RT5880 material was unfortunately not available in the IHE institute. Therefore it was necessary to redesign a MIMO antenna system with the same characteristics as the previous one but using another material. For the MIMO antenna system redesigned in this chapter the ROGERS RO4003 material is used. The ROGERS RO4003 can not be bent easily, which favors that the circuit will get broken when it is been used. Therefore the ROGERS RO4003 is not as suitable as the ROGERS RT5880 for this application.

The specifications of the microstrip line created in this project using ROGERS RO4003 are shown in Figure 5.1. In addition, in the table 5.1 the width values of the microstrip line are listed.

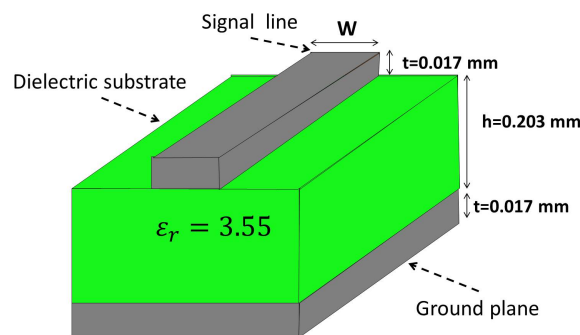


Figure 5.1: Microstrip line of the MIMO system

Width values (W) of the microstrip line	
W_{50}	0.4313 mm
W_{25}	1.184 mm
$W_{12.5}$	2.742 mm

Table 5.1: Width values (W) of the microstrip line

5.1 First fabricated MIMO system

The Figure 5.2 shows the fabricated MIMO antenna system. This system has exactly the same characteristics as the system described in the section 4.5, the only elements that have changed are the lengths of the stubs of the matching networks.

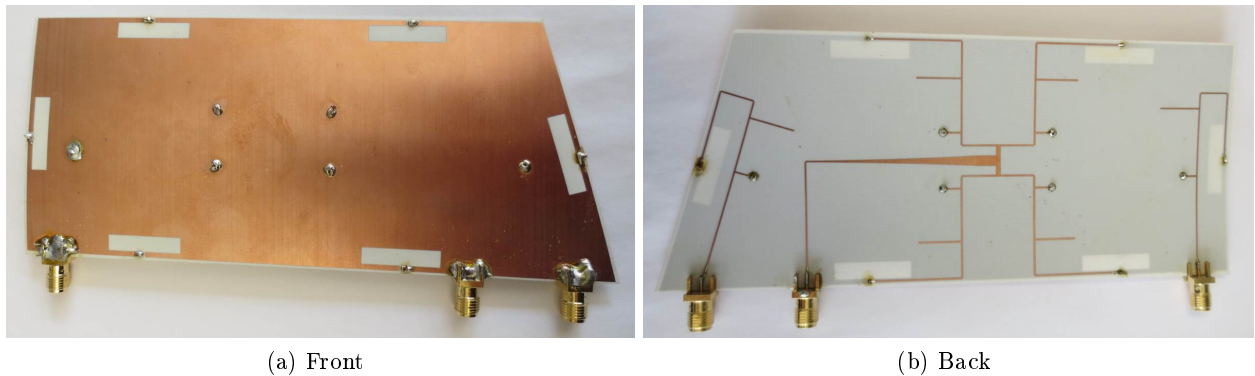


Figure 5.2: First fabricated MIMO antenna

5.1.1 Reflection coefficient measurements

In order to verify the performance of the fabricated circuit (Fig.5.2), the reflection coefficient of the system has been measured by VNA (Series Network Analyzer, E8363B, Agilent Technologies). The measurement of the reflection coefficient for the mode $J3$ has been done with an additional cable, as can be seen in the Figure 5.3. Two join the two cables connected to the two ports of the mode $J3$, a power divider had been used. Because of this power divider there is some reflection added to the measurement of the mode $J3$ as it can be seen in the Figure 5.4b. This behavior of the power divider is because it is not matched at 2.6 GHz.

As can be seen in the Figure 5.4, the matching point of the fabricated circuit had been moved to lower frequencies, this is due to tolerance of the circuit. As it was explained in the section 3.6, if some substrate is added in the borders of the MIMO antenna system the matching point will be moved towards lower frequencies. This tolerance problem could be solved using a CNC machine to fabricate the system.

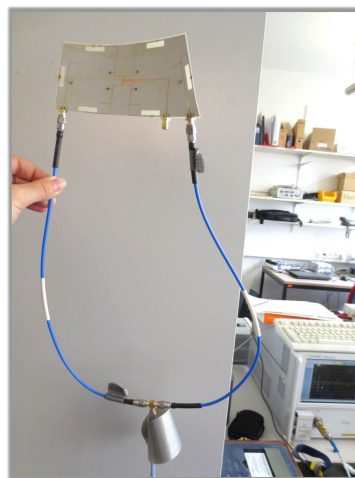
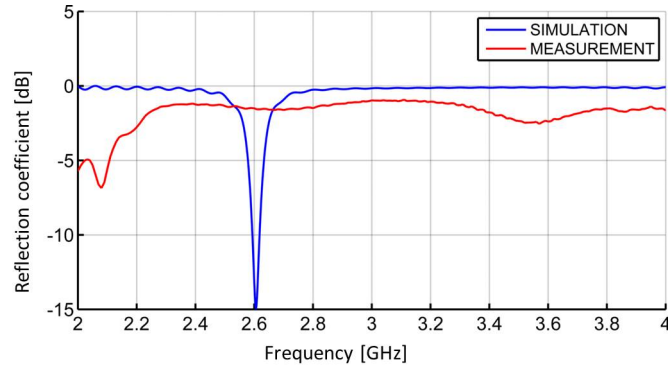
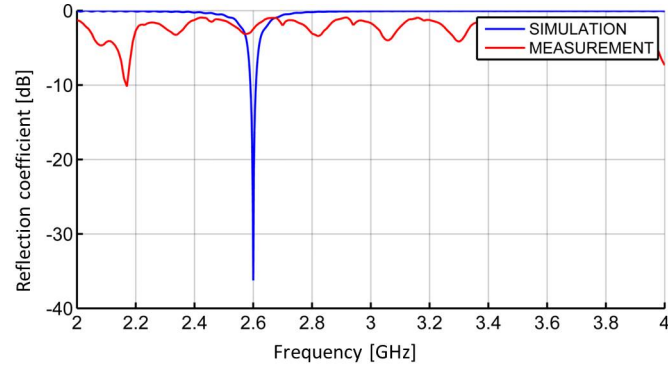


Figure 5.3: Measurement mode $J3$



(a) Reflection coefficient MODE 2

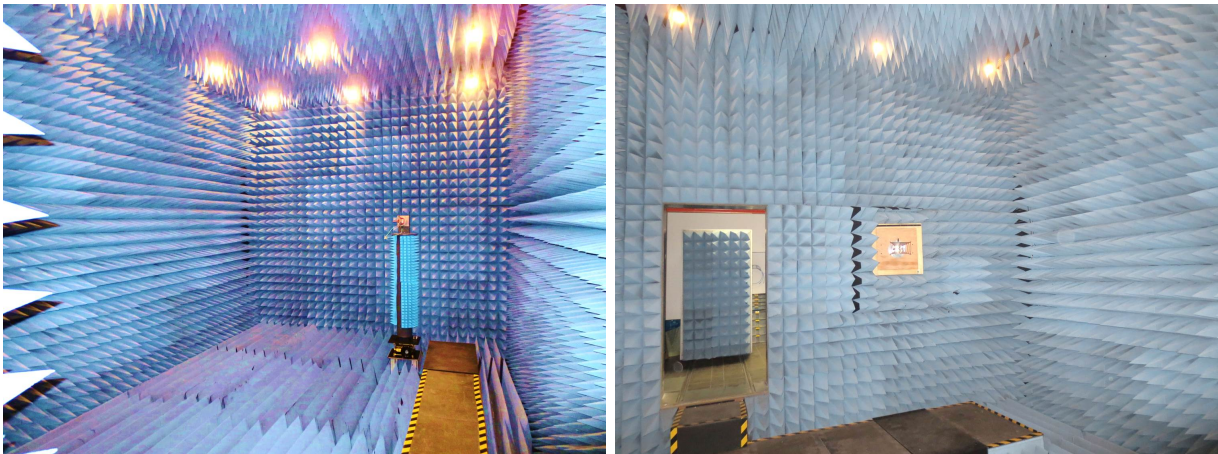


(b) Reflection coefficient MODE 3

Figure 5.4: Reflection coefficient first fabricated MIMO antenna system

5.1.2 Far field measurements

In this section the MIMO system radiation pattern measurements performed in the anechoic chamber are described. The anechoic chamber of the IHE institute can be seen in the Figure 5.5.



(a) Anechoic chamber

(b) Anechoic chamber

Figure 5.5: Anechoic chamber in the Institut für Hochfrequenztechnik und Elektronik (IHE)

The co-polarization and the cross-polarization of the MIMO antenna system have been measured in the anechoic chamber. The co-polarization is defined as that polarization that

the antenna is intended to radiate (receive) [37]. Whereas the cross-polarization is defined as the polarization orthogonal to the wanted polarization [37]. As the measurements of the reflection coefficient done in the previous section show that matched frequency has changed to around 2.2 GHz, the measurements of the co-polarization and the cross-polarization of the MIMO antenna system have been done at this frequency.

In the Figure 5.6 the measured cross-polarization and co-polarization of the antenna for the mode $J2$ can be seen. The Figure 5.7 represents the directivity patter of the mode $J2$ obtained in the simulation. Comparing the figure 5.6a with the figure 5.7 it can be conclude that the measurements are corresponding with the simulation. For example in the region from $\theta = 30^\circ$ to $\theta = 60^\circ$ the gain in the measurement and in the simulation has the same value (Gain=3.18 dB). However in the region from $\theta = -30^\circ$ to $\theta = -60^\circ$ there is a small mismatch of around 2 dB between the measurement and the simulation. Moreover, as it can be seen in the Figure 5.6b, the antennas system for the mode $J2$ have a low cross-polarization (below 0 dB).

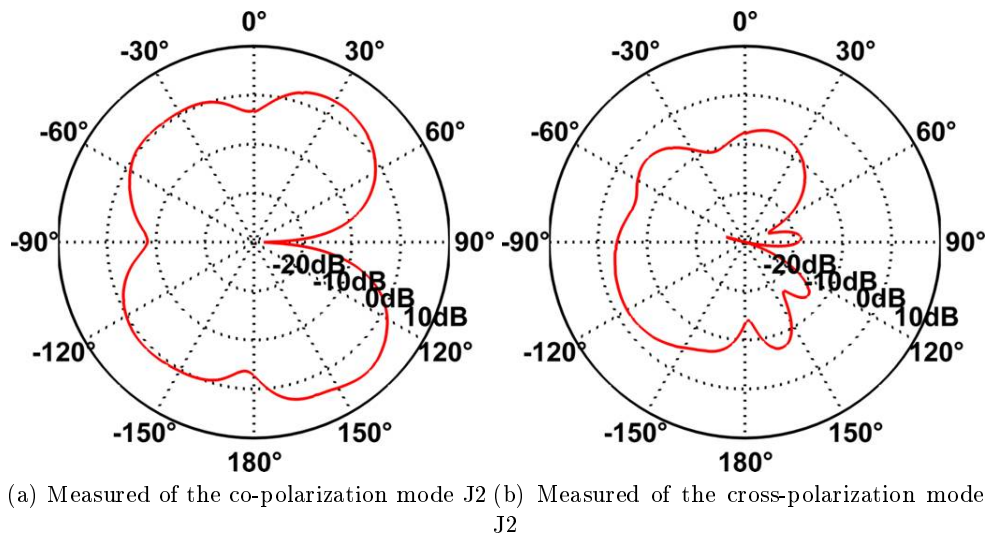


Figure 5.6: Measured directivity pattern at 2.2 GHz for $\theta = 90^\circ$ for mode J2

In the Figure 5.8 the measured cross-polarization and co-polarization of the antenna for the mode $J3$ can be seen. Unfortunately due to the substrate fragility the antenna was broken while performing the measurements. Consequently the measurements shown in the Figure 5.8

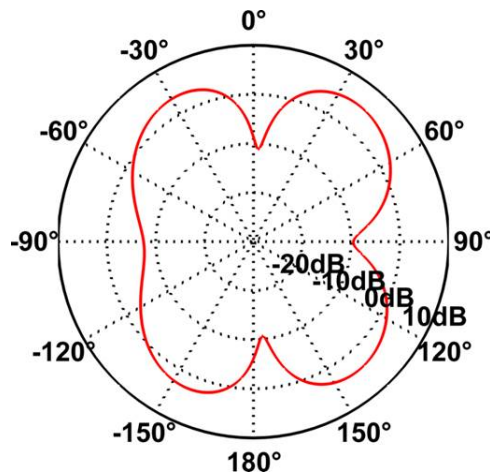


Figure 5.7: Simulated directivity pattern at 2.2 GHz for $\theta = 90^\circ$ for mode J2

can not be considered for characterization of the MIMO system. However the Figure 5.9 represents the directivity patter of the mode $J2$ obtained in the simulation. In this figure it can be seen that the simulated gain of the antenna system for the mode $J3$ is 3.18 dB in the main lobe ($\theta = 170^\circ$).

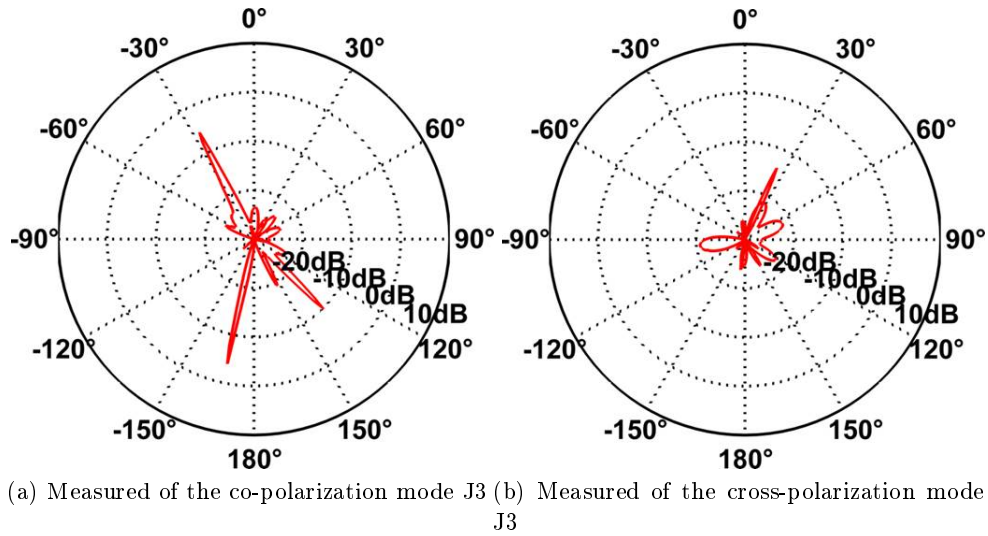


Figure 5.8: Measured directivity pattern at 2.2 GHz for $\theta = 90^\circ$ for mode J3

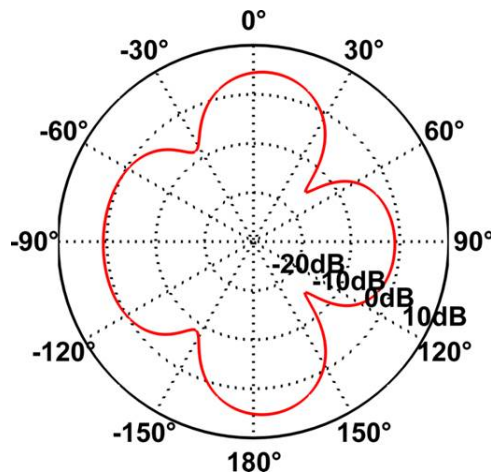


Figure 5.9: Simulated directivity pattern at 2.2 GHz for $\theta = 90^\circ$ for mode J3

5.2 Second fabricated MIMO system

After the fabrication of the antenna of the previous section, it was observed that improving the metallization of the vias is highly advantageous, because it makes the soldering of the vias easier. Therefore it was decided to fabricate a second circuit to include this same metallization in the vias that connect the slot line of the feeding network with the ground plane. The figure 5.10 shows this second fabricated MIMO antenna system. This system has exactly the same characteristics as the system described in the previous section since the metalization of the vias does not cause any change in the behavior of the system. Therefore in this case is not necessary to change the lengths of the stubs of the matching networks.

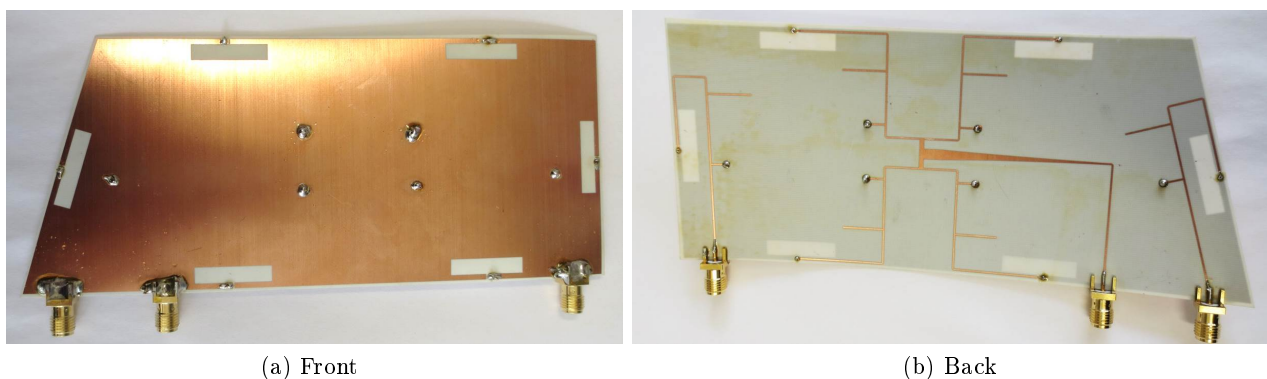


Figure 5.10: Second fabricated MIMO antenna

5.2.1 Reflection coefficient measurements

In order to verify the performance of the fabricated circuit (Fig.5.2), the reflection coefficient of the system has been measure by VNA (Series Network Analyzer, E8363B, Agilent Technologies).

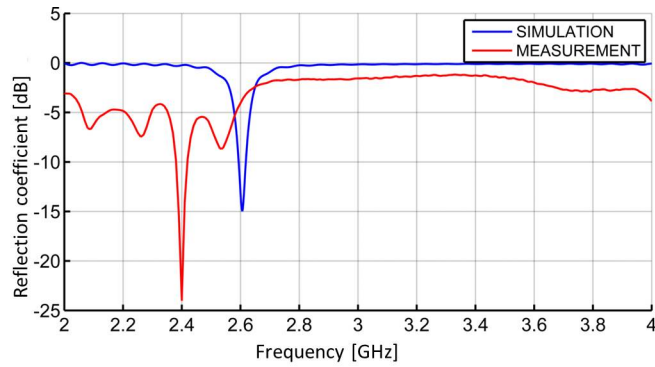
As can be seen in the Figure 5.11, the matching point of the second fabricated antenna is also shifted towards lower frequencies because of the fabrication tolerance. However the metallization of all the vias of the system makes the mismatch in frequency smaller. In the Figure 5.11a it can be seen that the mismatch of frequency is only from 2.6 GHz to 2.4 GHz.

5.3 Fabricated MIMO system on the side-mirror

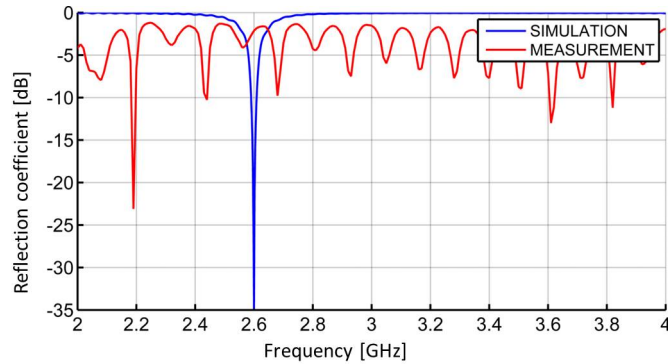
In the Figure 5.12 the fabricated MIMO antenna system placed on the side-mirror can be seen. This image is an example of how the MIMO antenna system should look like. In a real application the mirror should be cut and the MIMO antenna system should be glued using epoxy.

5.4 Conclusions

In this section a MIMO antenna system similar to the one described in the chapter 4. The difference between the fabricated MIMO antenna system and the one described in the chapter 4 is the material used in the design. The material used in the chapter 4 is ROGERS RT5880, which is a Teflon material with a great ease to be molded. However, the material used in



(a) Reflection coefficient MODE J2



(b) Reflection coefficient MODE J3

Figure 5.11: Reflection coefficient second fabricated MIMO antenna system

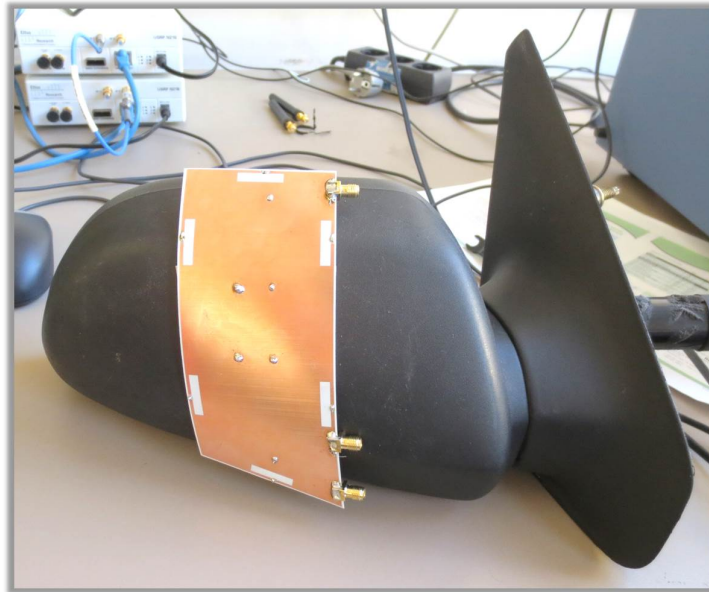


Figure 5.12: Fabricated MIMO system in the side-mirror

the fabrication of the antenna system in this chapter is ROGERS RO4003, which is a ceramic material. The ROGERS RO4003 can not be bent easily, which favors that the circuit will get broken when it is been used, as in the case of the measurement in the anechoic chamber for the mode J3.

First, from the measurements of the reflection coefficient, a frequency mismatching be-

tween the simulation and the measurements can be observed. This frequency mismatching is produce due to the excess of substrate around the fabricated system. This excess of substrate around the fabricated system can be avoided using a CNC machine to fabricate the MIMO antenna system.

On the other hand, the measurements of the radiation pattern of the J2 characteristic mode performed in the anechoic chamber show that there is a a reciprocity between the measurement and simulation. Therefore it can be concluded that the fabricated MIMO antenna system does not have a great loss in gain with respect to the simulated system.

To sum up, it can be conclude that the results have not been entirely satisfactory, however this was expected due to the type of material used for the manufacture of the MIMO antenna system.

6

MIMO antenna system in the side-mirror

6.1 Introduction

The design of the side-mirror in which the MIMO system is implanted is based on the study presented in [20]. In [20] it is clarified that the esthetic design of the side-mirror is more important than a good aerodynamic design. Therefore in this project have not been studied the aerodynamic properties of the side-mirror.

In the Figure 6.1 the MIMO system implemented in the side-mirror can be seen.

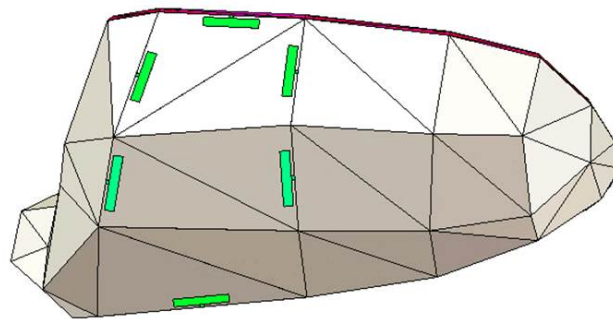


Figure 6.1: MIMO system in the side-mirror

To install the MIMO system in the car, different factors should be taken into account. These factors are listed in the following sections.

6.2 Attachment of the MIMO system with the side-mirror

The first factor that must be taken into account is how the MIMO system is going to be placed in the side-mirror. To fulfill this goal a powerful adhesive like epoxy [26] or acrylnitrilbutadienstyrol (ABS) [27] must be used. In this project epoxy adhesive is used, as the parameters of this material are well defined in CST. In the Figure 6.2a, the MIMO antenna surrounded by

the epoxy adhesive can be seen. Adding this glue to the structure does not cause any change to the system, leaving the reflection coefficient of the system intact (Figure 6.2b).

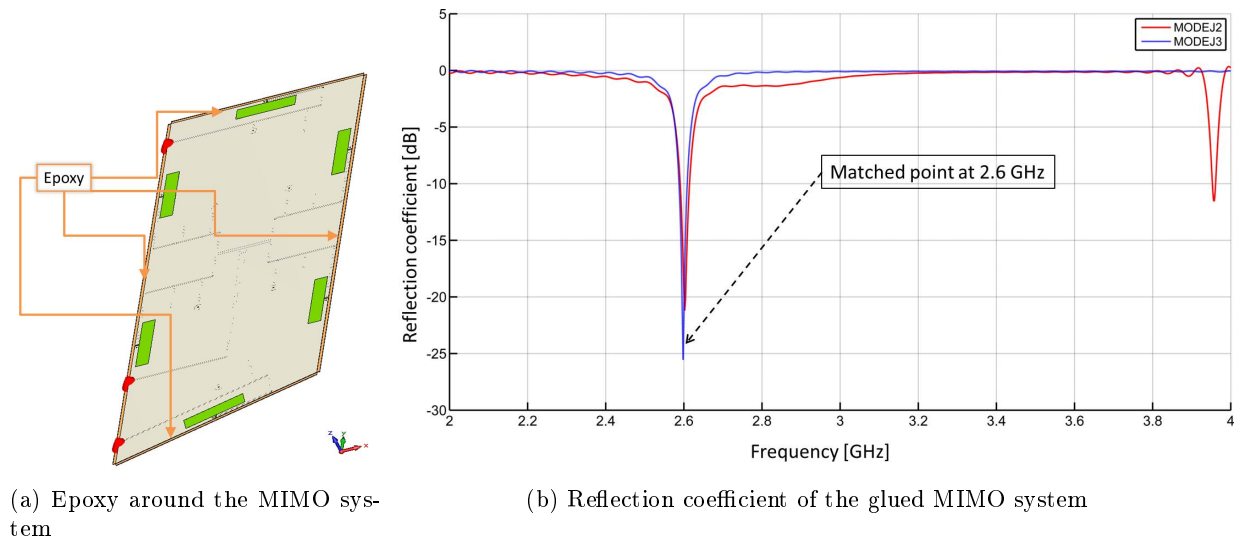


Figure 6.2: Glued MIMO system

6.3 MIMO system in the side-mirror

The next factor to be considered is how the rest of the metallic structure of the side-mirror will affect the MIMO system. In the Figure 6.3a two metallic blocks, to mimic the rest of the metallic structure of the side-mirror, had been added at the sides of the MIMO system. In this figure it is taken under consideration that the top and bottom of the MIMO system will be attached to the plastic part of the side-mirror. As can be seen in the Figure 6.3b, the only reflection coefficient that is affected is the one corresponding to mode $J2$. This is because the base of the Inductive Coupling Elements of the mode $J2$ are very close to the rest of the metallic structure of the side-mirror, and thus a frequency shift occurs.

There are at least two ways to solve this frequency shift. The first one is to take this effect in to account while designing the MIMO system. Thus, if the type of side-mirror metal is known, the matching networks of the MIMO system can be modified to match the system again to 2.6 GHz.

Another solution is to isolate Inductive Coupling Elements from the rest of the metallic structure of the side-mirror. Therefore it is necessary to add polyamide frame around the radiating structure. If a polyamide structure is added to the sides of the MIMO system, the system is not affected by the rest of the metallic structure of the side-mirror. The investigation have proved that the MIMO system will be isolated if between the MIMO system and the rest of the metallic structure of the side-mirror a polyamide block is placed. This polyamide block thickness must be at least 2.5 cm. A schema of the final isolated structure is shown in the Figure 6.4a. In the Figure 6.4b the reflection coefficient of the system after the isolation can be seen. Moreover, a possible aesthetic solution suitable for this propose is to use some tuning elements to design the side-mirror, as it can be seen in the Figure 6.5.

6.4 Influence of painting the car bodywork elements

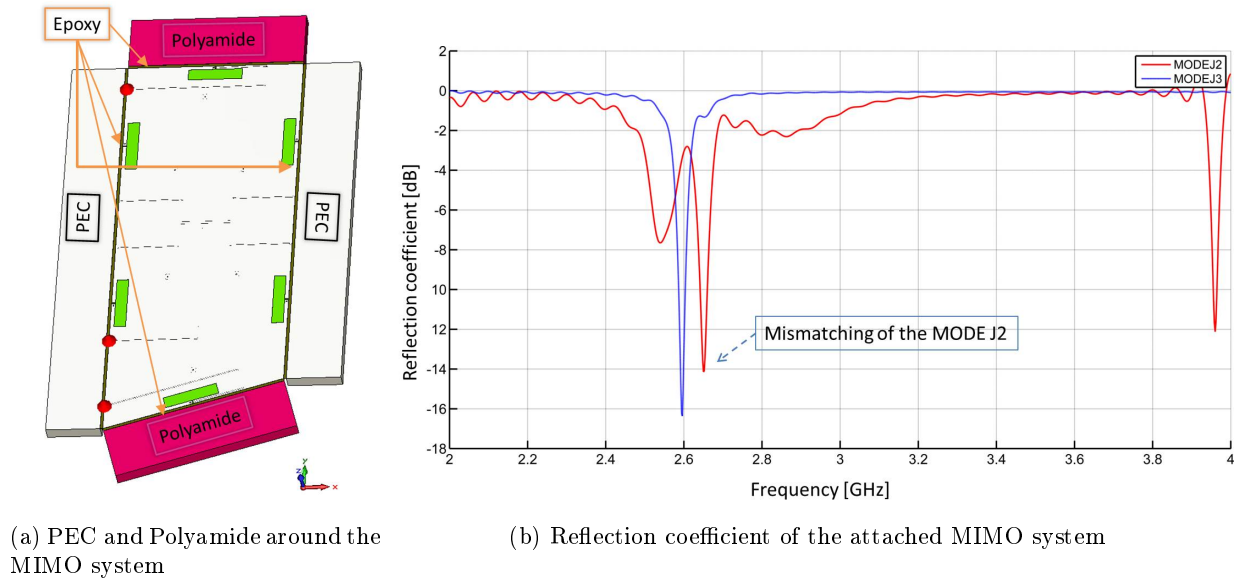


Figure 6.3: Attached MIMO system to the side-mirror

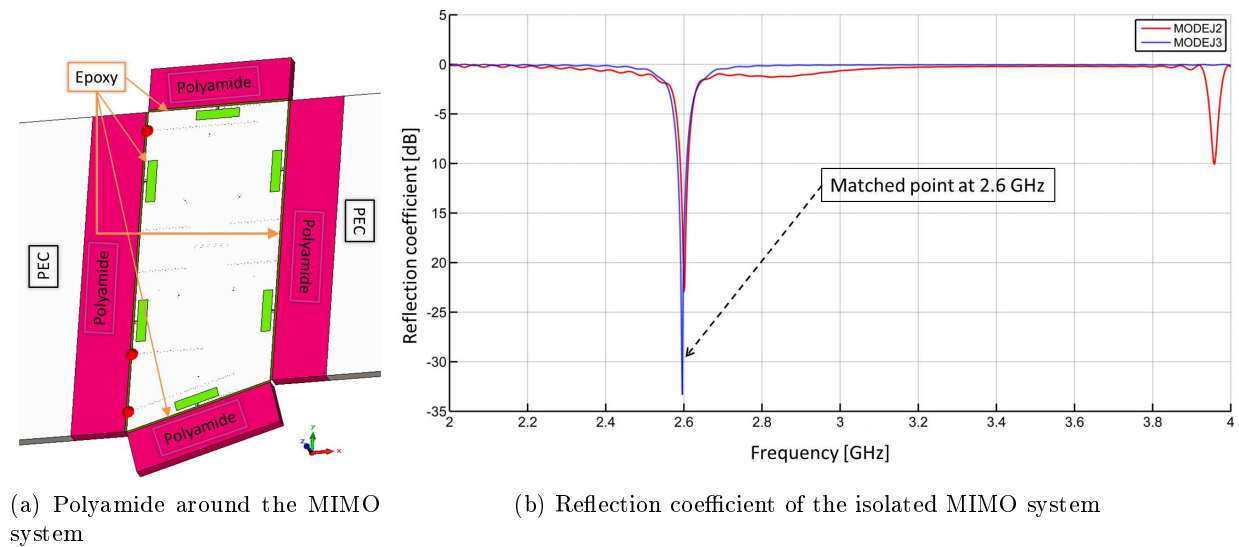


Figure 6.4: Isolated MIMO system to the side-mirror

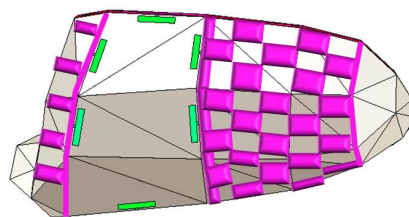


Figure 6.5: Tuning for the MIMO system

When the MIMO antenna fabricated in this project are designed, it is indispensable to take possible variations in the manufacturing process into account. One of this possible variation is the impact of adding the paint that covers the bodywork of the vehicle. In this section the behavior of the MIMO system when this paint is added is simulated. The paint should be considered in

the design because it acts as a protection for the MIMO system. The main ingredient of this paint are pigments of aluminum, this material gives a bright and metallic appearance to the side-mirror. Each type of paint has a concrete defined thickness. The parameters of the paint in this section are based on the study in [21]. Based on this study, a layer of aluminum paint with a thickness of 0.127 mm has been added to a MIMO system. This design can be seen in the Figure 6.6.

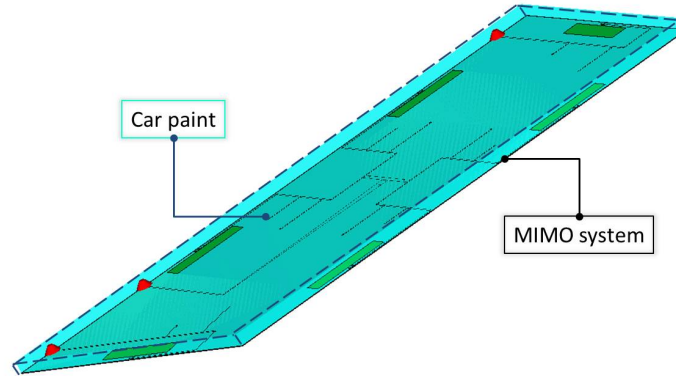
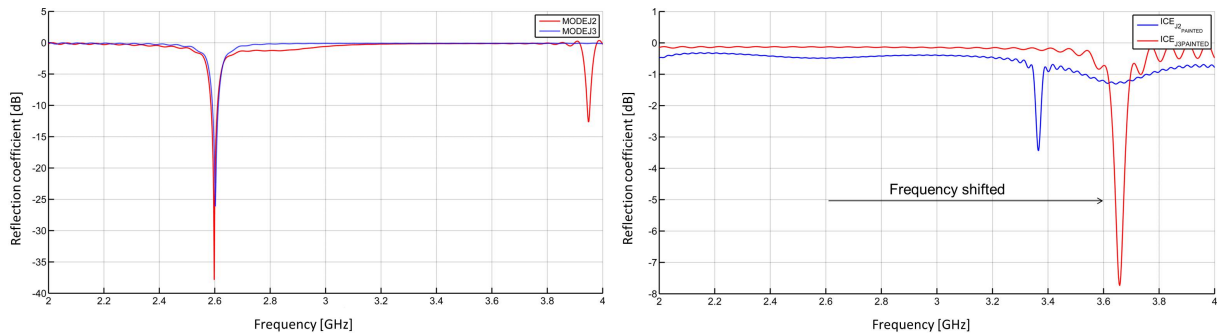


Figure 6.6: Painted MIMO system

The Figure 6.7a shows the reflection coefficient of the MIMO system before being painted. The Figure 6.7b shows the reflection coefficient of the MIMO system after painting. Seeing these two figures it can be concluded that the use of paint to cover the MIMO system causes a shift in the matched frequency. This frequency shift could be corrected easily by changing the matching network used in the MIMO system. Therefore it is required to make a study of the impact of the car paint in the MIMO system.



(a) Reflection coefficient of the NO painted MIMO system (b) Reflection coefficient of the painted MIMO system

Figure 6.7: Painted MIMO system

6.5 Feeding the MIMO system with a mini-coaxial cable

Using SMA connectors for feeding appears to be complicated in the side-mirror. Therefore in this section is proposed the used of 50 Ω mini-coaxial cable for this purpose. According to [28], [29], [30] and [31], a mini-coaxial cable as the outlined in the Figure 6.8a, could be used to transfer current to the microstrip line of the feeding network.

The dimension of the mini-coaxial cable can be seen in 6.8b, where $A=0.3797$ mm and $B=1.2714$ mm. An example of the existing mini-coaxial cable on the market can be found in [46] or [47].

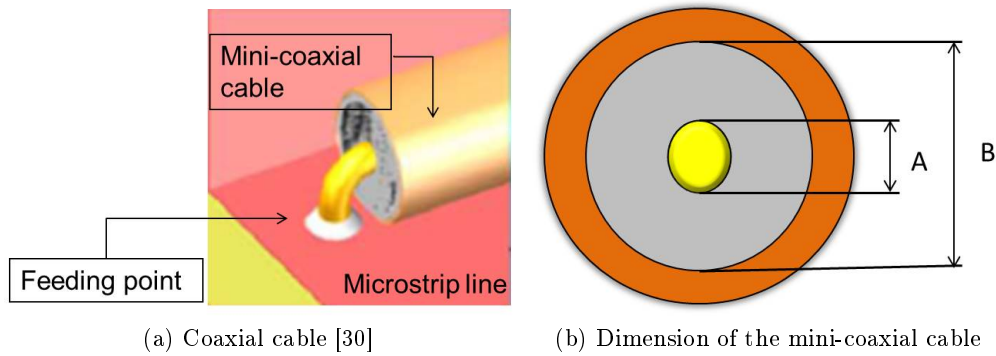
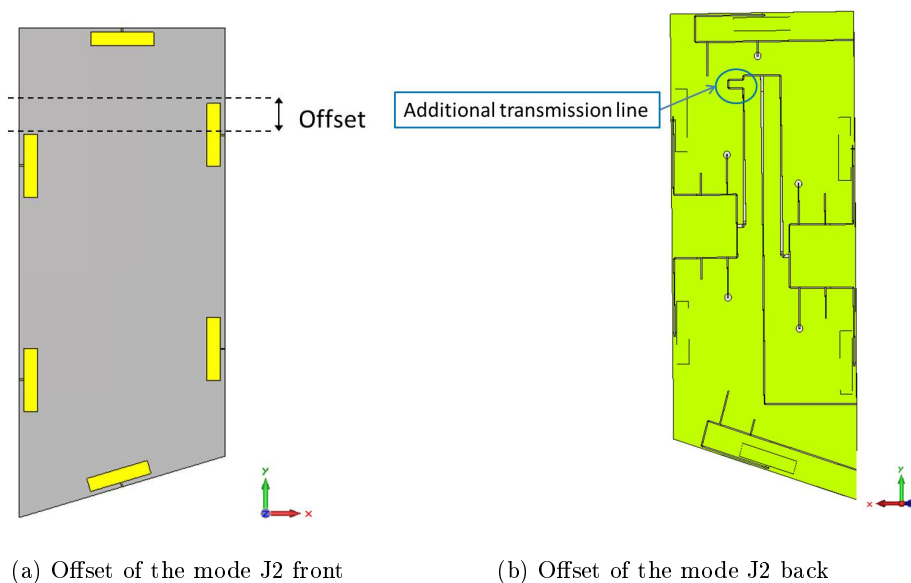


Figure 6.8: Feeding the MIMO system with a coaxial cable

6.6 Other considerations in the design of the MIMO system for the side-mirror

Recently the automotive industry tends to use the most advanced technologies. Therefore modern companies demand access to the newest technologies. Therefore if this MIMO system should be further developed into market-ready system, more factors must be taken into account. One of the most important factors is the geometry of the side-mirror. As explained in section 4.6, the Inductive Coupling Elements for the mode $J2$ must be facing two-to-two. However sometimes the structure of a side-mirror does not allow this feature, because there is not enough space in front of each Inductive Coupling Element. An example of the circuit is presented in the Figure 6.9. In this circuit it can be seen that the Inductive Coupling Elements are not faced two-to-two. However this does not affect the characteristics of the MIMO system. This problem only affects the design of the feeding network. It is necessary to add an additional segment of transmission line to compensate the phase shift between the ports of the Inductive Coupling Elements of the mode $J2$ (Figure 6.9b).

Figure 6.9: Offset of the mode $J2$

6.7 Conclusions

The integration and iteration of the MIMO antenna system inside a car bodywork element was analyzed in this section. Several simulations and measurements corroborate that this MIMO antenna system is suitable for automotive applications.

The goal of this section has been to study the behavior of the MIMO system when it is placed in the side-mirror. First it was necessary to attach the MIMO antenna system to the side-mirror, what can be done using epoxy. If an epoxy frame is placed around the MIMO antenna system the behavior of this does not change. Confirming that epoxy can be used to adhere the MIMO antenna system to the side-mirror.

Furthermore, in this section it has been studied how the rest of the metallic structure of the side-mirror influences the MIMO antenna system. After this study it can be concluded that it is necessary to isolate the MIMO system from the rest of the metallic structure of the side-mirror, this can be done by inserting plastic around the structure.

Another consideration carried in this section is the study of car metallic paint on the performance of the MIMO antenna system. From this it can be conclude that for future design of the MIMO antenna system the metallic paint of the car should be taken into account as it changes the matching frequency point.

In addition the feeding of the MIMO antenna system using a mini-coaxial cable has been proposed in this section. Likewise possible variation in the geometry of the side-mirror has been also considered in this section.

Finally, the influence of car's body on antenna performance was studied. In order to emulate the structure of the car a block of metal was placed 60 mm away from the MIMO antenna system. After the simulations, and combining the results from this simulation with the results of aerodynamics studies in [20], it is concluded that placing the side-mirror as far as possible from car's body is optimal for both aerodynamics and electrical compatibility. The regulations allow the mirror to protrude no more than (both sides included) 62.5 mm from the widest part of the car body. If the side-mirror is designed in this maximum distance, the behavior of the MIMO system will not be affected.

7

Conclusions

In this chapter a summary of the work carried out in this master thesis is presented, and conclusions extracted from the obtained results are drawn. In this master thesis a MIMO antenna system based on the excitation of car body elements has been designed. To design this system Inductive Coupling Elements have been used.

In the first place, the first three characteristic modes that could be excited on a rectangular metallic plate have been studied. For each of this characteristic modes a prototype circuit has been fabricated. From the simulation of this prototypes it can be conclude that the reflection coefficient for this three characteristic modes show that an inductive coupling elements can be successfully matched at 2.6 GHz using double tuning stubs circuits. Whereas the measurements of the fabricated prototype circuits show that this fabricated circuits do not function as expected from the simulation. However the fabricated circuits can be carefully redesigned in order to improve their performance.

Using the acquired knowledge of the characteristic modes, a single-layer MIMO antenna system has been design. This single-layer MIMO antenna system implements a combination of the characteristic modes J2 and J3. The use of the combination of this two characteristic modes will generate a beneficial directivity pattern, allowing a reception from all the directions around the antenna. Furthermore, using the combination of the modes J2 and J3 the channel capacity is increased. The feeding of this MIMO antenna system has been done using a microstrip line. From this design it can be conclude that a MIMO system matched at 2.6 GHz can be fabricated using Inductive Coupling Elements and a microstrip line as a feeding network.

As ROGERS RT5880 material used for the design of the MIMO antenna system was not available, ROGERS RO4003 which is a ceramic material was used to fabricate a prototype. The ROGERS RT5880 material is a Teflon based material which makes it a flexible material. However, the ROGERS RO4003 material is based on ceramic which makes it a fragile material. The fragility of the ROGERS RO4003 material favors that the circuit will get broken when it is been used, as in the case of the measurement in the anechoic chamber for the mode J3. Moreover, from the measurements of the reflection coefficient of the fabricated MIMO antenna system, a frequency shift between the simulation and the measurements is observed. This frequency shift is a result of the excess of substrate around the fabricated system. This excess of substrate around the fabricated system can be avoided using a CNC machine to fabricate the MIMO antenna system.

On the other hand, for the fabricated MIMO antenna system, the measurements of the radiation pattern of the J2 characteristic mode performed in the anechoic chamber show that there is a reciprocity between the measurements and the simulation. Therefore it can be concluded that the fabricated MIMO antenna system does not have a great loss in gain with respect to the simulated system.

Finally, the integration of the MIMO antenna system inside a car's side-mirror has been analyzed. Several simulations and measurements corroborate that the MIMO antenna system designed during this master thesis is suitable for automotive applications. Furthermore, it was investigated how the rest of the metallic structure of the side-mirror influences in the MIMO antenna system. After this study it can be concluded that it is necessary to isolate the MIMO system from the rest of the metallic structure of the side-mirror. This can be done by inserting plastic around the structure.

Another consideration carried out in this master thesis was how the MIMO antenna system behaves when it is covered with car metallic paint. From this investigation, it can be concluded that for future design of the MIMO antenna system the paint of the car should be taken into account as it changes the matching frequency point. In addition the feeding of the MIMO antenna system using a mini-coaxial cable has been proposed in this master thesis. Moreover, possible variation in the geometry of the side-mirror has been also considered.

8

Future work

To continue with the work carried out on this project, it intends to perform the same type of microstrip line circuit using a multi-layer structure and compare the results with those obtained in this project. A multi-layer structure is complex and expensive to be fabricated. In the Figure 8.1 a schematic of how this multi-layer circuit could be is shown.

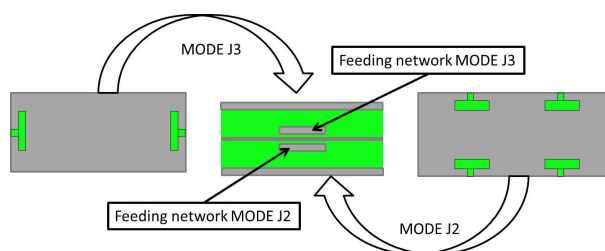


Figure 8.1: Multi-layer MIMO system

On the other hand, if new designs of a single-layer system should be performed, there are several factors that should be considered in the future. The most of this factors are related with the improvement of the fabrication process. The first of this factors is the tolerance of the circuit. In future designs the possibility of using a CNC machine to fabricate the system should be considered. The use of this machine would avoid the tolerance problems of the system.

In addition, another factor is associated with the design of the ports at the end of the microstrip line. In the system designed in this project the connection between the feeding network and the measurement equipment is made using SMA connectors. Therefore to avoid alterations in the line width, the end ports must be designed perpendicular to the edge of the metallic plate as is it shown in the figure 8.2. In future systems all the ports should be designed in this way.



Figure 8.2: SMA connected at the end of the microstrip line port

Another possible line of future work could be the study of the total Multi-Port Return Loss as a Figure of Merit for MIMO antenna systems [38].

Furthermore, other substrates that are easier to be bent should be investigated. This would result in a better adaptation of the system to the automotive industry.

Bibliography

- [1] M. Cabedo-Fabres, E. Antonino-Daviu, A. Valero-Nogueira, and M.F. Bataller. The Theory of Characteristic Modes Revisited: A Contribution to the Design of Antennas for Modern Applications. *Antennas and Propagation Magazine, IEEE*, 49(5):52–68, 2007.
- [2] R.J. Garbacz and R. Turpin. A generalized expansion for radiated and scattered fields. *Antennas and Propagation, IEEE Transactions on*, 19(3):348–358, May 1971.
- [3] Roger F. Harrington and J.R. Mautz. Theory of characteristic modes for conducting bodies. *Antennas and Propagation, IEEE Transactions on*, 19(5):622–628, Sep 1971.
- [4] Roger F. Harrington and J.R. Mautz. Computation of characteristic modes for conducting bodies. *Antennas and Propagation, IEEE Transactions on*, 19(5):629–639, Sep 1971.
- [5] R.J. Garbacz and David M. Pozar. Antenna shape synthesis using characteristic modes. *Antennas and Propagation, IEEE Transactions on*, 30(3):340–350, May 1982.
- [6] D. Liu, R.J. Garbacz, and David M. Pozar. Antenna synthesis and optimization using generalized characteristic modes. *Antennas and Propagation, IEEE Transactions on*, 38(6):862–868, Jun 1990.
- [7] Roger F. Harrington and J.R. Mautz. Control of radar scattering by reactive loading. *Antennas and Propagation, IEEE Transactions on*, 20(4):446–454, Jul 1972.
- [8] K.Y. Kabalan, A. El-Haji, and R.F. Harrington. Characteristic modes of a slot in a conducting cylinder and their use for penetration and scattering, TE case. *Microwaves, Antennas and Propagation, IEE Proceedings H*, 139(3):287–291, Jun 1992.
- [9] A. El-Hajj and K.Y. Kabalan. Characteristic modes of a rectangular aperture in a perfectly conducting plane. *Antennas and Propagation, IEEE Transactions on*, 42(10):1447–1450, Oct 1994.
- [10] Constantine A. Balanis. *Antenna Theory. Analysis and Design*. John Wiley and Sons Inc, 3 edition, 2005.
- [11] David M. Pozar. *Microwave Engineering*. John Wiley and Sons Inc, 4 edition, 2012.
- [12] R. Martens and D. Manteuffel. A feed network for the selective excitation of specific characteristic modes on small terminals. In *Antennas and Propagation (EUCAP), 2012 6th European Conference on*, pages 1842–1846, 2012.
- [13] S.K. Chaudhury, W.L. Schroeder, and H.J. Chaloupka. MIMO antenna system based on orthogonality of the characteristic modes of a mobile device. In *Antennas, 2007. INICA '07. 2nd International ITG Conference*, pages 58–62, 2007.
- [14] R. Martens, E. Safin, and D. Manteuffel. Inductive and capacitive excitation of the characteristic modes of small terminals. In *Antennas and Propagation Conference (LAPC), 2011 Loughborough*, pages 1–4, 2011.

- [15] D. Manteuffel and R. Martens. A concept for MIMO antennas on small terminals based on characteristic modes. In *Antenna Technology (iWAT), 2011 International Workshop on*, pages 17–20, 2011.
- [16] R. Martens, E. Safin, and D. Manteuffel. Selective excitation of characteristic modes on small terminals. In *Proceedings of the 5th European Conference on Antennas and Propagation (EUCAP)*, pages 2492–2496, 2011.
- [17] W.L. Schroeder, A.A. Vila, and C. Thome. Extremely Small, Wide-band Mobile Phone Antennas by Inductive Chassis Mode Coupling. In *Microwave Conference, 2006. 36th European*, pages 1702–1705, 2006.
- [18] S.K. Chaudhury, H.J. Chaloupka, and A. Ziroff. Multiport antenna systems for MIMO and diversity. In *Antennas and Propagation (EuCAP), 2010 Proceedings of the Fourth European Conference on*, pages 1–5, 2010.
- [19] E. Antonino-Daviu, M. Fabres, M. Ferrando-Bataller, and V.M.R. Penarrocha. Modal Analysis and Design of Band-Notched UWB Planar Monopole Antennas. *Antennas and Propagation, IEEE Transactions on*, 58(5):1457–1467, 2010.
- [20] Martin Olsson. Designing and Optimizing Side-View Mirrors. 2011.
- [21] I.J.G. Zuazola, A. Sharma, J.C. Batchelor, I. Angulo, A. Perallos, W.G. Whittow, J.M.H. Elmighani, and R. Langley. Radio frequency identification miniature interrogator antenna sprayed over an in-vehicle chassis. *Microwaves, Antennas Propagation, IET*, 6(15):1674–1680, December 2012.
- [22] Mauro Biagi and Enzo Baccarelli. A simple multiple-antenna ultra wide band transceiver scheme for 4th generation wlan. In *Vehicular Technology Conference, 2003. VTC 2003-Fall. 2003 IEEE 58th*, volume 3, pages 1903–1907 Vol.3, Oct 2003.
- [23] Niels Koch. Antennas for automobiles, new advances in vehicular technology and automotive engineering. 2012.
- [24] Brendan Pell Edin Sulic Wayne Rowe Kamran Ghorbani Sabu John. Antennas for automobiles. new advances in vehicular technology and automotive engineering. 2012.
- [25] E. Gschwendtner, D. Loffler, and W. Wiesbeck. Spiral antenna with external feeding for planar applications. In *Africon, 1999 IEEE*, volume 2, pages 1011–1014 vol.2, 1999.
- [26] A. Kilian, J. Weinzierl, and L. Schmidt. Investigation of the hot embossing technology for low-cost antennas printed on polymer substrates. In *Microwave Conference, 2008. EuMC 2008. 38th European*, pages 1–4, Oct 2008.
- [27] A. Kilian and L. Schmidt. A novel fabrication process for printed antennas integrated in polymer multi-layer car body panels. In *Microwave Conference, 2009. EuMC 2009. European*, pages 578–581, Sept 2009.
- [28] Saou-Wen Su and Fa-Shian Chang. Compact coaxial-line-fed printed monopole antenna for lower-band ultrawideband applications. In *Antennas and Propagation Society International Symposium, 2009. APSURSI '09. IEEE*, pages 1–4, June 2009.
- [29] Saou-Wen Su, Tzi-Chieh Hong, and Fa-Shian Chang. Compact and printed, coupled-fed, 2.4 ghz loop antenna. In *Applications of Electromagnetism and Student Innovation Competition Awards (AEM2C), 2010 International Conference on*, pages 157–161, Aug 2010.

- [30] Chia-Mei Peng, I-Fong Chen, Ching-Chih Hung, Su-Mei Shen, Chia-Te Chien, and Chih-Cheng Tseng. Bandwidth enhancement of internal antenna by using reactive loading for penta-band mobile handset application. *Antennas and Propagation, IEEE Transactions on*, 59(5):1728–1733, May 2011.
- [31] Cheng-Tse Lee, Saou-Wen Su, and Fa-Shian Chang. Novel, compact, flat-plate antenna for 2.4/5.2/5.8-GHz WLAN operation. In *Antennas and Propagation (EUCAP), 2012 6th European Conference on*, pages 1847–1850, March 2012.
- [32] S. Blanch, J. Romeu, and I. Corbella. Exact representation of antenna system diversity performance from input parameter description. *Electronics Letters*, 39(9):705–707, May 2003.
- [33] S.L.Zuo, Y.Z.Yin, W.J.Wu, Z.Y.Zhang, and J.Ma. Investigations of reduction of mutual coupling between two planar monopoles using two slots. 19:9–18, 2010.
- [34] Y.A.S.Dama, R.A.Abd-Alhameed, S.M.R.Jones, D.Zhou, N.J.McEwan, M.B.Child, and P.S.Excell. An envelope correlation formula for (n,n) mimo antenna arrays using input scattering parameters, and including power losses. *International Journal of Antennas and Propagation*, August 2011.
- [35] George Tatsis Constantinos Votis and Panos Kostarakis. Envelope correlation parameter measurements in a mimo antenna array configuration. *Int. J. Communications, Network and System Sciences*, April 2010.
- [36] S. Zhang, A.A. Glazunov, Z. Ying, and S. He. Reduction of the envelope correlation coefficient with improved total efficiency for mobile lte mimo antenna arrays: Mutual scattering mode. *Antennas and Propagation, IEEE Transactions on*, 61(6):3280–3291, June 2013.
- [37] Ieee standard definitions of terms for antennas. *IEEE Std 145-1993*, pages 1–32, July 1993.
- [38] W.L. Schroeder and A. Krewski. Total multi-port return loss as a figure of merit for mimo antenna systems. In *Microwave Conference (EuMC), 2010 European*, pages 1742–1745, Sept 2010.
- [39] Servicios Inalambricos. Como elegir una antena, 2012.
- [40] Graph Software for Scientists and Engineers. BESSELJ(x,order), 2013.
- [41] Teletech Aerials, 2012.
- [42] Air-Stream Wireless Incorporated. Antenna polarisation, 2010.
- [43] Rockshore.
- [44] Alphaomegaem.
- [45] Auto-types.
- [46] I-PEX.
- [47] Hirose Electric.

Appendices



Introducción

A.1 Motivación

En los últimos años, las personas pasan más y más tiempo en sus coches, esto significa que los coches son esenciales en nuestra sociedad. En consecuencia los consumidores cotidianos exigen más servicios en sus coches. Esta demanda conduce a un creciente desarrollo de las nuevas tecnologías en los vehículos. Estas nuevas tecnologías promueven la mejora de diferentes factores tales como el tamaño del producto, la reducción del precio del producto y una mejor adaptación del producto con el medio ambiente. Ergo hay una constante investigación y desarrollo de nuevas soluciones que proporcionan una alta calidad de servicio. El aumento en la cantidad de servicios como la radio, la navegación GPS, la TV o el teléfono requieren un continuo aumento de la cantidad de antenas instaladas en un coche. Sin embargo, el número de lugares adecuados para posicionar estas antenas en el coche está disminuyendo.

La demanda de más servicios requiere mayores velocidades de datos que pueden ser llegadas a cabo por sistemas de antenas Multiple-Input Multiple-Output (MIMO) [22, 23, 24]. MIMO es una parte esencial de todos los futuros estándares inalámbricos móviles [18]. Por lo tanto, el diseño de un sistema de antenas MIMO para vehículos es un gran atractivo en la industria del automóvil.

Además, como la localización adecuada de un sistema de antenas dentro de los vehículos está limitada, ya sea por las especificaciones de diseño o por posibles interferencias con otros equipos electrónicos, se debe considerar el uso de antenas de tamaño reducido. Así, el diseño de un sistema MIMO basado en la generación de modos característicos en los elementos de la carrocería de un coche [1, 2, 3, 4, 5, 6, 7] parece ser una solución prometedora para cubrir la creciente demanda de servicios móviles en automóviles. Si a la ventaja de una alta velocidad de datos y un tamaño reducido, se le añade la facilidad de fabricación y el bajo coste de los circuitos de microstrip, un sistema de antenas de comunicación puede ser diseñado.

Debido a las razones nombradas anteriormente, un sistema de antenas MIMO [13, 15, 18] basado en la excitación de los elementos de carrocería de automóviles utilizando elementos de acoplamiento inductivo con una red de alimentación microstrip es desarrollado y verificado en este proyecto final de carrera.

A.2 Objetivos

El objetivo general de este proyecto es el diseño, construcción y medida de un sistema de antenas MIMO utilizando elementos de acoplamiento inductivo. La banda de funcionamiento de este sistema de antenas es desde 2.5 GHz hasta 2.7 GHz, esta banda de frecuencia es usada en LTE (Long Term Evolution).

Los objetivos de este proyecto son los siguientes:

- 1) Estudio de las posibilidades de la excitación multimodo de los elementos de carrocería de automóviles
- 2) Diseño y optimización de elementos de acoplamiento inductivo en una placa metálica
- 3) Diseño de una red de alimentación para los elementos de acoplamiento inductivo utilizando la tecnología microstrip y las redes de adaptación
- 4) Fabricación de un prototipo para los diferentes modos característicos
- 5) Diseño de un sistema MIMO utilizando elementos de acoplamiento inductivo con la red de alimentación
- 6) Fabricación del sistema MIMO

A.3 Estructura del documento

Este documento está estructurado de la siguiente manera:

- **Capítulo 1: Introducción**
Presentación de la motivación para el proyecto, sus objetivos y la estructura de la memoria.
- **Capítulo 2: Estado del arte**
Descripción del estado del estado del arte, profundización en los sistemas MIMO, en los modos característicos y en la tecnología microstrip.
- **Capítulo 3: Red de alimentación para los elementos de acoplamiento inductivo**
El diseño completo de la red de alimentación está organizado en tres partes:
 - Diseño y caracterización de los elementos de acoplamiento inductivo
 - Diseño de la red de alimentación para cada uno de los modos característicos
 - Fabricación de prototipos y verificación experimental
- **Capítulo 4: Sistema de antenas MIMO basado en la excitación de los elementos de la carrocería de vehículos automóviles**
Diseño del sistema MIMO aplicando los conocimientos adquiridos sobre elementos de acoplamiento inductivo en la generación de modos característicos.
- **Capítulo 5: Fabricación del sistema MIMO**
El proceso de fabricación del sistema MIMO y sus resultados experimentales se detallan en este capítulo.
- **Capítulo 6: sistema de antenas MIMO en el espejo retrovisor**
La implementación final del sistema MIMO en el espejo retrovisor se describe en este capítulo.

- **Capítulo 7: Trabajo futuro**

Finalmente, este capítulo sugiere posibles mejoras y futuras líneas de trabajo.

B

Conclusiones

En este capítulo se describe un resumen del trabajo llevado a cabo en este proyecto final de carrera, y se detallan las conclusiones extraídas de los resultados obtenidos. En este proyecto final de carrera se ha diseñado un sistema de antenas MIMO basado en la excitación de los elementos de la carrocería de un coche. En el diseño de este sistema se ha utilizado elementos de acoplamiento inductivo.

En primer lugar, se han estudiado los tres primeros modos característicos que podrían ser excitados en una placa metálica rectangular. Para cada uno de estos modos característicos se ha fabricado un prototipo. A partir de la simulación de estos prototipos se puede concluir que el coeficiente de reflexión para estos tres modos característicos muestra que los elementos de acoplamiento inductivo pueden ser adaptados con éxito a 2.6 GHz usando una red de adaptación de doble-stub. Mientras que las mediciones de los prototipos fabricados muestran que estos circuitos fabricados no funcionan como se esperaba comparando los con la simulación. Sin embargo, los circuitos fabricados pueden ser rediseñados con el fin de mejorar su rendimiento.

Utilizando los conocimientos adquiridos sobre los modos característicos, se ha diseñado un sistema de antena MIMO de una sola capa. Este sistema de antena MIMO de una sola capa implementa una combinación de los modos característicos J2 y J3. El uso de la combinación de estos dos modos característicos generará un patrón de directividad beneficioso, lo que permite una recepción de señal en todas las direcciones alrededor del sistema. Además, el uso de la combinación de los modos J2 y J3 incrementa la capacidad del canal. La red de alimentación de este sistema de antena MIMO se ha realizado utilizando una línea microstrip. A partir de este diseño se puede concluir que un sistema MIMO adaptado a 2.6 GHz puede ser fabricado usando elementos de acoplamiento inductivo y una línea microstrip como una red de alimentación.

Como el material ROGERS RT5880 utilizado para el diseño del sistema de antena MIMO no estaba disponible, se utilizó ROGERS RO4003 que es un material cerámico para fabricar un prototipo. El material ROGERS RT5880 es un material a base de teflón que hace que sea un material flexible. Sin embargo, el material ROGERS RO4003 es cerámico que hace que sea un material frágil. La fragilidad del material ROGERS RO4003 favorece que el circuito se rompa cuando es utilizado, como en el caso de la medición en la cámara anecoica para el modo de J3. Por otra parte, partir las mediciones del coeficiente de reflexión del sistema de antena MIMO fabricado, se observa un desplazamiento en frecuencia entre la simulación y las mediciones. Este desplazamiento en frecuencia es el resultado de un exceso de sustrato alrededor del sistema

fabricado. Este exceso de sustrato alrededor del sistema fabricado se puede evitar con el uso de una máquina CNC para fabricar el sistema de antena MIMO.

Por otro lado, para el sistema de antena MIMO fabricado, las mediciones del patrón de radiación del modo característico J2 realizadas en la cámara anecoica muestran que hay una reciprocidad entre las mediciones y la simulación. Por lo tanto se puede concluir que el sistema de antena MIMO fabricado no tiene una gran pérdida en ganancia con respecto al sistema simulado.

Finalmente, se ha analizado la integración del sistema de antena MIMO dentro de los espejos retrovisores de un coche. Varias simulaciones y mediciones corroboran que el sistema de antena MIMO diseñado en este proyecto final de carrera es adecuado para aplicaciones de automoción. Además, se investigó cómo el resto de la estructura metálica del espejo retrovisor influye en el sistema de antena MIMO. Después de este estudio se puede concluir que es necesario aislar el sistema MIMO del resto de la estructura metálica del espejo retrovisor. Esto se puede hacer mediante la inserción de plástico alrededor de la estructura.

Otra consideración realizada en este proyecto final de carrera fue cómo el sistema de antena MIMO se comporta cuando está cubierto con pintura metálica. A partir de esta investigación, se puede concluir que para futuros diseños del sistema de antena MIMO la pintura del coche se debe tener en cuenta ya que cambia el punto de adaptación del sistema. Además en este proyecto final de carrera se ha propuesto la alimentación del sistema de antena MIMO mediante un cable mini-coaxial. Por otra parte, la posible variación en la geometría del espejo retrovisor también se ha considerado.

B.1 Publicaciones

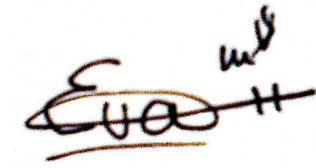
Del trabajo llevado a cabo en este PFC, se ha escrito un artículo enviado a la conferencia Asia-Pacific Microwave Conference (APMC 2014, <http://apmc2014.org/index.html>).



Presupuesto

1) Ejecución Material	
• Compra de ordenador personal (Software incluido)	2.000 €
• Material de oficina	150 €
• Total de ejecución material	2.300 €
2) Gastos generales	
• 16% sobre Ejecución Material	712 €
3) Beneficio Industrial	
• 6% sobre Ejecución Material	267 €
4) Honorarios Proyecto	
• 850 horas a 15 €/hora	12.750 €
5) Material fungible	
• Gastos de impresión	100 €
• Encuadernación	200 €
6) Subtotal del presupuesto	
• Subtotal Presupuesto	18.479 €
7) I.V.A. aplicable	
• 16% Subtotal Presupuesto	2.957 €
8) Total presupuesto	
• Total presupuesto	21.436 €

Madrid, Mayo de 2014
El Ingeniero Jefe de Proyecto

A handwritten signature in black ink, appearing to read 'EVA MASAGUER VELASCO', with a horizontal line drawn through the middle of the signature.

Fdo.: Eva Masaguer Velasco
Ingeniero Superior de Telecomunicación



Pliego de condiciones

Este documento contiene las condiciones legales que guiarán la realización, en este proyecto, de un Sistema de antenas MIMO basado en la excitación de los elementos de la carrocería de un coche. En lo que sigue, se supondrá que el proyecto ha sido encargado por una empresa cliente a una empresa consultora con la finalidad de realizar dicho sistema. Dicha empresa ha debido desarrollar una línea de investigación con objeto de elaborar el proyecto. Esta línea de investigación, junto con el posterior desarrollo de los programas está amparada por las condiciones particulares del siguiente pliego.

Supuesto que la utilización industrial de los métodos recogidos en el presente proyecto ha sido decidida por parte de la empresa cliente o de otras, la obra a realizar se regulará por las siguientes:

Condiciones generales.

- 1) La modalidad de contratación será el concurso. La adjudicación se hará, por tanto, a la proposición más favorable sin atender exclusivamente al valor económico, dependiendo de las mayores garantías ofrecidas. La empresa que somete el proyecto a concurso se reserva el derecho a declararlo desierto.
- 2) El montaje y mecanización completa de los equipos que intervengan será realizado totalmente por la empresa licitadora.
- 3) En la oferta, se hará constar el precio total por el que se compromete a realizar la obra y el tanto por ciento de baja que supone este precio en relación con un importe límite si este se hubiera fijado.
- 4) La obra se realizará bajo la dirección técnica de un Ingeniero Superior de Telecomunicación, auxiliado por el número de Ingenieros Técnicos y Programadores que se estime preciso para el desarrollo de la misma.
- 5) Aparte del Ingeniero Director, el contratista tendrá derecho a contratar al resto del personal, pudiendo ceder esta prerrogativa a favor del Ingeniero Director, quien no estará obligado a aceptarla.
- 6) El contratista tiene derecho a sacar copias a su costa de los planos, pliego de condiciones y presupuestos. El Ingeniero autor del proyecto autorizará con su firma las copias solicitadas por el contratista después de confrontarlas.

- 7) Se abonará al contratista la obra que realmente ejecute con sujeción al proyecto que sirvió de base para la contratación, a las modificaciones autorizadas por la superioridad o a las órdenes que con arreglo a sus facultades le hayan comunicado por escrito al Ingeniero Director de obras siempre que dicha obra se haya ajustado a los preceptos de los pliegos de condiciones, con arreglo a los cuales, se harán las modificaciones y la valoración de las diversas unidades sin que el importe total pueda exceder de los presupuestos aprobados. Por consiguiente, el número de unidades que se consignan en el proyecto o en el presupuesto, no podrá servirle de fundamento para entablar reclamaciones de ninguna clase, salvo en los casos de rescisión.
- 8) Tanto en las certificaciones de obras como en la liquidación final, se abonarán los trabajos realizados por el contratista a los precios de ejecución material que figuran en el presupuesto para cada unidad de la obra.
- 9) Si excepcionalmente se hubiera ejecutado algún trabajo que no se ajustase a las condiciones de la contrata pero que sin embargo es admisible a juicio del Ingeniero Director de obras, se dará conocimiento a la Dirección, proponiendo a la vez la rebaja de precios que el Ingeniero estime justa y si la Dirección resolviera aceptar la obra, quedará el contratista obligado a conformarse con la rebaja acordada.
- 10) Cuando se juzgue necesario emplear materiales o ejecutar obras que no figuren en el presupuesto de la contrata, se evaluará su importe a los precios asignados a otras obras o materiales análogos si los hubiere y cuando no, se discutirán entre el Ingeniero Director y el contratista, sometiéndolos a la aprobación de la Dirección. Los nuevos precios convenidos por uno u otro procedimiento, se sujetarán siempre al establecido en el punto anterior.
- 11) Cuando el contratista, con autorización del Ingeniero Director de obras, emplee materiales de calidad más elevada o de mayores dimensiones de lo estipulado en el proyecto, o sustituya una clase de fabricación por otra que tenga asignado mayor precio o ejecute con mayores dimensiones cualquier otra parte de las obras, o en general, introduzca en ellas cualquier modificación que sea beneficiosa a juicio del Ingeniero Director de obras, no tendrá derecho sin embargo, sino a lo que le correspondería si hubiera realizado la obra con estricta sujeción a lo proyectado y contratado.
- 12) Las cantidades calculadas para obras accesorias, aunque figuren por partida alzada en el presupuesto final (general), no serán abonadas sino a los precios de la contrata, según las condiciones de la misma y los proyectos particulares que para ellas se formen, o en su defecto, por lo que resulte de su medición final.
- 13) El contratista queda obligado a abonar al Ingeniero autor del proyecto y director de obras así como a los Ingenieros Técnicos, el importe de sus respectivos honorarios facultativos por formación del proyecto, dirección técnica y administración en su caso, con arreglo a las tarifas y honorarios vigentes.
- 14) Concluida la ejecución de la obra, será reconocida por el Ingeniero Director que a tal efecto designe la empresa.
- 15) La garantía definitiva será del 4.
- 16) La forma de pago será por certificaciones mensuales de la obra ejecutada, de acuerdo con los precios del presupuesto, deducida la baja si la hubiera.
- 17) La fecha de comienzo de las obras será a partir de los 15 días naturales del replanteo oficial de las mismas y la definitiva, al año de haber ejecutado la provisional, procediéndose si no existe reclamación alguna, a la reclamación de la fianza.

- 18) Si el contratista al efectuar el replanteo, observase algún error en el proyecto, deberá comunicarlo en el plazo de quince días al Ingeniero Director de obras, pues transcurrido ese plazo será responsable de la exactitud del proyecto.
- 19) El contratista está obligado a designar una persona responsable que se entenderá con el Ingeniero Director de obras, o con el delegado que éste designe, para todo relacionado con ella. Al ser el Ingeniero Director de obras el que interpreta el proyecto, el contratista deberá consultarle cualquier duda que surja en su realización.
- 20) Durante la realización de la obra, se girarán visitas de inspección por personal facultativo de la empresa cliente, para hacer las comprobaciones que se crean oportunas. Es obligación del contratista, la conservación de la obra ya ejecutada hasta la recepción de la misma, por lo que el deterioro parcial o total de ella, aunque sea por agentes atmosféricos u otras causas, deberá ser reparado o reconstruido por su cuenta.
- 21) El contratista, deberá realizar la obra en el plazo mencionado a partir de la fecha del contrato, incurriendo en multa, por retraso de la ejecución siempre que éste no sea debido a causas de fuerza mayor. A la terminación de la obra, se hará una recepción provisional previo reconocimiento y examen por la dirección técnica, el depositario de efectos, el interventor y el jefe de servicio o un representante, estampando su conformidad el contratista.
- 22) Hecha la recepción provisional, se certificará al contratista el resto de la obra, reservándose la administración el importe de los gastos de conservación de la misma hasta su recepción definitiva y la fianza durante el tiempo señalado como plazo de garantía. La recepción definitiva se hará en las mismas condiciones que la provisional, extendiéndose el acta correspondiente. El Director Técnico propondrá a la Junta Económica la devolución de la fianza al contratista de acuerdo con las condiciones económicas legales establecidas.
- 23) Las tarifas para la determinación de honorarios, reguladas por orden de la Presidencia del Gobierno el 19 de Octubre de 1961, se aplicarán sobre el denominado en la actualidad "Presupuesto de Ejecución de Contrata 2 anteriormente llamado "Presupuesto de Ejecución Material" que hoy designa otro concepto.

Condiciones particulares.

La empresa consultora, que ha desarrollado el presente proyecto, lo entregará a la empresa cliente bajo las condiciones generales ya formuladas, debiendo añadirse las siguientes condiciones particulares:

- 1) La propiedad intelectual de los procesos descritos y analizados en el presente trabajo, pertenece por entero a la empresa consultora representada por el Ingeniero Director del Proyecto.
- 2) La empresa consultora se reserva el derecho a la utilización total o parcial de los resultados de la investigación realizada para desarrollar el siguiente proyecto, bien para su publicación o bien para su uso en trabajos o proyectos posteriores, para la misma empresa cliente o para otra.
- 3) Cualquier tipo de reproducción aparte de las reseñadas en las condiciones generales, bien sea para uso particular de la empresa cliente, o para cualquier otra aplicación, contará con autorización expresa y por escrito del Ingeniero Director del Proyecto, que actuará en representación de la empresa consultora.
- 4) En la autorización se ha de hacer constar la aplicación a que se destinan sus reproducciones así como su cantidad.

- 5) En todas las reproducciones se indicará su procedencia, explicitando el nombre del proyecto, nombre del Ingeniero Director y de la empresa consultora.
- 6) Si el proyecto pasa la etapa de desarrollo, cualquier modificación que se realice sobre él, deberá ser notificada al Ingeniero Director del Proyecto y a criterio de éste, la empresa consultora decidirá aceptar o no la modificación propuesta.
- 7) Si la modificación se acepta, la empresa consultora se hará responsable al mismo nivel que el proyecto inicial del que resulta el añadirla.
- 8) Si la modificación no es aceptada, por el contrario, la empresa consultora declinará toda responsabilidad que se derive de la aplicación o influencia de la misma.
- 9) Si la empresa cliente decide desarrollar industrialmente uno o varios productos en los que resulte parcial o totalmente aplicable el estudio de este proyecto, deberá comunicarlo a la empresa consultora.
- 10) La empresa consultora no se responsabiliza de los efectos laterales que se puedan producir en el momento en que se utilice la herramienta objeto del presente proyecto para la realización de otras aplicaciones.
- 11) La empresa consultora tendrá prioridad respecto a otras en la elaboración de los proyectos auxiliares que fuese necesario desarrollar para dicha aplicación industrial, siempre que no haga explícita renuncia a este hecho. En este caso, deberá autorizar expresamente los proyectos presentados por otros.
- 12) El Ingeniero Director del presente proyecto, será el responsable de la dirección de la aplicación industrial siempre que la empresa consultora lo estime oportuno. En caso contrario, la persona designada deberá contar con la autorización del mismo, quien delegará en él las responsabilidades que ostente.